Office of Naval Research

Contract N50RI-76 • Task Order No.1 • NR-071-012

RECTIFICATION OF NEARLY GAUSSIAN NOISE

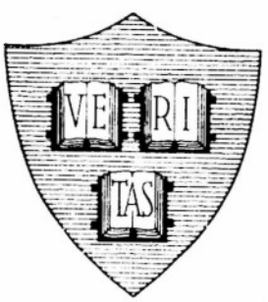

By

James A. Mullen
and
David Middleton

June 1, 1954

Technical Report No. 189

Cruft Laboratory
Harvard University
Cambridge, Massachusetts

Office of Naval Research

Contract N5ori-76

Task Order No. 1

NR-071-011

Technical Report

on

Rectification of Nearly Gaussian Noise

by

James A. Mullen and David Middleton

June 1, 1954

The research reported in this document was made possible through support extended Cruft Laboratory, Harvard University, jointly by the Navy Department (Office of Naval Research), the Signal Corps of the U. S. Army, and the U. S. Air Force, under ONR Contract N5ori-76, T. O. 1.

Technical Report No. 189

Cruft Laboratory

Harvard University

Cambridge, Massachusetts

TR189

Rectification of Nearly Gaussian Noise

by

James A. Mullen and David Middleton

Cruft Laboratory, Harvard University

Cambridge, Massachusetts

Abstract

Nongaussian noise occurs sufficiently often that a study of its points of similarity to and difference from gaussian noise is desirable. This report considers an important sub-class of non-normal statistics, viz., nearly normal noise. A new form for the nearly gaussian probability densities has been found; this is discussed, compared to the conventional Edgeworth series, and related to earlier work. Next a survey of physical noise sources is made in order to classify the statistical nature of the noise that each produces. The rectification of nearly normal noise and a c-w signal in a half-wave νth-law detector is analyzed and the correlation functions of the output obtained. The behavior of the output is compared to the corresponding results for gaussian noise of the same input intensity. For the linear and square-law detectors, the cases of prime interest, detailed figures and a number of more tractable formulas are given. Finally, the problem of finite averaging is briefly considered.

- - - - - -

I

Introduction

This report considers the rectification of a-m signals and nongaussian noise. The corresponding problem in which the noise is gaussian is particularly important because most noise sources are gaussian ones and because the normal distribution is easy to handle analytically. Quite properly, early work considered gaussian noise nearly exclusively. Nonetheless, certain types of noise do not have normal distributions, so that an analysis of the non-normal case is desirable, both to apply directly to problems where it is applicable, and to help to indicate in uncertain cases how critical the assumption of gaussian statistics is. We note that because of the presence of a non-

linear element in the receiver, viz., the rectifier, the output moments depend on the entire input distributions, so that the input statistics affect even the simplest of the output properties.

The noise of the present paper is nearly gaussian so that the probability distributions can be expanded asymptotically in terms of the corresponding normal probability distribution and its derivatives. This is the well-known Edgeworth series [1]; however, the form that we have found most useful, which involves derivatives with respect to the second moments of the distribution, has apparently not been mentioned before. Pearson [2] used the idea for a special distribution in order to facilitate deriving the usual Edgeworth series and Crofton [3] has obtained similar equalities between different kinds of derivatives in a separate derivation of the Edgeworth series. The application of our results depends partly on the fact that, after passing through the tuned stages of the receiver, the noise is narrow-band. We have obtained relations connecting the distributions of the envelope and phase of the noise wave to those of the instantaneous value, which also appear to be new.

A survey of physical sources of noise has been made to determine, whenever possible, whether the noise produced is gaussian or nongaussian and to suggest noise models for use in the analysis of the detector. The correlation function at the output of an idealized a-m receiver with a νth-law rectifier has been found when the input is a nearly normal noise and a c-w signal. The result is fairly intractable in general, but formulas have been obtained. Graphs have been drawn for the two most important cases, linear and square-law rectifiers, with various representative types of noise inputs. The general effect of nongaussian noise compared to gaussian noise of the same input power has been found for both the output power and the output correlation function. Finally, the effect of averaging the output over a finite time has been examined, again qualitatively, in general, and with explicit results and figures for the quadratic detector.

II

Probability Distributions of Nearly Gaussian Noise

2.1 General Properties of Probability Distributions

A sufficient characterization of systems containing noise requires a statistical description of the noise, viz., the joint probability densities of the noise at a set of different values of the time, or alternatively, knowledge of the ensemble from which the sample functions actually observed are drawn [4,5,6]. The noise processes with which this report is concerned are Markoffian [7,8], which means that knowledge of the joint distribution at two times is enough to describe the process completely. Thus two distributions will be needed for each variable.

$W_1(y,t)dy$ = the probability that y will lie in the interval y, y and dy at time t and,

$W_2(y_1,t_1; y_2,t_2)dy_1dy_2$ = the joint probability that y will lie in y_1, $y_1 + dy_1$ at time t_1, and that y will lie in y_2, $y_2 + dy_2$ at time t_2.

As the time difference between the two times of observation is increased, the dependence of y_2 on y_1 is lessened until with sufficient separation, y_1 and y_2 are independent; that is

$$\lim_{t\to\infty} W_2(y_1,t_1; y_2,t_2 = t_1 + t) = W_1(y_1,t_1)W_1(y_2,t_2). \qquad (2.1)$$

The characteristic function of the noise is the Fourier transform of the probability distribution [9,10].

$$F_2(\xi_1,t_1;\xi_2,t_2) = \int_{-\infty}^{\infty}\int e^{i\xi_1y_1 + i\xi_2y_2} W_2(y_1,t_1;y_2,t_2)dy_1dy_2. \qquad (2.2)$$

This function is introduced because problems are often simpler when phrased in terms of transforms than when stated directly in terms of the probability densities.

A further important concept is that of stationarity [11], which means

that the distributions are invariant under a linear shift of all the times of observation. W_1 thus does not depend on t, and W_2 depends only on the time difference t_2-t_1.

An important set of parameters associated with a distribution are its moments, defined by

$$\mu_{mn}^{(t)} = \iint_{-\infty}^{\infty} y_1^m y_2^n W_2(y_1,y_2;t)dy_1dy_2. \tag{2.3}$$

Because of its particular importance, $\mu_{11}(t)$ is given a special symbol, R(t), and a name, the correlation function. It serves as a simple but not entirely reliable test of independence of the noise values at two times separated by an interval t.* Also, the spectral distribution of the noise power can be found from the correlation function by using the Wiener-Khintchine theorem [12,13],

$$\begin{aligned} W(f) &= 4\int_o^{\infty} R(t)\cos\omega t\, dt, \\ R(t) &= \int_o^{\infty} W(f)\cos\omega t\, dt. \end{aligned} \tag{2.4}$$

When all the Kth-order moments exist, the characteristic function possesses an expansion in terms of the moments [9,10],

$$\begin{aligned} F_2(\xi_1,\xi_2;t) &= \langle \exp(i\xi_1 y_1 + i\xi_2 y_2)\rangle_{av}, \\ &= \sum_{\substack{M=0 \\ m+n=M}}^{K} \frac{\mu_{mn}(t)}{m!n!}(i\xi_1)^m(i\xi_2)^n + 0([\xi_1^2+\xi_2^2]^{k/2}). \end{aligned} \tag{2.5}$$

A different set of parameters of the distribution are the semi-invariants, defined from the expansion of the logarithm of the characteristic function [9,10].

- - - - - - -

*It is in fact a "wide sense" test for independence, in the sense of Doob, sec 2.3.

$$\ln F_2(\xi_1,\xi_2;t) = \sum_{\substack{K=1 \\ k+l=K}}^{\infty} \frac{\lambda_{kl}^{(t)}}{k!\,l!}(i\xi_1)^k(i\xi_2)^l. \tag{2.6}$$

By comparing the two power series, relations between the moments and semi-invariants can be found.

The sources of noise considered in the succeeding section are Markoffian and stationary; furthermore, they are representative of Poisson ensembles, a particular class of distributions of sums of independent random variables.

2.2 The Poisson ensemble

The Poisson noise ensemble is composed of sums of independent variables with common distributions and uniformly distributed times of occurrence, t_j, viz.,

$$V(t;K,\{t_j\}) = \sum_{j=1}^{K} v_j(t-t_j).$$

Physically, the basic random variables represent pulses produced randomly by a noise source. These hypotheses imply that the number of pulses occurring, K, is a random variable with a Poisson distribution [13,14], so that K, as well as the set of t_j's, is an ensemble parameter. The variability of K distinguishes the Poisson model from the random walk problem where K is a fixed, known number [2,15]. This difference is not a necessary consequence of either model. However, with superposed pulses, the natural condition of uniformly distributed occurrence times leads at once to a distribution of K. In a random walk, on the other hand, a fixed number of steps seems more natural. In this paper, "random walk" and "Poisson" models will always refer to ensembles with a fixed or variable K, respectively.

The distributions of V can now be derived following Middleton [16].

Because of the independence between pulses the characteristic function for V when K pulses occur is the Kth power of the characteristic function for v.

$$F_{2V}(\xi_1,\xi_2)_K = [F_{2v}(\xi_1,\xi_2)]^K. \tag{2.7}$$

The desired characteristic function is the above one averaged over the values of K.

$$F_{2V}(\xi_1,\xi_2) = \sum_{K=0}^{\infty} \frac{\gamma^K}{K!} e^{-\gamma} [F_{2v}(\xi_1,\xi_2)]^K = \exp\left\{\gamma[F_{2v}(\xi_1,\xi_2) - 1]\right\} . \quad (2.8)$$

Here γ is the average pulse density, the average number of pulses per second times the average duration of a pulse.

The above equations exhibit a consequence of the different ensembles for Poisson or random walk models. In the Poisson case, the semi-invariants of V equal γ times the moments of v; in the random walk (Eq. 2.7), the semi-invariants of V equal γ times the semi-invariants of v, i.e., the fixed value of K is γ.

In the general model, individual pulses are themselves random variables with distributions of amplitude, phase, duration, and occurrence time, viz.,

$$v(t-t') = a\, h(\beta[t-t']; r) \cos[\omega_o(t-t') + \psi] . \quad (2.9)$$

Here a is the amplitude of the pulse; h, its shape factor, which depends on the occurrence time, t', and the duration, r(the time variable has been normalized by dividing by the mean duration $\bar{r} = 1/\beta$); and ψ is the phase of the pulse. Most systems in which noise is important are spectrally narrow-band; accordingly v(t) has been written as a slowly varying envelope factor, h(βt;r) times a rapidly varying "carrier" wave. In terms of these random variables, the characteristic function for a single pulse is

$$F_{2v}(\xi_1,\xi_2) = \int da_1 da_2 dr_1 dr_2 d\psi_1 d\psi_2 d\beta t'_1 d\beta t'_2 d\beta t_1 \times w(a_1,a_2,r_1,r_2,\psi_1,\psi_2,\beta t_1,\beta t'_2)$$

$$\exp\left\{ia_1\xi_1 h(\beta[t_2-t'_1]; r_1) + ia_2\xi_2 h(\beta[t-t'_2]; r)\right\} . \quad (2.10)$$

A specific noise source will not usually produce pulses variable in all these quantities, so that the problem of evaluating the above integral is not so formidable as it may appear.

The moments of a distribution are always of interest; in this paper, they are particularly so since we shall be concerned with nearly gaussian

distributions where only the first four sets of moments appear, not the general form of the exact distribution.

For simplicity, let us consider a noise source that produces pulses at random times but with specific amplitude, shape, and phase. Then the semi-invariants of the output are

$$\lambda_{mn}(t) = \gamma \left\langle a^{m+n} \int_{-\infty}^{\infty} h^m(x;r)h^n(x+\beta t;r) \cos^m(\omega_o x/\beta - \psi)\cos^n(\omega_o x/\beta - \psi + \omega_o t)dx \right\rangle_{av}, \tag{2.11}$$

where βt_1 has been set equal to a new variable, x, and t_2 has been changed to $t_1 + t$.

As is justified in Appendix I, because of the narrow-band structure the phase may be assumed to be distributed uniformly. Carrying out the phase average first then simplifies the form of $\lambda_{mn}(t)$ considerably in specific cases. In general, one has

$$\lambda_{mn}(t) = 0 \quad m + n \text{ odd},$$

$$\lambda_{mn}(t) = \lambda_{nm}(-t), \tag{2.12}$$

which last follows directly from Eq. (2.7) above, quite independent of the narrow-band assumption. The second and fourth order semi-invariants are then

$$\begin{cases} \lambda_{11}(t) = \gamma\frac{1}{2}\left\langle a^2 \int_{-\infty}^{\infty} h(x;r)h(x+\beta t;r)dx \right\rangle_{av} \cos\omega_o t, \equiv \psi r_o(t)\cos\omega t \equiv \psi r(t); \\ \lambda_{20} = \lambda_{02} = \lambda_{11}(0) \equiv \psi \ . \end{cases} \tag{2.13}$$

$$\begin{cases} \lambda_{22}(t) = \gamma\frac{1}{8}\left\langle a^4 \int_{-\infty}^{\infty} h^2(x;r)h^2(x+\beta t;r)dx \right\rangle_{av} (2 + \cos 2\omega_o t), \\ \lambda_{31}(t) = \lambda_{13}(-t) = \gamma\frac{3}{8}\left\langle a^4 \int_{-\infty}^{\infty} h^3(x;r)h(x+\beta t;r)dx \right\rangle_{av} \cos\omega_o t, \end{cases}$$

$$\lambda_{40} = \lambda_{04} = \lambda_{31}(0) = \lambda_{22}(0). \tag{2.14}$$

It is convenient to separate the low-and high-frequency variations in the fourth-order semi-invariants just as, in $\lambda_{11}(t)$, the $\psi r_o(t)$ is distinct from the carrier part. Defining a low-frequency factor $\Lambda_{mn}(t)$, so that $\Lambda_{mn}(0) = \lambda_{mn}(0)$, we have

$$\lambda_{22}(t) = \Lambda_{22}(t)[\,2/3 + 1/3 \cos 2\omega_o t\,]. \tag{2.15}$$

$$\lambda_{31}(t) = \Lambda_{31}(t) \cos \omega_o t$$

$$\lambda_{40} = \Lambda_{40}.$$

2.3 Nearly gaussian distributions

A nearly normal distribution may be asymptotically expanded in terms of the limiting gaussian form in inverse powers of γ. To get the asymptotic series, we write (2.6) as

$$F_2(\xi_1,\xi_2;t) = \left\{ 1 + \frac{\lambda_{40}}{4!}\xi_1^4 + \frac{\lambda_{31}(t)}{3!}\xi_1^3\xi_2 + \frac{\lambda_{22}(t)}{2!2!}\xi_1^2\xi_2^2 + \frac{\lambda_{13}(t)}{3!}\xi_1\xi_2^3 + \frac{\lambda_{04}}{4!}\xi_2^4 + O_T(\gamma^{-2}) \right\} \times \exp\left\{ -\frac{\psi}{2}[\xi_1^2 + 2r(t)\xi_1\xi_2 + \xi_2^2] \right\}. \tag{2.16}$$

The symbol $O_T(\gamma^{-2})$ means that, after the transform is taken, the neglected part is of order γ^{-2}. All the semi-invariants are of order γ; V^2 is of order $\langle V^2 \rangle$, so that ξ_i is of order $\gamma^{-1/2}$. Thus the M = 4 terms are of order γ^{-1}; the next succeeding terms, M = 6 and the square of M = 4 terms, will be of order γ^{-2} (odd order semi-invariants, when not equal to zero, introduce fractional powers)[17]. The probability density corresponding to the above characteristic function is

$$W_2(V_1,V_2;t) \simeq \left\{ 1 + \frac{\lambda_{40}}{4!}\frac{\partial^4}{\partial V_1^4} + \frac{\lambda_{31}(t)}{3!}\frac{\partial^4}{\partial V_1^3 \partial V_2} + \frac{\lambda_{22}(t)}{2!2!}\frac{\partial^4}{\partial V_1^2 \partial V_2^2} + \right.$$

$$+\frac{\lambda_{13}(t)}{3!}\frac{\partial^4}{\partial V_1 \partial V_2^3}+\frac{\lambda_{04}}{4!}\frac{\partial^4}{\partial V_2^4}+O(\gamma^{-2})\Bigg]\frac{\exp\left\{-\dfrac{V_1^2+V_2^2-2V_1V_2r(t)}{2\psi\sqrt{1-r^2(t)}}\right\}}{2\pi\psi\sqrt{1-r^2(t)}} \tag{2.17}$$

This is the two-dimensional form of the well-known Edgeworth series [1].

Another form of this probability distribution is possible, in which derivatives are taken with respect to the second moments (for the derivation of this result, see Appendix II).

The characteristic function is

$$F_2(\xi_1,\xi_2;t)=\left\{1+\frac{\Lambda_{40}}{3!}\left[\frac{\partial^2}{\partial\psi_1^2}+\frac{\partial^2}{\partial\psi_2^2}\right]+\frac{2}{3!\psi}\frac{\partial}{\partial r_o}\left[\Lambda_{31}(t)\frac{\partial}{\partial\psi_1}+\Lambda_{13}(t)\frac{\partial}{\partial\psi_2}\right]\right.$$

$$\left.+\frac{\Lambda_{22}(t)}{3!}\left[\frac{1}{\psi^2}\frac{\partial^2}{\partial r_o^2}+2\frac{\partial^2}{\partial\psi_1\partial\psi_2}\right]+O_T(\gamma^{-2})\right\} \tag{2.18}$$

$$\times\exp\left\{-\frac{1}{2}\left[\psi_1\xi_1^2+2\psi r_o(t)\xi_1\xi_2\cos\omega_o t+\psi_2\xi_2^2\right]\right\}\Bigg|_{\psi_1=\psi_2=\psi}$$

The probability distribution can be obtained from this by transforming the exponential alone.

The series (2.18) was first found by Pearson [2] for the first order density in the random walk, using the properties of Bessel functions; but apparently it has not previously been extended to any general class of distributions. The only condition needed is that the random variables be isotropic. Even if this is not so, a similar series involving also derivatives with respect to the first moments may be found. However, the latter is sufficiently involved so that little advantage is to be expected in using it rather than the Edgeworth series.

For moments after a nonlinear operation, the comparative simplicity

in the analysis when the noise possesses a gaussian distribution is often a strong point in favor of the series of parametric derivatives. Applying the differential operator to the result for (nonstationary) gaussian noise is likely to be involved, but is certainly straightforward. Furthermore, where the narrow-band structure of the output is important, this characteristic function possesses the very considerable advantage of having the high-frequency part appearing only in the exponent, while the Edgeworth form has high-frequency terms of different orders scattered about in the various semi-invariants as well as in the exponent.

2.4 Envelope and phase distributions

In narrow band problems, it is sometimes more convenient to take the slowly varying parts of the noise wave as the random variables, rather than the instantaneous value. The distributions obtained are more complicated, but in return this technique entirely eliminates high-frequency terms in the probability distribution. A narrow-band ensemble can be written as

$$V(t;\alpha,\beta) = R(t;\alpha)\cos\left[\omega_o t - \theta(t;\beta)\right], \tag{2.19}$$

where the envelope and phase are random variables not, in general, independent (which means that the ensemble parameters α and β are functionally related). In terms of in-phase and quadrature components,

$$V(t;\gamma[\alpha,\beta],\delta[\alpha,\beta]) = X(t;\gamma)\cos\omega_o t + Y(t;\delta)\sin\omega_o t. \tag{2.20}$$

X and Y are not usually independent either. It is frequently easier to find the distributions of X and Y and afterward, by transforming to polar coordinates, find the distributions of envelope and phase.

From the equation above, it is evident that knowledge of the distributions of V is equivalent to knowledge of those of X and Y. The explicit connection between these two different representations of the noise wave has been found under the condition that the phase is distributed uniformly.*

- - - - - - -

*A general four-dimensional distribution has thirty-one non-zero fourth-order semi-invariants while the corresponding distribution of V has only five. Finding that a connection between the two distributions is highly desirable in the interest of algebraic simplicity alone.

In case only the marginal distributions of envelope and phase changes are needed, the condition on the phase distribution may be dispensed with. It should be pointed out that, while the fact that V is narrow-band and nearly gaussian implies that it is isotropic, because of the high-frequency variations, that is not true of the slowly varying components, precisely because the high-frequency part has been removed. Furthermore, while the requirement that the phase be uniformly distributed is satisfied for a good many noise sources of interest, an almost equal class will not fit this scheme, so that the restriction is more severe than desirable. Fortunately, for the detection problem, and indeed for all cases where only the low-frequency output is needed, the isotropy condition can be eliminated by working with the distributions of the envelope alone.

The high-frequency variation of the characteristic function of V contains always $\cos \omega_o t$. To put the high-frequency dependence in evidence let us write the characteristic function as $F_{2V}(\xi_1, \xi_2; t, \cos \omega_o t)$. Then, if the characteristic function for X and Y is transformed into polar coordinates,

$$F_{2X,Y}(\chi_1, \eta_1, \chi_2, \eta_2; t) = F_{2X,Y}(\xi_1 \cos \phi_1, \xi_1 \sin \phi_1, \xi_2 \cos \phi_2, \xi_2 \sin \phi_2; t), \tag{2.21}$$

the connection between the two is

$$F_{2X,Y}(\xi_1 \cos \phi_1, \xi_1 \sin \phi_1, \xi_2 \cos \phi_2, \xi_2 \sin \phi_2; t) = F_{2V}(\xi_1, \xi_2; t, \cos [\phi_2 - \phi_1]), \tag{2.22}$$

a result derived in Appendix III, on the assumption of a uniform phase distribution. Without any restrictions on the phase, however, the distribution of envelopes and phase difference may be found. We have

$$W_2(R_1, R_2, \theta) = R_1 R_2 \int_0^\infty \int_0^\infty \int_0^{2\pi} \frac{d\phi}{(2\pi)^2} \xi_1 \xi_2 \, d\xi_1 d\xi_2$$

$$\times J_o([\xi_1^2 R_1^2 + \xi_2^2 R_2^2 + 2\xi_1 \xi_2 R_1 R_2 \cos(\theta - \phi)]^{1/2} \tag{2.23}$$

$$\times F_{2V}(\xi_1, \xi_2; t, \cos \phi),$$

where $\theta = \theta_2 - \theta_1$, $\phi = \phi_2 - \phi_1$

As an important special case, one finds

$$W_1(R) = R \int_0^\infty \xi J_o(\xi R) F_V(\xi)\, d\xi. \tag{2.24}$$

The above relations are true of narrow-band distributions in general; these must now be applied to the nearly gaussian distributions which are our primary concern. If there is an unmodulated carrier present as well as the nearly gaussian noise, the instantaneous value of the sum of the two may be written variously as

$$\left.\begin{aligned} Z(t) &= A_o \cos\omega_o t + V(t), \\ &= [A_o + X(t)] \cos\omega_o t + Y(t) \sin\omega_o t, \\ &= x(t) \cos\omega_o t + y(t) \sin\omega_o t. \end{aligned}\right\} \tag{2.25}$$

Using Eqs. (2.1), (2.21), (2.25) together, the distribution of the envelope is found to be

$$\begin{aligned} W_1(R) &= \left[1 + \frac{\Lambda_{40}}{3!} \frac{\partial^2}{\partial\psi^2} \right] \frac{R}{\psi} I_o\left(\frac{A_o R}{\psi}\right) e^{\frac{-R^2 + A_o^2}{2\psi}}, \\ &= \left[I_o\left(\frac{A_o R}{\psi}\right) + \frac{\Lambda_{40}}{4!\psi^2} \left\{ \frac{4A_o^2 R^2}{\psi^2} I_2\left(\frac{A_o R}{\psi}\right) \right.\right. \\ &\quad + \left[\frac{2A_o R}{\psi} - \frac{4A_o R}{\psi^2}(A_o^2 + R^2) \right] I_1(A_o R/\psi) \\ &\quad \left.\left. + \left[\frac{(R^2 + A_o^2)^2}{\psi^2} - \frac{8(A_o^2 + R^2)}{\psi} + 8 \right] I_o\left(\frac{A_o R}{\psi}\right) \right\} \right] \frac{R}{\psi} e^{-\frac{R^2 + A_o^2}{2\psi}}. \end{aligned} \tag{2.26}$$

A nearly gaussian distribution is shown in Fig. 1 for various values of signal-to-noise-power ratio together with gaussian noise of the same mean square value. Before the nearly gaussian distribution can be plotted, a value of the fourth-order semi-invariant must be assigned. The graph

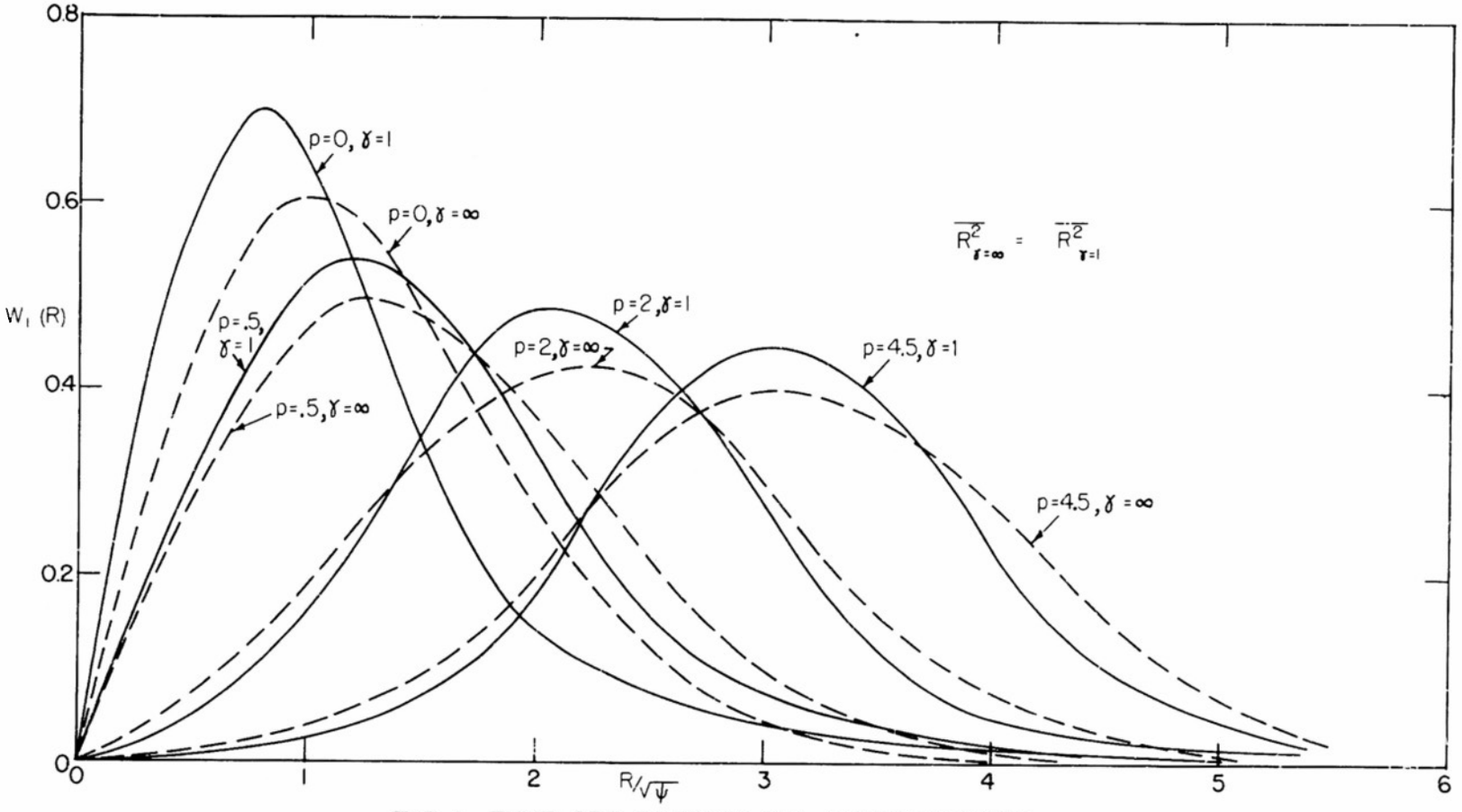

FIG. 1 ENVELOPE PROBABILITY DISTRIBUTIONS

here represents a noise source producing square c-w pulses of constant amplitude, serving as an approximation to clutter in a radar system. $\Lambda_{40}/3!\,\psi^2$ then becomes $1/4\gamma$, where γ is the density parameter previously defined (Eq. 2.8). The nearly gaussian distribution has more small deviations from the mode and a larger tail than does the gaussian.

As pointed out previously, the random walk model is not equivalent to the Poisson one. For this noise source, the deviation of the random walk distribution from the gaussian are equal in sign but opposite in magnitude to the deviation of the Poisson model distribution in the figure (for equal densities). In general,

$$\left.\frac{\Lambda_{40}}{\psi^2}\right|_{\text{Poisson}} = \left.\frac{\Lambda_{40}}{\psi^2}\right|_{\substack{\text{Random}\\ \text{Walk}}} + \frac{3}{\gamma} \quad , \tag{2.27}$$

when the Poisson and random walk densities are the same.

The phase distribution presents a more difficult problem. The sum of a sine wave and narrow-band noise will not have a uniform phase distribution since the phase of the carrier takes a preferred value. If, however, the noise by itself has a uniform phase distribution, then the desired distribution may be found by transforming coordinates from X,Y of Eq. (2.20) to x,y of Eq. (2.25).

The joint distribution of envelope and phase is thus

$$W_1(R,\theta) = \left[1 + \frac{\Lambda_{40}}{3!}\frac{\partial^2}{\partial\psi^2}\right]\frac{R}{2\pi\psi}\exp\left\{-\frac{R^2 + A_o^2 - 2A_oR\cos\theta}{2\psi}\right\} \tag{2.28}$$

whence

$$W_1(\theta) = \left[1 + \frac{\Lambda_{40}}{3!}\frac{\partial^2}{\partial\psi^2}\right]\frac{e}{2\pi}^{-p\sin^2\theta}\left[\sqrt{p\pi}\cos\theta + {}_1F_1(-\tfrac{1}{2},\tfrac{1}{2};p\cos^2\theta)\right]$$

or as a Fourier series.

$$W_1(\theta) = \sum_{m=o}^{\infty}\frac{\epsilon_m p^{m/2}\cos m\theta}{m!}\Gamma(\tfrac{m}{2}+1)\left\{F(\tfrac{m}{2};\,m+1;\,-p) - \frac{\Lambda_{40}}{3!\,\psi^2}\frac{m(m+2)}{4}F(\tfrac{m}{2}+2;\,m+1;\,-p)\right\} \tag{2.29}$$

The envelope distribution, Eq. (2.26) can also be derived from Eq. (2.28) by integrating over the phase, but its previous derivation directly from

Eq. (2.24) emphasizes that no assumption on the phase distribution is necessary.

The second-order distribution is needed for calculating correlation functions. For a nearly normal noise alone, from Eq. (2.23) we have

$$W_2(R_1,R_2,\theta_1,\theta_2;t) = R_1R_2\left\{1+\frac{\Lambda_{40}}{3!}\left[\frac{\partial^2}{\partial\psi_1^2}+\frac{\partial^2}{\partial\psi_2^2}\right]+\frac{2}{3!\psi}\frac{\partial}{\partial r_o}\left[\Lambda_{31}(t)\frac{\partial}{\partial\psi_1}+\Lambda_{13}(t)\frac{\partial}{\partial\psi_2}\right]\right.$$

$$\left.+\frac{\Lambda_{22}(t)}{3}\left[\frac{1}{\psi^2}\frac{\partial^2}{\partial r_o^2}+2\frac{\partial^2}{\partial\psi_1\partial\psi_2}\right]+0(\gamma^{-2})\right\}\exp\left\{-\frac{\psi_2R_1^2-2\psi r_oR_1R_2\cos\theta+\psi_1R_2^2}{2(\psi_1\psi_2-\psi^2r_o^2)}\right\}\Bigg|_{\psi_1=\psi_2=\psi}$$

$$\frac{}{(2\pi)^2(\psi_1\psi_2-\psi^2r_o^2)} \tag{2.30}$$

where $\theta = \theta_2 - \theta_1$, and the parameters are those of Eq. (2.18).

If a sine-wave signal is also present, the distribution of the envelopes and phases of the sum can be found by transforming variables in Eq. (2.25) to the polar coordinates corresponding to Eq. (2.20). The result for a signal and noise is

$$W_2(R_1,\theta_1,R_2,\theta_2;t)_{S+N} = \left\{1+\frac{\Lambda_{40}}{3!}\left[\frac{\partial^2}{\partial\psi_1^2}+\frac{\partial^2}{\partial\psi_2^2}\right]+\frac{2}{3!\psi}\frac{\partial}{\partial r_o}\left[\Lambda_{31}(t)\frac{\partial}{\partial\psi_1}+\Lambda_{13}(t)\frac{\partial}{\partial\psi_2}\right]\right.$$

$$\left.+\frac{\Lambda_{22}(t)}{3}\left[\frac{1}{\psi^2}\frac{\partial^2}{\partial r_o^2}+2\frac{\partial^2}{\partial\psi_1\partial\psi_2}\right]+0(\gamma^{-2})\right\}\frac{R_1R_2}{(2\pi)^2(\psi_1\psi_2-\psi^2r_o^2)}$$

$$\exp\left\{\frac{-A_o^2(\psi_1-2\psi r_o+\psi_2)}{2(\psi_1\psi_2-r_o^2\psi^2)}-\frac{R_1^2\psi_2-2\psi r_oR_1R_2\cos\theta+\psi_1R_2^2}{2(\psi_1\psi_2-\psi^2r_o^2)}+\frac{A_oR_1(\psi_2-\psi r_o)\cos\theta_1+A_oR_2(\psi_1-\psi r_o)\cos\theta_2}{\psi_1\psi_2-\psi^2r_o^2}\right\}\Bigg|_{\psi_1=\psi_2=\psi}$$

(2.31)

III

Physical Noise Sources

3.1 Introduction

A search through the literature has shown that the Poisson noise model is applicable to most actual noise sources, although the range of densities characteristic of nearly gaussian noise is found only occasionally. The five principal groups of noise sources (not all microscopically distinct), considered below in the same order, are those associated primarily with (1) radar, (2) sonar, (3) atmospheric disturbances, (4) extra-terrestrial generators, and (5) the quantization of charge.

3.2 Sources of noise in radar

Undesired echoes in radar are an example of Poisson noise. Besides the desired target echoes the radar picks up signals from the surface of the sea or ground, from storms, and from "window" – metal strips used to provide spurious target indications. All these are lumped under the general title of "clutter" [18,19].

In a pulsed radar (with a fixed pulse repetition frequency), the input signal following a transmitter pulse represents the echo obtained from a range proportional to the time elapsed since the initiation of the transmitter pulse. At the start of the next pulse, the range is set back to zero and then increases again, as shown in Fig. 2a and b. In analyzing clutter, we want the return signal from one fixed range, R_o, which, as shown in Fig. 2c, is a number, viz., the amplitude of the echo. Before being presented to the observer, the signal from a fixed range is converted to "boxcars," Fig. 2d, and then smoothed, as in Fig. 2e, to give the final form. The display is presented on a cathode-ray tube where the persistence of the phosphor serves as the boxcar generator. Variations in the clutter return between successive pulses are quite small, so that the smoothed representation is an accurate one.

The return, nominally from a single range, R_o, actually comes from

a small volume around R_o within which targets cannot be resolved. The non-zero angular widths of the antenna beam, Θ and Φ,* mean that targets in a solid angle $\Theta\Phi$ will be illuminated simultaneously. With a pulse duration, τ, targets in a range interval of length $c\tau/2$, where c is the propagation velocity, produce echoes which overlap the return from R_o; thus the resolving volume is $R_o^2 \Theta \Phi c \tau/2$. For typical radars, the pulse duration is about 1 μsec corresponding to a range interval of 150 yards and the beam widths, 0.5-5°, so that, up to ranges of 1-10 miles, the shape of the resolving volume is narrow and deep, while at greater ranges it is broad and shallow.

The clutter return at the detector is represented by, as in Eq. (2.9),

$$V(t_1) = \sum_{1}^{K} A_{1k}\, h([t_1 - t'_{1k}]/\tau) \cos(\omega_o[t_1 - t'_{1k}] - \psi_k), \qquad (3.1)$$

where the scatterers are independent and uniformly distributed throughout the resolving volume. Here A_k is the amplitude of the echo from the kth scatterer in the resolving volume and ψ_k its phase; e is the pulse shape, a constant of the transmitter, but also a function of the time of arrival of the received pulse; τ is the duration of the pulse, also constant; and ω_o is the i-f frequency. The average number of scatterers in the resolving volume is the density parameter of the clutter, because the ordinary definition of γ as the average number of pulses per second times the mean duration of a pulse must be divided by the amount of time that the radar receives echoes from the single range R_o.

If the obstacles are moving relative to the radar, the clutter at a later time will contain variations because of a shift in the epochs t'_k. The effect of motion can be important; however, the problem is treated in Appendix IV, since the analysis is moderately involved and does not bear directly on the noise density, our primary concern in this section.

Echoes from "window"

One important type of clutter is "window," echoes from metal strips. Analysis of the echo from a strip [20] shows that the amplitude depends on

---

* Θ and Φ are equivalent rectangular beam widths in their respective directions.

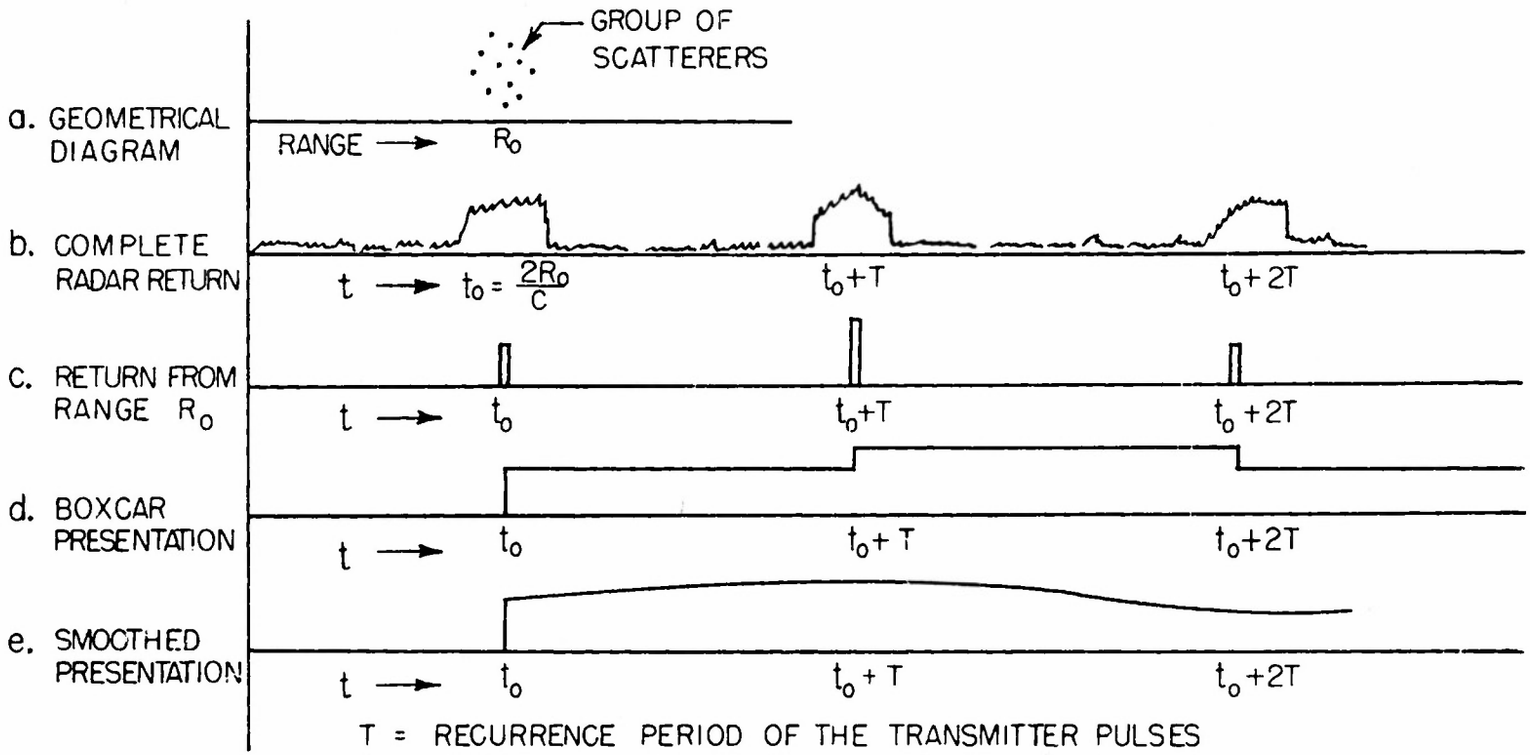

FIG. 2 WAVEFORMS FOR A SINGLE-POINT RANGE DISPLAY

the orientation with respect to the direction of propagation, but that the time over which the correlation function differs from zero is much smaller than the rotation time of a strip, so that the amplitude return is effectively constant in time i.e., $a_1 = a_2$). The total number of strips in a resolving volume is large enough so that the noise is gaussian if the strips are physically independent; however, they might cohere in clumps so that there are only a small number of effectively independent scatterers. Unfortunately, present measurements of distributions [21,22] contain enough experimental uncertainty to mask any nearly gaussian deviations.

Echoes from precipitation

Rain, hail, and snow also may give radar echoes, particularly at higher microwave frequencies [23]. This particular problem may be formulated in terms of reflections of a plane wave from an aggregate of spheres. Trinks [24] has shown that for Rayleigh scattering interaction is negligible if neighboring spheres are two or three diameters apart. Meteorological observations of rainfall [25,26,27,28] have shown this requirement to be well satisfied. Humphreys [29] gives the weight of rain water in the air per cubic meter as a function of the rate of rainfall, while the NEL group [27] and Laws and Parsons [26] give distributions of drop sizes as a function of rate of rainfall. The drop distributions are apparently not single-valued functions of rain intensity, but they are consistent enough to make an approximate calculation of the density parameter, γ, possible.

As the rate of rainfall varies from 0.25-100 mm/hr. (from drizzle to cloudburst), the weight of suspended water goes from 0.1-5 g/m^3; and the average drop radius, from 0.05-0.15 cm. The drop distribution gives the relative amount of water at the ground contributed by drops of a given radius. This is the important distribution, since what is needed here is the amount of water in drops of a given radius, not the number of such drops. The distribution should be corrected by dividing by the terminal velocity distribution of the drops; this will give the drop distribution in the air. Since the larger drops travel faster, this correction reduces the average drop size, and so increases the density parameter. As the lower figure is found to be large enough to provide gaussian noise, additional refinements were felt to be unnecessary.

The average number of drops per cubic meter is then 150-400, varying with the rate of rainfall. This corresponds to an average distance between drops of 12-8 cm. Since the distance required for negligible interaction between scattering for different drops is 0.3-0.9 cm, it seems clear that any lack of independence in the scattering is small enough to be ignored. This many drops. scattering independently, give a normal noise return from each cubic meter.

The same conclusion may be reached with more careful reasoning, by dividing a cubic meter into cubic cells such that the scattering from pairs of drops is interdependent only if the drops are in neighboring cells. The cells prove to be numerous enough (several million to the cubic meter) that the possibility of having more than one drop per cell is negligible. Since the drops are distributed uniformly and independently, the conditions for a Poisson distribution are satisfied. The number of interacting pairs also possesses a Poisson distribution. A calculation of probabilities shows that for all rain intensities, 99.9 per cent of the time, less than 1 per cent of the return will be from interacting drops. These "exact" figures should not be taken too literally, but they do illustrate the overwhelming likelihood of independence.

One of the salient characteristics of rainfall is its inhomogeneity, both temporally and spatially. With rain gauges less than 5 meters apart, Rado [28] found variations of from 5 to 20 per cent in the measured rainfall, while the NEL group [27], with gauges 200 meters apart, found much larger differences.

Thus, in one resolving volume, the rain is almost certain to be non-uniform. If the non-uniformity represents merely a statistical fluctuation, then unquestionably the noise is gaussian. If this is not so, on the other hand, the volume may have to be split into subvolumes, each of which has different statistical parameters. In this case, the subvolumes will be larger than a cubic meter, so that the total return will be a superposition of gaussian noise from each subvolume, and therefore gaussian itself. The conclusion from the above is that clutter from meteorological precipitation is effectively always gaussian.

Echoes from the sea surface

Another source of clutter is sea return—echoes from the sea surface [30,31]. Exactly what reflects the incident pulse is an unsettled question; quite possibly the mechanism may differ for different grazing angles of the incident beam. There are three possibilities; (i) specular reflection from the waves themselves, (ii) reflections from ripples on the surface of size comparable to a wavelength, or (iii) reflections from spray droplets.

The radar cross section* of the sea for high grazing angles shows large values that apparently are due to specular reflection. The data for low grazing angles do not show this effect, so that it is not sufficient to explain all the results [31,32].

The dependence of cross section on polarization favors the droplet theory. For fairly calm seas, the cross section for horizontal polarization is smaller than that for vertical; the difference becomes smaller for rougher seas and at moderate roughness becomes negligible. This can be explained by destructive interference between the incident and reflected waves above the surface at the height of the droplets. A rough sea destroys the interference pattern, making the cross sections for the two different polarizations equal. The shifting of interference patterns with grazing angle suffices to explain the observed dependence of cross section on grazing angle [33].

On the other hand, measurements of the dependence of cross section on wavelength [32], indicate a λ^{-4} behavior, which favors ripples as against both droplets and specular reflection. Also, the drops needed to produce the observed magnitude of sea echo are much larger than those found in practice. The approach to a limit of the cross section at low wave heights (2-4 ft) also favors ripples, since with high waves, more and bigger drops and steeper wave fronts are present. The last two factors would favor a

- - - - - - -

*The radar cross section of an obstacle is defined as the area intercepting that amount of power which, when scattered isotropically, produces an echo equal to that observed from the target. For sea return, the cross section is expressed as a dimensionless ratio by referring it to unit area of the sea surface; it may be greater than one if the actual scatterers are not isotropic.

continued increase of cross section with wave height, if drops or specular reflection were the primary mechanism.

The nature of the scatterers is not settled; the observed distributions are usually gaussian to within the limits of error of the measurements. This cannot be accepted as conclusive, however, because of the major effect of deviations from the normal law appear in regions of large amplitude, which is the part of the distribution most difficult to obtain accurately. A long period of observation is necessary to accumulate enough high-amplitude returns to decide whether the clutter is gaussian or nearly gaussian. Because of the finite lifetime of the scatterers, whether drops, ripples or waves, it is entirely possible that the clutter statistics be non-stationary over the times necessary to measure the tail of the probability distribution. In fact, the only sea return distribution in Kerr [34] that includes the larger amplitude region is distinctly non-normal, from whatever cause.

The measured relative cross section is -30 to -70 db, i.e., as though 10^{-3} to 10^{-7} of the illuminated area were isotropically reflecting. This is so low a value as to argue against specular reflection. In a typical resolving area, there are 10^4 or 10^5 sq. ft., and, assuming a ripple reflector to cover several square feet, we see that the noise may well be nearly gaussian; no more definite conclusion can validly be drawn.

3.3 Sources of noise in sonar

Sonar, considered as an echo-ranging device, is very much like radar in its basic operation. The wavelength and resolving volume are of the same order of magnitude as in radar, because of compensating changes in the other parameters. Typical values for a sonar [35] are: transmitter frequency 24 Kc/s, pulse length 0.2 sec, bandwidth 6-10°, and the velocity of sound in the sea, 1600 M/s. Then the resolving area is about 300 yards in range, varying laterally with range, and the wavelength is about 6 cm. Serious additional problems arise, however, because of the dispersive properties of sea water.

Reverberation

Sonar clutter comes from reflections from irregular inhomogeneities

of the ocean, and from the irregular boundaries at the surface and bottom; it is usually called reverberation rather than clutter [36,37,38]. The importance of the three types, "volume," "surface," and "bottom" reverberation varies with circumstances as shown in Table 3.1.

Volume reverberation is caused by sound scattered by air bubbles suspended solid matter (e.g., plankton, fish), and small thermal inhomogeneities. The measured relative cross section, i.e., scattering area per unit volume varies from 10^{-8} to 10^{-5} yd^{-1} at a medium range, 800 yds. This makes the total scattering area in one resolving volume (c. $10^{6} yd^{3}$) .01-10 $yd.^{2}$ All of the above-mentioned scatterers, except for fish, are much smaller than a wavelength, so that the individual cross sections should be very small, except for those few scatterers of a size resonant for the particular transmitter frequency. Then the received noise is "dense" enough to be gaussian.

Table 3.1

Predominant Type of Reverberation

	volume	surface	bottom
Deep Water, Smooth sea			✓
Deep Water, Smooth sea	✓		
Deep Water, Rough sea, short range		✓	
Deep Water, Rough sea, long range (> 1 mile)	✓		

At ranges less than 500 yards, reverberation from the surface may be 20 to 30 db higher than that from the volume. Surface reverberation drops off at long ranges faster than volume reverberation; in addition, it depends strongly on the sea state.

As a function of wind speed, the return starts to increase at 8 mph, when whitecaps start to form, and continues to rise until it saturates at 20 mph with the reverberation intensity 35 db higher than the initial level. This wind-speed dependence favors bubbles or ripples as the cause of scattering; however, again definite conclusions cannot be reached. An analysis of the scattering from a dense layer of bubbles shows that their cross sections are not large enough to account for the experimental results by themselves. Scattering from ripple patches can provide the necessary return alone; however, the observed reverberation is probably a combination of the two [39]. Bubbles provide a gaussian return; the return from the ripples cannot be calculated without some knowledge of the ratio of the geometrical cross section to the scattering one. An estimate of γ is attempted here to point out the lacunae in our knowledge that preclude definite results.

The relative cross section for surface reverberation varies from 10^{-3} to 10^{-6}. At 300 yd, the resolving area is 9000 yd^2, which corresponds to 9 to 9 x 10^{-3} yd^2 of perfect isotropic reflectors. The simplest assumption for the actual reflectors is that they are "perfectly diffuse," so that Lambert's law applies. At 300 yd, the angle of incidence with the surface is about 6 degrees, with both incident and reflected flux corrected to normal incidence, 900-0.9 yd^2 is the area of the scatterers. Since the reverberation intensity is found to be frequency-independent, it follows that the scatterers must be several times as large as a wavelength, say 1 yd^2 for 24 Kc/s sound. There are then 900-0.9 scatterers per resolving area, a density range including both gaussian and nearly gaussian noise.

The above figures must be considered as simply illustrative. A proper estimate requires knowledge, rather than assumptions, of the backscattering from a ripple and the average size and structure of ripples. In addition, some knowledge of bubble-density is needed in order to estimate how much of the surface scattering is caused by bubbles.

Bottom reverberation is important only in shallow water; however, there it is likely to be the dominant factor. This scattering arises from irregular features of the bottom, comparable to surface reverberation from ripples; again, not enough is known about the back scattering from the types of obstacles likely to be encountered to make a density estimate possible.

Noise from marine life

A type of noise that has no counterpart in radar is that produced by marine life [40,41]. The important distinction is that not echoes, but externally generated noise is present. Most of these noises are markedly diurnal and seasonal; one important type, generated by the snapping shrimp, is both widespread geographically and continually produced. Results for this noise are available in sufficient detail to permit an estimate of the expected density [42,43].

The shrimp that produce this noise are of several species, all of which are small (about two inches long) and possess a large snapping claw, which is directly responsible for the noise. These shrimp are distributed in tropical and subtropical waters at depths less than 60 meters, with a rock or coral bottom. Investigation off San Diego has definitely located the shrimp as the source of crackling noise found along the California coast. Among other areas in which both snapping shrimp and loud underwater crackling noise are found are Beaufort, N. C., Cape Hatteras, the Bahamas, Puget Sound, and several locations in the Central and Southwest Pacific.

One of the important features of this noise is that its spectrum is very nearly flat from 1 to 15 kc, while most underwater noise varies according to a (1/f) law. Shrimp noise is thus particularly prominent at the higher frequencies. Measurements on an individual snap show an average excess pressure of 60 db above 2×10^{-4} dyne/cm^2 at a range of 1 meter. Corresponding figures from four shrimp beds found off San Diego are 43 db and 16 m, 34 db and 30 m, 35 db and 44 m, and 45 db and 20 m. The density can be found as the total power divided by the power per snap, both measured at the same range. For the four measurements above, γ is 5,2,6, and 12 respectively, values characteristic of the lower range of nearly gaussian density. The noise has been described as "like static crashes" or "coal going down a metal chute," which qualitatively tends to

indicate a fairly low noise density.

3.3 Atmospheric noise: lightning

Lightning also causes noise; however, each stroke produces only one pulse so that the noise is not dense enough to be nearly gaussian. Study of lightning shows that initially there is a moderately slow downward stroke followed by a rapid upward discharge, of durations roughly 10 and .05 Mc/s respectively. After this, there is a further slow change to equilibrium. Superimposed on all these field changes are small, more rapid variations caused by fluctuations in the resistance of the ionized path; furthermore, multiple reflections from the ionosphere may occur (44,45). One result of the presence of several different components is that the received wave form depends strongly on the distance of the receiver from the lightning stroke. Near to the stroke, the induction field will predominate and a slowly varying aperiodic wave form will be observed; far away, the radiation field produces a quasi-periodic wave form. The various components all belong to the same stroke and different strokes are spaced widely enough so that the noise is of low density.

A different type of atmospheric noise comes from snow squalls [46]. This is also an electric discharge, but the strokes are much shorter and weaker than in thunderstorms. While the strokes are more frequent, the essentially distinct character of the individual received waveforms shows that this noise is also of the low-density type.

Precipitation static

Airplanes flying through precipitation in the atmosphere become frictionally charged. If the storm is at all severe, a corona discharge occurs on the pointed parts of the aircraft, e.g., the wing tips or radio antenna. The noise thus produced limits radio reception considerably and may cause a total loss of intelligible functioning. Because of the close connection between the noise and the weather in which it is produced, it is known as precipitation noise [47,48].

The most intense noise is produced from corona on the antenna. Since aircraft surfaces in practical use charge negatively, the problem is that of

negative corona from a wire [49]. Initially there is a glow along the wire, which with increasing potential, collects into an active spot giving pulses from a recurring breakdown. The discharge is initiated by an electron avalanche in the high field-strength region near the wire. The positive ions left behind, moving slowly, eventually fall into the negative wire and quench the discharge by momentarily lowering the potential difference across the gap. After a recovery time, the field strength becomes high enough to cause a discharge again. In air the pulse itself lasts about 0.1-0.5 μsec while the recovery time is of the order of 1 Mc/s. These recurring pulses are called Trichel pulses after their discoverer [50].

As the field strength at the wire increases, the frequency of the Trichel pulses does also, but before the successive pulses merge into a continuous discharge the first spot saturates and another active spot forms. Because of the regular recurrence of the Trichel pulses, the individual pulses do not fit the Poisson noise model; however, the sequences from different spots will do so, and, as seen above, more spots will form with increasing field strength or discharge current.

From the results on airplanes [51], a check with the corona investigations is possible by calculating the threshold field. At the corona threshold, the field on the belly of the test airplane was 250-300 volt/cm which corresponds to voltages of 25-30,000 volts. For an antenna 0.04 inch in diameter, this means a field at the surface of 250-300,000 volt/cm, which is the range of values found experimentally [49,52]. The density factor may be determined from

$$\gamma = (\text{total current})/(\text{current/spot}).$$

The total current figures here are taken from the results of Gunn [51], but data for the current per spot are not available from the results of Miller and Loeb [49], since they measured the total corona current rather than the current per spot. This makes a quantitative determination of γ impossible. In air, currents start at 0.1-1 μa at the threshold (this is from one spot) and increase to values of 50-100 μa, by which time multiple spots have formed. The total discharge current from the airplane will be from 1 μa to 2000 μa, depending on the severity of the storm. While a calculation of γ as a function

of field strength is not possible, it seems clear that the noise density, varying continuously from low to high, will be in the nearly gaussian range for storms of intermediate intensity. This is qualitatively borne out by aural observations of the character of the noise [53].

3.4 Celestial noise

A further source of noise is the electromagnetic radiation from celestial objects, particularly the sun [54]. Galactic and extra-galactic radiation is present over most of the sky. Since the sources are so distant, the mechanism of generation is not completely certain; however, it appears that the radiation can all come from point sources. The continuous radiation of known point sources indicates that the mechanism is probably a thermal one, since an equilibrium process appears necessary. A thermal source, which here means a star, contains so many elementary noise generators that the noise is certainly gaussian.

Solar radiation

The relative nearness of the sun provides the possibility of determining much more about its radiation. Several different types of radiation in the meter-to-centimeter bands have been discerned, one kind always present, and several only occasionally present. The ever-present radiation [55,56] is spoken of as produced by the quiet sun, since it provides a minimum solar noise level. As it is always present, it represents an equilibrium process and thus is thermal and gaussian.

The occasional radiation, produced by the "active sun," is of three types; isolated bursts, outbursts, and enhanced radiation. Isolated bursts occurring for a few seconds are sometimes present in solar radiation with peak magnitudes 30-50 db above the level of the quiet sun. The bursts are unpolarized and have a sharp but smooth rise and a slow decay. Their infrequent occurrence marks them as low-density noise [57].

"Outbursts" are the most spectacular of the various forms of solar radiation. Intensity recordings have gone off-scale after 70 db increases in power. Outbursts last for several minutes at a time; they are apparently connected with visible solar flares--at least the larger of them are—and are

often the cause of complete interruption of short-wave reception. Outbursts do not seem to be separable into superposed pulses and so can not be considered as Poisson noise [58,59].

Enhanced solar radiation

The enhanced radiation from the active sun can be of considerable importance. While not the strongest form of solar radiation, it is 30 db higher (in power) than the quiet radiation and lasts longer than the other active forms [60,61]. The distinguishing characteristics of enhanced radiation are its duration (several days rather than minutes or seconds,) its circular polarization, and its correlation with sunspots. Enhanced radiation is particularly important for our purposes, since it is the only type which experimental results show to be nearly normal. At least two widely different origins have been proposed to account for this noise. One model assumes that the radiation is due to the thermal motion of the electrons in the fields near a sunspot [56,62]. This is incoherent and depends on the mean thermal energy; extremely high temperatures (about 10^{10} degrees Kelvin) are required to account for the observed intensities. The alternative proposal is that coherent oscillations of the plasma may exist [63,69]. This model avoids the temperature difficulty, but must explain how the coherence can be maintained in the presence of the large random thermal velocities [63-67,69] in the solar atmospheres and how the energy can radiate from the generating regions where the group velocity is zero [63,66-68]. Opinions are too unsettled, and detailed knowledge of the solar atmosphere near sunspots too vague to make a detailed discussion of present theories worth while here; nevertheless, the experimental results show the features needed for Poisson noise [5 ,70].

Records of moderately dense noise where individual bursts can not be resolved give correlation times comparable to the duration of individual bursts discernible on quiet days [70]. Wild [60] has made a careful study of enhanced noise over the frequency band 70-130 Mc/s for a period of several months. From his values of average power received and the observed distributions of bursts large enough to be individually measurable, one can estimate the density of the noise. Wild gives an experimental intensity distribution for the bursts. The middle of the curve follows an exponential law fairly closely; at the low end the pulses were occasionally

lost in the background, and so the observed number of burstsis too small; and at the high end, the infrequent appearance of large amplitude bursts makes the sampling error large. The average peak power in a burst is found to be 2.5×10^{-20} watts/m^2-c/s). The average spectral width of a burst was 4.5 Mc/s between quarter maximum points. Since the spectral shape was found to be essentially gaussian, the width of the equivalent rectangular-filter with the same peak value is 3.2 Mc/s. Then the average total power in a burst is 8×10^{-20} watts/m^2.

In order to find γ, only the total power received needs further to be calculated. For purposes of observation, Wild separated the received wave into a continuum and bursts of amplitude 10^{-20} watts / (m^2-c/s). With the observed intensity distribution, the average value of the continuum is 0.33 of the total power; including the 60 Mc/s bandwidth, and using the observed continuum $.75 \times 10^{-20}$ watts/(m^2-c/s), the total power is found to be 135×10^{-20} watts/m^2, whence γ equals 17, in the nearly gaussian range.

3.5 Noise arising from the quantization of charge: shot noise

The various kinds of noise caused by the discreteness of the elementary particles fit the Poisson model. Of these, shot noise is the simplest to analyze. In a vacuum tube, the current contains fluctuations because of the discrete nature of the charge [71]. As long as each electron is emitted from the cathode independently of the others, viz., in the temperature-limited and retarding field regions, the Poisson noise requirement is satisfied, and a density estimate is straightforward. The transit time in an ordinary tube is about 10^{-9} sec, so that

$$\gamma = \langle I \rangle \tau / e = 5 \times 10^{10} \langle I \rangle \qquad (3.2)$$

The noise is broad-band, so that the leading correction term will be of the order of $\gamma^{-1/2}$; for a current of 1 ma, this is about 10^{-4}; and the correction does not rise to 10^{-2} until the current drops to 0.2 μa, or less.

In the space-charge region of the characteristic, the electrons are not emitted independently and a different approach to the density problem is demanded. The problem now is that each emitted electron modifies the space charge so that succeeding electrons find a larger potential barrier [72]

Obviously, the change in the space charge is produced in a fairly small volume around the individual electron. In an ordinary receiving tube the potential minimum is about 3 volts; the potential due to the moving electron is $e/4\pi r_o$, so that 4×10^{-7} cm away from the trajectory of the emitted electron, the modification of the potential minimum is less than 1 per cent of its prior value. The quasi-stationary potential suffices because the electrons are moving in small enough fields so that the retarded potentials are not necessary.

The cathode surface may be divided into square areas of such size that only 1 per cent of the electrons emitted in the area will produce appreciable effects outside it, i.e., a fringe of width r_o around the edges of the square contains 1 per cent of the total area of the square. Then the various areas are effectively independent and a noise density may be estimated. Note that, since the number of independent areas is fixed, the random-walk model is applicable, not the Poisson noise model. The linear dimension of one of these areas is $400\, r_o$, or 1.6×10^{-4} cm. With a typical cathode area of 0.5 cm^2, γ is 2×10^7, safely in the gaussian noise region. This estimate is at the anode of the tube. If the network intervening between this anode and the output has a rise time longer than the transit time of the electron in the tube, the noise pulses will be stretched and γ increased.

A consistency check with the previous result is instructive. Certainly the effective density when all electrons are independent will be greater than that when they are not. In fact, $\gamma_{Poisson}/\gamma_{space\ charge}$ is $2 \times 10^3 \langle I \rangle$. The space-charge region may then be expected to start with currents of about 0.5 ma.

A second estimate of the current needed for a space-charge effect may be made as follows: if, on the average, one electron is present in each elementary area, there is sufficient overlapping of electron emissions so that the assumption of independence is untenable. Only about 0.1 of the emitted electrons have enough energy to pass the potential minimum, and consequently the charge carried from one elementary area is 6×10^{-13} coulomb/cm^2. For the transit time of 10^{-9} sec, a 1 cm plate to cathode spacing, and the cathode area 0.5 cm^2, as before, this is a tube current of 0.3 ma, in order of magnitude agreement with the previous estimate.

Photo-multiplier noise

Photo-multiplier tubes are also sources of noise [73-75]. The im-

portant distinction between these and other tube sources is that the several stages of electronic amplification produce shot noise with elementary pulses containing many electrons instead of single ones, as in the ordinary shot effect. This means that the photo-multiplier noise current fluctuates more intensely than ordinary tube current of the same mean value [73].

Besides the shot effect, noise can be caused by spontaneous emission from the photo cathode or any of the dynodes. This current is initially very small (perhaps 10^{-14}a.), but electron multiplication again magnifies the effect to a level requiring consideration. Such emission is called a "dark" current since it flows regardless of the illumination on the photo cathode.

Photo-multiplier tubes are used mainly for two different purposes, to measure light intensities, or to count scintillations in radioactivity measurements.

In scintillation counters, radiation causes a fluorescent screen to produce glowing spots that activate the photo-multiplier [76,77].

The signal pulses then have a duration of the order of the time constant of the fluorescent screen, a few microseconds. The noise pulses, on the other hand, have durations of the order of the transit time through the tube, about 10^{-9} sec [74]. The input time constant of the counter pulse amplifier is made equal to the phosphor decay constant, which is short enough to resolve signal pulses and long enough to discriminate against the noise pulses. The noise pulses at the anode may then be considered δ-functions since they are of such short duration compared to the input time constant. In a 931A tube, about 5×10^4 "dark-current" pulses are emitted per second [75]; this gives a γ of about 0.1. Dark current noise is thus of the low-density type in scintillation counters.

For light intensity measurements, the input time constant is large, (of the order of seconds in fact) in order to smooth out fluctuations. In this case, the dark current is certainly gaussian, since γ is about 10^5. However, the signal current is so much larger that the noise may be taken as entirely shot effect, with the dark current completely neglected. The transit time is so short compared to the input time constant that the spread

may be neglected. The current pulses are then

$$i(t) = ae \exp\left\{ - t/\tau \right\} , \tag{3.3}$$

where a is the overall multiplier gain.

Now, we observe from Eq. (2.11) and (3.3) that

$$\lambda_k = \frac{\gamma}{k\tau} \langle a^k \rangle e^k \quad . \tag{3.4}$$

In particular

$$\lambda_2 = \frac{\gamma}{2\tau} \langle a^2 \rangle e^2 = \frac{e\langle I \rangle}{2\tau} \frac{\langle a^2 \rangle}{\langle a \rangle} . \tag{3.5}$$

Notice that the fluctuation is increased by at least a factor $\langle a \rangle$ over the ordinary shot effect, and that fluctuations in gain produce even larger output current fluctuations.

Since λ_1 equals the mean current, we have

$$\gamma = \langle I \rangle \tau / \langle a \rangle e, \tag{3.6}$$

which shows that γ is smaller by the gain of the multiplier than for shot noise of the same mean value and time constant. The gain of the tube is 10^5 or 10^6, so that this effect is quite important, particularly for the current at the photo-multiplier anode, since then τ is the transit time of the tube. In the input circuit of the voltage amplifier following the photo-multiplier tube, the time constant is about 1 sec, so that γ is large enough for correction terms to be safely neglected.

Thermal noise in resistors

Thermal noise from resistors is one of the commonest sources of noise. From a macroscopic point of view the noise is sufficiently well characterized as gaussian with the well-known power spectrum $W(f) = 4k\,TR$ [78,79]. The noise is caused by the random motion of the conduction electrons of the resistor, achieving its randomness by collisions with atoms of the lattice structure, which is not completely regular. For an order-of-magnitude estimate of the noise density, the Drude theory will be sufficient [80,81]. In this simple theory, the conduction electrons are independent, which is necessary for the Poisson noise model to be directly applicable. Furthermore, the mean free path is independent of the electron

velocity, while the scattering from a given collision is isotropic.

Here γ equals the mean time between collision times the average number of current pulses passing through a cross section per unit time. This last is one third the average number of conduction electrons per cubic centimeter multiplied by the product of the mean velocity and cross-sectional area. Using the Maxwell-Boltzmann velocity distribution and the independence of the mean free path, γ is found equal to $4/3\pi$ times the product of mean free path, cross section, and number of conduction electrons per cubic centimeter.

One has

$$\gamma = \frac{4}{3\pi} \ell NA, \tag{3.7}$$

where ℓ is the mean free path, N the number of conduction electrons per cubic centimeter, and A the cross-sectional area. The mean free path may be expressed in terms of the interatomic distance, d; also, the number of conduction electrons is proportional to the number of atoms, which should vary as d^{-3}. We have

$$\gamma = \frac{4k_\ell k_N}{3\pi d^2} A \ ; \tag{3.8}$$

d is of the order of 10^{-8} cm., k_ℓ, about 100, and k_N of the order unity, so that

$$\gamma \doteq 4 \times 10^{17} \ A(cm^2) \tag{3.9}$$

The leading correction term to the normal distribution is of order $\gamma^{-1/2}$, which is certainly negligible here.

Non-equilibrium sources of noise

Besides thermal noise, conduction in solids causes current noise, semiconductor noise, and flicker noise. These last are nonequilibrium effects; their spectrum is directly proportional to the mean-square current and inversely proportional to frequency. These phenomena are complex, each depending apparently on several different mechanisms whose relative importance is critically dependent on factors not ordinarily under control.

Flicker Noise

Flicker noise is caused by variations in the emission from thermionic

cathodes over times large compared to a single transit time [82,83,84]. For some reason, certain regions of the cathode surface emit particularly strongly for short times. This corresponds to fluctuations in the work function, probably caused by diffusing ions. A diffusion process leads to a $1/(1+\omega^2\tau^2)$ spectrum, where τ is the lifetime of a diffusing ion; however, if an appropriate distribution of lifetimes is assumed, a $1/\omega$ spectrum can be obtained over any finite interval [84]. At present knowledge of the mechanism is insufficient to warrant an estimate of noise density.

Excess noise in solids

Certain types of resistors develop noise in excess of the Nyquist formula when current is passing through them [83-85]. Besides the dependence of noise power on the construction of the resistor (e.g., whether it is carbon composition or "metallized"), different resistors of the same kind of construction and of the same value of resistance, can give noise powers differing by a factor 20. Here again, exactly to what the fluctuations should be ascribed is not known in enough detail to allow a calculation of γ.

In semiconductors, two types of current carriers are present, each of which produces noise. Excess noise, with the characteristic 1/f spectrum, is apparently caused by fluctuations in the number of minority carriers [86]. Minority carriers affect the conductivity strongly, since they add to the total number of current carriers themselves and by lessening the space charge, also increase the number of majority carriers [87]. In the material not near an electrode, the current density will be nearly uniform; using the same reasoning as for thermal noise, we see that $\gamma \doteq \ell NA$. The cross-sectional area is about the same as for thermal noise; and the mean free path is comparable [88]; however, the concentration of minority carriers is much less, 10^{-7} or 10^{-8} of the total number of atoms [89]. The excess noise is thus much less "dense" than thermal noise; nevertheless, γ will be sufficiently large so that the noise is effectively gaussian. Evidence has been presented that another component, due to majority carriers, is present, becoming relatively more important at the higher frequencies (above 10 kc/s) [90,91].

Since this noise is denser than minority carrier noise, it will be gaussian also.

Barkhausen noise

The noise in ferromagnetic materials caused by changes in the domain structure [92] is called Barkhausen noise. As a magnetic field is applied, two different processes take place. At low values of the impressed field, the domain boundaries move, with the result that favorably oriented domains become larger at the expense of slightly misoriented domains. With greater impressed fields, the direction of magnetization of domains originally oriented nearly perpendicular to the field is rotated toward alignment with the field, without any wall motion. Domain rotation produces noise because of the discrete character of the changes of magnetization [93,94]. Inhomogeneities making the wall motion irregular may also produce noise [95]. As the domain wall moves past an imperfection, subsidiary walls reaching from the irregularity to the main front are formed; with continued expansion of the main wall, the subsidiary walls stretch until they break, giving a smooth main wall and leaving a small stationary domain around the imperfection. Barkhausen noise has been observed when no domain rotation was occurring, favoring the above mechanism. Quantitative statements about the relative importance of these two mechanisms or estimates of the noise density, do not yet appear possible.

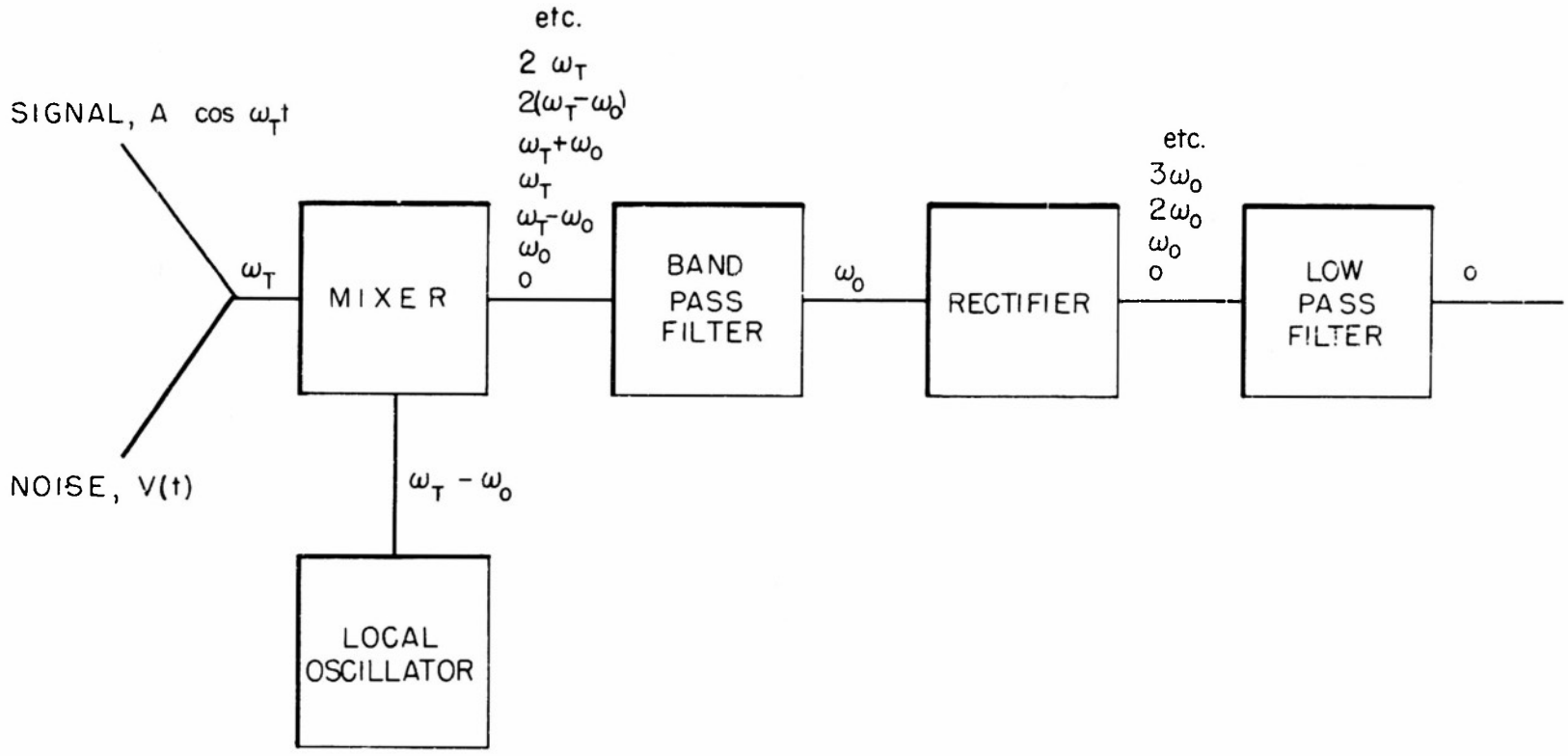

FIG. 3 BLOCK DIAGRAM OF AN A-M RECEIVER

IV

Rectification of Nearly Gaussian Noise

The next task is to use the distributions previously found in section II, with specific forms of the correlation function and semi-invariants suggested by section III, to determine the most important statistical parameters of the output of an a-m receiver with a c-w signal and nearly gaussian noise impressed on the input.

4.1 Model of an a-m receiver

In an amplitude modulation system, the signal is transmitted from source to receiver at a relatively high frequency, which is demodulated by the receiver to recover the envelope of the high-frequency variation, which represents the original signal. The noise is generated in the channel and in the first sections of the receiver. The receiver contains a band-pass filter which eliminates all spectral components except those in a narrow-band around the central frequency, and a demodulator, composed of a half-wave ν-th law detector followed by a low-pass filter. The relation between output and input of a nonlinear device is called the dynamic transfer characteristic; for the half-wave ν th-law device, we have

$$I = g(V) = \begin{cases} \beta V^{\nu} & V > 0 \\ 0 & V < 0 \end{cases}, \qquad (4.1)$$

where I is the output, V the input, and β an appropriate proportionality constant. The input, V, is a narrow-band signal and narrow-band noise, but the nonlinear device changes the spectral composition, so that the output is composed of spectral zones lying at multiples of the central frequency of the input; the (ideal) low-pass filter eliminates all these zones except the low-frequency one, corresponding to the zeroth harmonic. A block diagram is shown in Fig. 3, together with typical waveforms and spectra at various points in the circuit.

The system treated here is of course, an idealization of actual ones. Two of the more critical approximations are those of representing actual

modulations, which are functions of time, by a constant value and representing the dynamic detector characteristic by a simple power law, without including saturation effects at high voltages and smoothing of the discontinuity in the slope at the origin. Nevertheless, the idealized system in most applications is a sufficiently close representation to warrant analysis.

Since there is noise present, a complete analysis should give the probability distributions of the output. This is a difficult problem which has been solved only for the quadratic detector ($\nu = 2$), [96,97] an important and particularly simple special case. We shall calculate the correlation function of the output, a much simpler problem and one whose solution yields considerable insight into the effects of noise in the system. Two different methods can be applied, corresponding to the different statistical descriptions of the input by the distributions of either the instantaneous value or of the envelope and phase. The former of these is better suited to the major problem, but the envelope and phase description give a better picture of the zonal structure, so we shall use it initially.

4.2 Output power

The output can be expanded in a Fourier series,

$$I = g[R\cos(\omega_o t - \theta)] = \sum_{n=0}^{\infty} \epsilon_n a_n(R)\cos n(\omega_o t - \theta), \qquad (4.2)$$

$$a_n(R) = \frac{1}{2\pi}\int_{-\pi}^{\pi} g[R\cos(\omega_o t - \theta)]\cos n(\omega_o t - \theta)\, d\omega_o t\,,$$

in which ϵ_n is the Neumann discontinuous factor, $\epsilon_o = 1$, $\epsilon_n = 2$ for $n \geq 1$. The envelope and phase are also functions of time, but they vary so little during one period of $\cos\omega_o t$ that they may be considered constant in calculating $a_n(R)$.

The output correlation function is then

$$R(t) = \langle I_1 I_2 \rangle_{av} = \sum_{n=0}^{\infty} \epsilon_n \langle a_n(R_1) a_n(R_2) \cos n(\omega_o t - \theta_2 + \theta_1) \rangle_{av}. \tag{4.3}$$

Note that only the phase difference occurs in this equation, so that the required probability distribution can always be found, as in Eq. (2.22), from the distribution of instantaneous values. The power in each spectral zone, P_n, can be found from the correlation function for $t = 0$, $P_n = \epsilon_n \langle a_n^2(R) \rangle_{av}$ since now $\theta_2 = \theta_1$. The d-c power equals the square of the mean value. $P_{d\text{-}c} = \langle a_o(R) \rangle^2_{av}$. For the half-wave detector, we find

$$a_n = \frac{\beta R^{\nu} \Gamma(\nu + 1)}{2^{\nu+1} \Gamma\left(\frac{\nu + n}{2} + 1\right) \Gamma\left(\frac{\nu - n}{2} + 1\right)} \tag{4.4}$$

Equation (4.4) shows that the detector output possesses the same dependence on the input envelope for all zones, so that the only difference between zones, is in a multiplying factor. Blackman [98] has previously pointed out this result, though stating the implication in less general terms. This is that the relative power per zone is a constant independent of the statistics, i.e., regardless of what the input is, the detector places the same percentage of the total output power in each spectral zone.

Such a result is worthy of note, since it is by no means intuitively obvious. Indeed, it seems possible that some input could be found that would contribute an extra share of power to the higher zones, and a different input whose power would be distributed mostly to the lower zones. For the ν th-law detector, no such input exists; however, this detector is apparently a very special case.*

- - - - - - -

*Clearly, a sufficient condition that the result should hold is that $g(R\cos\theta) = g_1(R) g_2(\cos\theta)$, and the ν-th law detector does, in fact, satisfy this. Necessary and sufficient conditions are not obvious; however, it seems likely that they are somewhat but not very much weaker than the above, the point being that if the envelope and cosine factors can not be separate before the integration is performed, n and R are likely to be inextricably mingled in the result. As an example, if a half-wave rectifier with saturation is represented by $g(v) = \beta[1 - \exp(-\alpha v)]$, then $a_n(R) = \beta[\delta_{no} - I_n(\alpha R)]$, and the relative power in the zones quite definitely depends on the input statistics.

The low-frequency zone is the most important in the treating of the receiver problem, so that all results are given in terms of it. These results can be altered to give the power in a different zone, if desired, by multiplication by an appropriate constant factor. The averages are evaluated in Appendix V; for the total low-frequency power, we have

$$P_o = \frac{\beta^2 \Gamma^3(\nu+1)}{4\Gamma^4(\frac{\nu}{2}+1)} \left(\frac{\psi}{2}\right)^\nu \left\{ {}_1F_1(-\nu;1;-p) + \frac{\lambda_{40}\,\nu(\nu-1)}{3!\,\psi^2}\, {}_1F_1(-\nu+2;1;-p) + O(\gamma^{-2}) \right\}; \tag{4.5}$$

and, for the d-c power,

$$P_{d\text{-}c} = \frac{\beta^2 \Gamma^2(\nu+1)}{4\Gamma^2(\frac{\nu}{2}+1)} \left(\frac{\psi}{2}\right)^\nu \left\{ {}_1F_1(-\frac{\nu}{2};1;-p) + \frac{\lambda_{40}\frac{\nu}{2}(\frac{\nu}{2}-1)}{3!\,\psi^2}\, {}_1F_1(-\frac{\nu}{2}+2;1;-p) + O(\gamma^{-2}) \right\}^2, \tag{4.6}$$

where $p = A_o^2/2\psi$ is the input signal-to-noise ratio. If ν in Eq. (4.5) or $\nu/2$ in Eq. (4.6) is a positive integer, the nearly gaussian series terminates and the above expressions become exact; furthermore, the confluent hypergeometric functions reduce to polynomials.

These equations are plotted in Figs. 4 and 5 for gaussian noise and for a nearly gaussian noise of comparatively low density. As these graphs show, the change in the output power caused by the nongaussian statistics is small for small values of ν, and small for large values of p. When ν is greater than one, the nongaussian output power, (Fig. 4), is greater than in the gaussian case; while for ν less than one, either may predominate, depending on the signal-to-noise ratio.

When ν and p are both less than one, the nongaussian power is always less than the corresponding gaussian one; however, if p is greater than one, the nongaussian power is first greater, then less, the crossover point increasing from ν equals zero to ν equals one as p increases from one to infinity. For large signal-to-noise ratios, the output power is composed mostly of S × S (signal × signal) and S × N (signal × noise) interaction, while with small signal-to-noise ratios, the power arises mostly from n × n (noise × noise) interaction. There is no <u>a priori</u> reason to believe that the

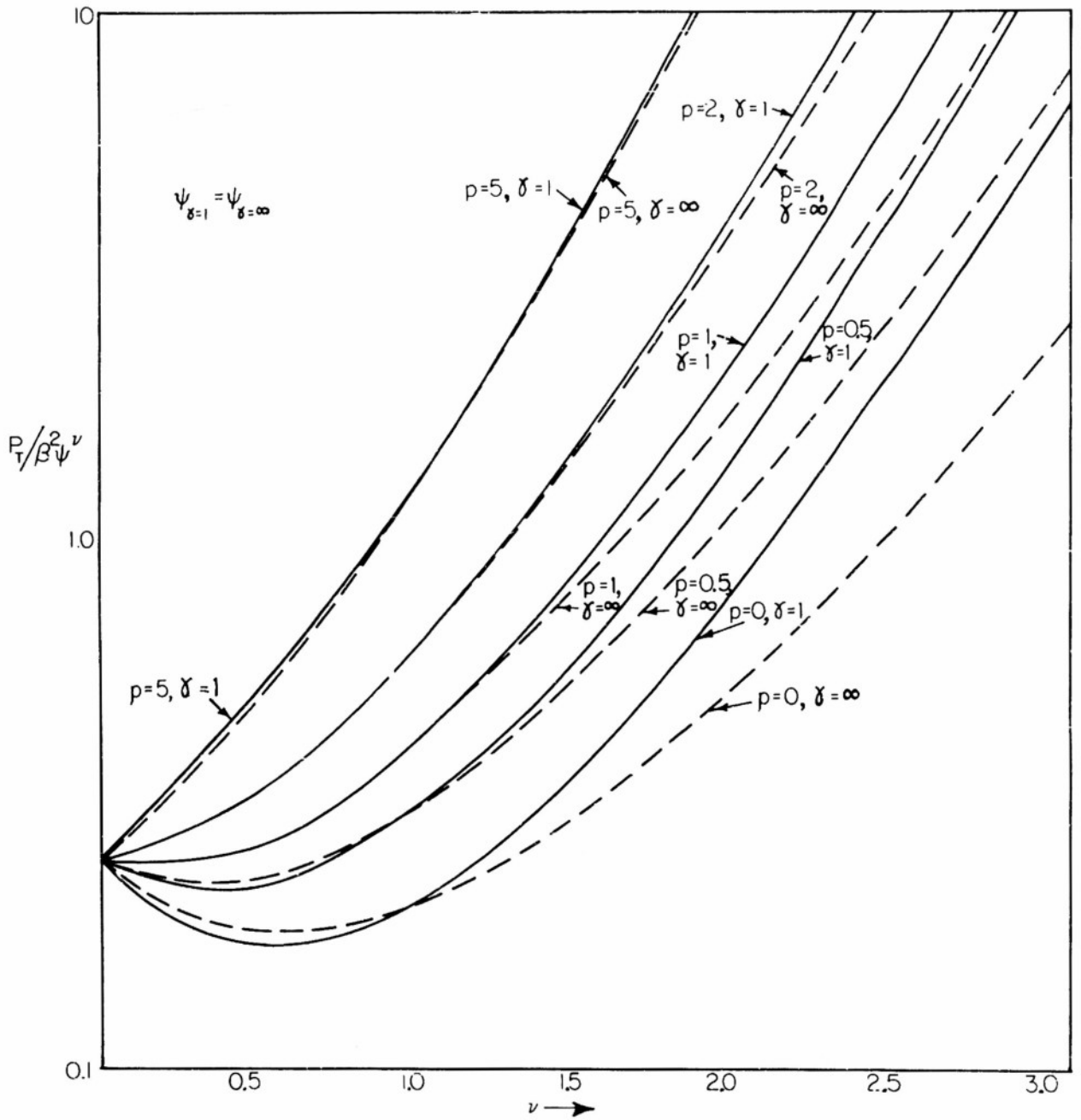

FIG. 4 TOTAL LOW-FREQUENCY OUTPUT POWER

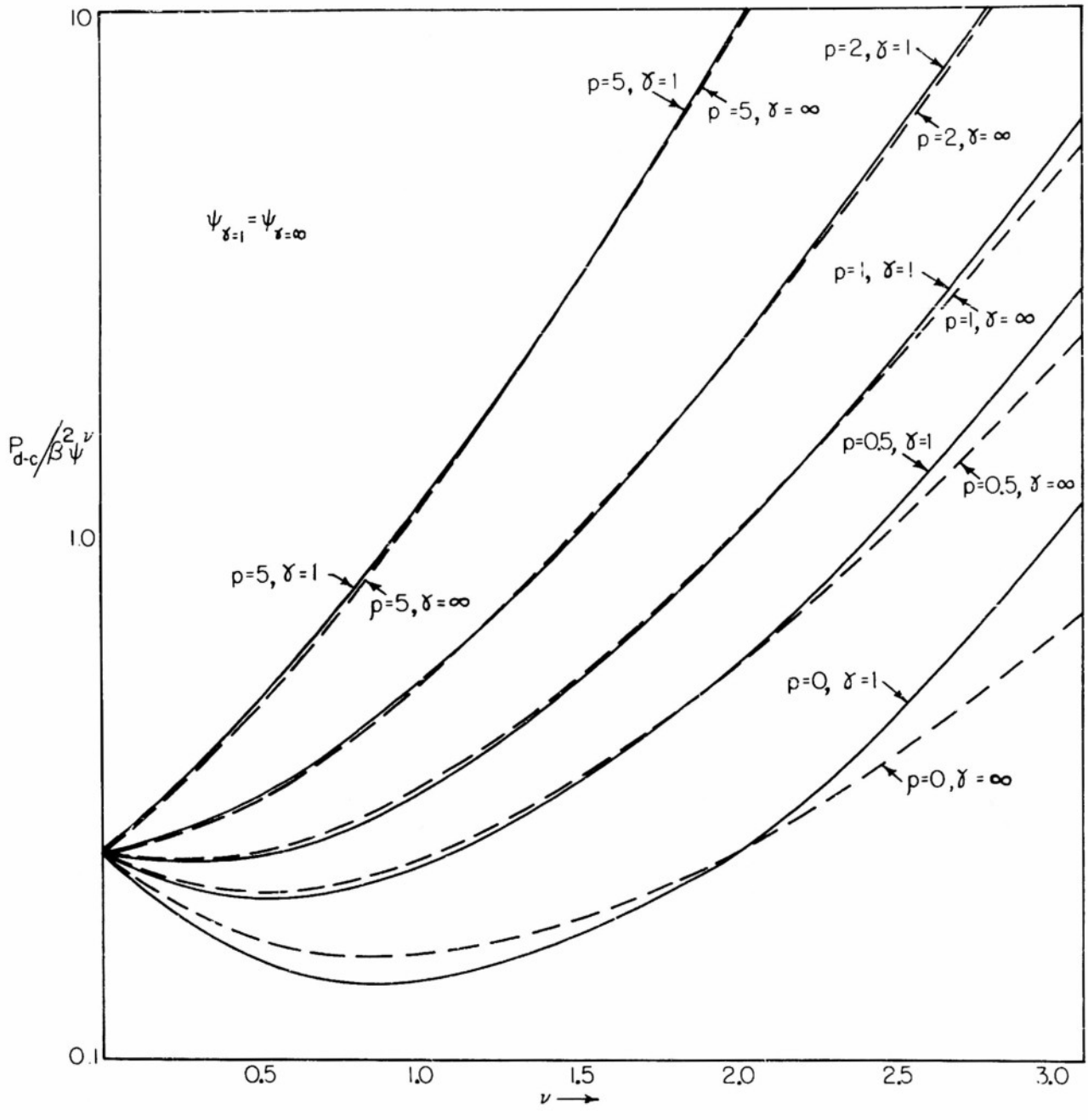

FIG. 5 D – C OUTPUT POWER

nongaussian result will bear the same relation to the gaussian in the one case as in the other, and in fact, Eq. (4.5) shows that they do not. Analytically, these facts depend on the behavior of the confluent hypergeometric functions, which are discussed in more detail in Appendix V. The discussion on the total power carries over immediately to the d-c power except that all the values of ν previously mentioned must now be multiplied by two.

The asymptotic series for the hypergeometric functions of Eqs. (4.5) and (4.6) show that the leading nongaussian term is of order p^{-2}, while the leading noise term is of order p^{-1}. Thus, in the strong signal case, as well as the usual suppression of noise relative to signal, there is an additional suppression of deviations from gaussian statistics (except for values of ν near 1). The figures and equations show that in order to detect the type of statistics present in an experimental problem by a power measurement, the detector used should have a high power law and the noise power should be measured without any signal present. The first of these requirements is intuitively reasonable, because, since the tails of a distribution are particularly sensitive to the exact type of statistics, a large value of ν, which accentuates the effect of the tails, is desirable.

From a practical point of view, however, large values of ν will be more sensitive to saturation effects. In an actual detector the maximum output will always be limited, either from saturation in the detector itself or in the i-f amplifier preceding it. The law of the detector, of course, has no bearing on the overloading of the i-f amplifier, but large values of ν will require the detector to produce large outputs without distortion when only moderate inputs are present. Four or five would probably be as high a value of ν as one would want to choose.

The second requirement above is not obvious, since a locally injected signal of known strength increase the output noise power because of the cross-modulation products of the signal and the noise present in the output of the detector. For low input noise levels, it may be important to be able to adjust the output noise power to a level large enough to be convenient. One might think that cross-modulation would also accentuate the difference between gaussian and nongaussian noise; however, the above figures and

equations show that quite the contrary is the case; in fact, the power difference is not only less relative to the total output power with increasing signal-to-noise ratio, but even decreases in numerical value. Thus, although adding a signal may be worthwhile in order to measure noise power, the method is entirely unsuitable for distinguishing different types of statistics.

4.3 The output correlation function

For evaluating the correlation function, the distribution of the instantaneous value is preferable. While the envelope and phase distributions can be used, the final result is then in a less tractable form. The correlation function can be expressed in terms of the characteristic function by using the complex Fourier transform of the dynamic characteristic [99,100],

$$f(iz) = \int_{-\infty}^{\infty} g(V)e^{-iVz}\,dV,$$

$$g(v) = \frac{1}{2\pi}\int_{C} f(iz)e^{iVz}\,dz, \tag{4.7}$$

where $g(V)$ is zero for V less than some V_o, and of no greater than exponential order at infinity, and C is a horizontal contour in the complex z-plane lying below the singularities of $f(iz)$. The output correlation further becomes

$$R_T(t) = \langle g(V_1)g(V_2)\rangle = \frac{1}{(2\pi)^2}\int_{C} dz_1 \int_{C} dz_2\, f(iz_1)f(iz_2)\,\langle \exp(iz_1V_1+iz_2V_2)\rangle_{av} \tag{4.8}$$

and the average of the exponential defines the second-order characteristic function (Eq. 2.2).

The input signal to the detector in this case is the sum of a sine wave and random noise which are independent of each other, so that the characteristic function in Eq. (4.8) is the product of the separate characteristic functions of the signal and the noise. Since both inputs are narrow-band, the two characteristic functions are expanded in Fourier series in order to exhibit the zonal structure of the correlation function; for the detector problem, we need only the correlation function of the low-frequency zone, R(t).

The detailed evaluation is carried out in Appendix VI; here we mention that two forms of the correlation function are possible, a convergent power series in p, the input signal-to-noise power ratio, useful when the signal is small, and an asymptotic series in 1/p useful when the signal is large relative to the noise. These series are given in Eq. (VI.13) and (VI.14) of the appendix, respectively. The general results are sufficiently complicated so that a study of various special cases is desirable.

The leading terms of the series in p can easily be found from Eq. (VI.15); however, the equation remains difficult to interpret unless the hypergeometric functions involved reduce to simpler functions. The two most important values of ν are one and two, corresponding to the linear and square-law detector, respectively. The square-law case is particularly simple, viz.,

$$R(t) = \frac{\beta^2\psi^2}{4}\left[1 + r_o^2 + \frac{2\Lambda_{22}(t)}{3\psi^2} + 2p(1 + r_o) + p^2\right]; \quad \nu = 2. \tag{4.9}$$

This result is exact for all p and γ, all other terms in the general result vanishing. For this particular value of ν, the output voltage is the same, except for a scale factor, as that from a full-wave squaring device; accordingly, the correlation function can be calculated directly as a moment,

$$R_T(t) = \frac{\beta^2}{4}\left\langle\left[V(t_o) + A_o\cos\omega_o t_o\right]^2\left[V(t_o + t) + A_o\cos\omega_o(t_o + t)\right]^2\right\rangle_{av}. \tag{4.10}$$

This is by far the simplest way to obtain the output correlation function; unfortunately, the method can only be applied when ν is an even integer.

For the linear detector, the hypergeometric functions reduce to complete

elliptic integrals, and the leading terms are

$$R(t) = \frac{\beta^2\psi}{\pi^2}\left\{E + r_o^2 B + \frac{\lambda_{40}}{12\psi^2}(K-2E) - \frac{\Lambda_{31}(t)+\Lambda_{13}(t)}{12\psi^2} 2r_o D + \frac{\Lambda_{22}(t)}{12\psi^2}(2D+K)\right.$$

$$+ p\left[E + r_o B + \frac{\lambda_{40}}{12\psi^2}\left\{4E - 2K - \frac{E}{1-r_o^2} + r_o\frac{2E-B}{1-r_o^2}\right\}\right.$$

$$\left.\left. + \frac{\Lambda_{31}(t)+\Lambda_{13}(t)}{12\psi^2} 2\frac{Er_o - B}{1-r_o^2} + \frac{\Lambda_{22}(t)}{12\psi^2}\left\{-\frac{E+2B}{1-r_o^2} + r_o\left[\frac{3B}{1-r_o^2} - 2C\right]\right\}\right]\right.$$

$$\left. + O(\gamma^{-2}, p^2)\right\}; \quad \nu=1. \tag{4.11}$$

In this equation, the functional dependence of $r_o(t)$ on t, and of the elliptic integrals on r_o, e.g., $E(r_o)$, has not been explicitly expressed. If it is thought preferable, the various elliptic integrals appearing can be expressed in terms of any two, preferably $K(r_o)$ and $E(r_o)$ the complete elliptic integrals of the first and second kind respectively, by using the relations [101]

$$E + (1-r_o^2)K = r_o^2 B,$$

$$K - E = r_o^2 D,$$

$$(2-r_o^2)K = 2E + r_o^4 C. \tag{4.12}$$

All five integrals have been tabulated, e.g., in Jahnke and Emde. This result for the linear detector is not exact, either in p or in γ; furthermore, there is no essentially simpler way of obtaining this result, in contrast to the case of the quadratic detector.

The correlation function when the signal is much stronger than the noise is considerably simpler than for the weak-signal case. The leading terms of the result for a νth-law detector are

$$R(t) \simeq \frac{\beta^2\Gamma^2(\nu+1)}{4\Gamma^4(\frac{\nu}{2}+1)}\left(\frac{p\psi}{2}\right)^\nu\left\{1 + 2\left(\frac{\nu}{2}\right)^2\frac{1+r_o}{p} + \frac{\left(\frac{\nu}{2}\right)^2}{p^2}\left[\left\{\left(\frac{\nu}{2}\right)^2 + \left(\frac{\nu}{2}-1\right)^2\right\}(1+r_o^2) + 4\left(\frac{\nu}{2}\right)\left(\frac{\nu}{2}-1\right)r_o\right. + \right.$$

$$+ \frac{1}{3\psi^2}\left[\left(\frac{\nu}{2}-1\right)^2\Lambda_{40} + 2\frac{\nu}{2}\left(\frac{\nu}{2}-1\right)(\Lambda_{31}) + (\Lambda_{13}) + \left[2\left(\frac{\nu}{2}\right)^2 + \left(\frac{\nu}{2}-1\right)^2\right]\Lambda_{22}\right]$$

$$+ O(p^{-3}, \gamma^{-2})\Big\} . \qquad (4.13)$$

The correlation function shows the same suppression effects previously mentioned in connection with the output power, viz., the first noise term is of lower order (in p) than the signal, and the first non-gaussian term is of lower order than the first gaussian one.

4.4 Noise models

To proceed further requires explicit models of the noise statistics in order to fix the time dependence of the semi-invariants. An immense variety of types is naturally possible; three models among those felt to be the most important are treated here. The amplitude, shape of the envelope, and the phase of the individual pulses are able to affect the time dependence of the statistics, while, in our models, time dependence enters through the shape of the pulse envelope alone. This apparent restriction is justified as being usually true of actual noise sources (cf. Appendix IV where this point is treated in connection with radar clutter) and as being irrelevant to the real problem of choosing a suitable time variation. By this last is meant that the time dependence of the semi-invariants is what really matters and this can remain the same whether ascribed to pulse envelope, amplitude, phase, or some combination of all three.

Pertinent data on the three models are summarized in Table 4.1. The exponential pulses represent impulses after having passed through a single-tuned circuit, as might occur with precipitation static in an aircraft receiver of shrimp noise in a sonar.

Although a single tuned circuit is not an accurate model of the tuned stages of a receiver, this type of time dependence is important because it is necessary (and sufficient) if the process is to be Markoffian in the limit of increasing density [102].

The pass band of an actual receiver is an involved function of the number of stages and the exact coupling network between stages. As

an abstraction from the details associated with any particular i-f strip, we shall take a pass band of gaussian shape as our model, which preserves the essential features of a pass band while remaining analytically tractable. Admittedly, a gaussian pass band is not physically realizable, but it is a good approximation to the magnitude-frequency curve of actual amplifiers (if not to the phase-frequency curve), and possesses the important virtue of simplicity.* Impulses passing through this i-f amplifier will become gaussian pulses as in the second model of Table 4.1.

The third type chosen is that of square pulse envelopes of finite duration. This illustrates noise whose values are independent when separated by a sufficiently long, but finite time. The model fits the sonar and radar clutter problem when relative motion between the transceiver and scatterers is slight.

Notice that, for these three cases, all the semi-invariants can be expressed as functions, in fact powers, of the input correlation. Accordingly, the time enters only on a normalized scale and only implicitly through the input correlation function. Figure 6 shows the time dependence of the fourth-order semi-invariants compared to the correlation function, showing the extent of the more rapid decrease to zero of the higher semi-invariants.** The corresponding figure for the linear model is obvious.

4.5 Results for the quadratic and linear detectors

Table 4.2 lists the correlation functions after a quadratic detector for the three different noise models. The unnormalized values of the functions in the table are not of primary interest here since the parallel problem concerning output power has been discussed earlier. The correlation function

- - - - - - -

*H. Wallman has shown that the pass band of cascaded networks whose individual step function responses have no overshoot tends toward the gaussian (Second Symposium in Applied Mathematics, Am. Math. Soc. 1950, p. 91). Furthermore it seems likely that one can extend these results to any cascaded network except to those tuned for a Butterworth response.

**The linear model is one extreme of possible time behavior in that its semi-invariants of all orders decrease no faster than the correlation function. One may conjecture that no $\Lambda_{22}(t)$ can decrease faster than the square of the correlation function, in which case the other two models represent the other extreme; however, we have been unable to prove this.

TABLE 4.1

NOISE MODELS

Pulse Envelope $h(x)$	$\begin{cases} e^{-x}, & x > 0 \\ 0, & x < 0 \end{cases}$	e^{-x^2}	$\begin{cases} 1, & 0 < x < 1 \\ 0, & \text{elsewhere} \end{cases}$
Normalized Correlation Function $r_o(t)$	$e^{-\beta\lvert t\rvert}$	$e^{-\frac{\beta^2 t^2}{2}}$	$\begin{cases} 1-\beta\lvert t\rvert, & \beta\lvert t\rvert < 1 \\ 0, & \beta\lvert t\rvert > 1 \end{cases}$
Normalized Semi-invariants $\frac{\Lambda_{40}}{3!\psi^2}$	$1/4\gamma$	$1/4\gamma\sqrt{\pi}$	$1/4\gamma$
$\frac{\Lambda_{31}(t)+\Lambda_{13}(t)}{3!\,\psi^2}$	$\frac{r_o + r_o^3}{4\gamma}$	$r_o^{3/2} / 2\gamma\sqrt{\pi}$	$r_o/2\gamma$
$\frac{\Lambda_{22}(t)}{3!\psi^2}$	$r_o^2/4\gamma$	$r_o^2/4\gamma\sqrt{\pi}$	$r_o/4\gamma$
$\frac{2^{\frac{m+n}{2}}}{(m+n)!}\frac{\Lambda_{mn}(t)}{\psi^{\frac{m+n}{2}}}$	$\frac{\gamma(2/\gamma)^{\frac{m+n}{2}}}{(m+n)\Gamma^2(\frac{m+n}{2}+1)}$ $\begin{cases} r_o^m, & t > 0 \\ r_o^n, & t < 0 \end{cases}$	$\frac{\gamma\sqrt{\pi}\,(\frac{i}{\gamma}\sqrt{\frac{2}{\pi}})^{\frac{m+n}{2}}\, r_o^{\frac{2mn}{m+n}}}{\sqrt{m+n}\,\Gamma^2(\frac{m+n}{2}+1)}$	$\frac{r_o}{\gamma^{\frac{m+n}{2}-1}\,2(\frac{m+n}{2}+1)}$

TABLE 4.2

CORRELATION FUNCTIONS FOR

THE QUADRATIC DETECTOR

1. Exponential Model: $r_o = e^{-\beta|t|}$

$$R(t) = \frac{\beta^2\psi^2}{4}\left[(1+p)^2 + 2pr_o + \left(1+\frac{1}{\gamma}\right)r_o^2\right]$$

2. Gaussian Model: $r_o = e^{-\frac{\beta^2 t^2}{2}}$

$$R(t) = \frac{\beta^2\psi^2}{4}\left[(1+p)^2 + 2p\,r_o + \left(1+\frac{1}{\gamma\sqrt{\pi}}\right)r_o^2\right]$$

3. Linear Model: $r_o = \begin{cases} 1-\beta|t| & ,\ \beta|t| < 1 \\ 0 & ,\ \beta|t| > 1 \end{cases}$

$$R(t) = \frac{\beta^2\psi^2}{4}\left[(1+p)^2 + \left(2p+\frac{1}{\gamma}\right)r_o + r_o^2\right]$$

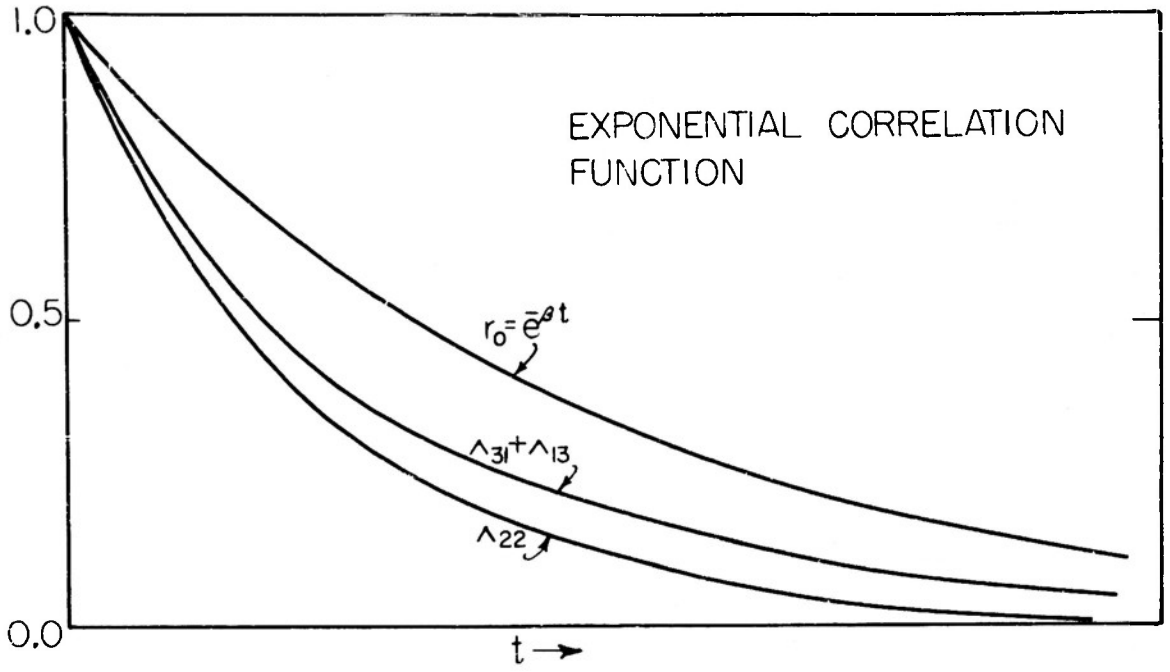

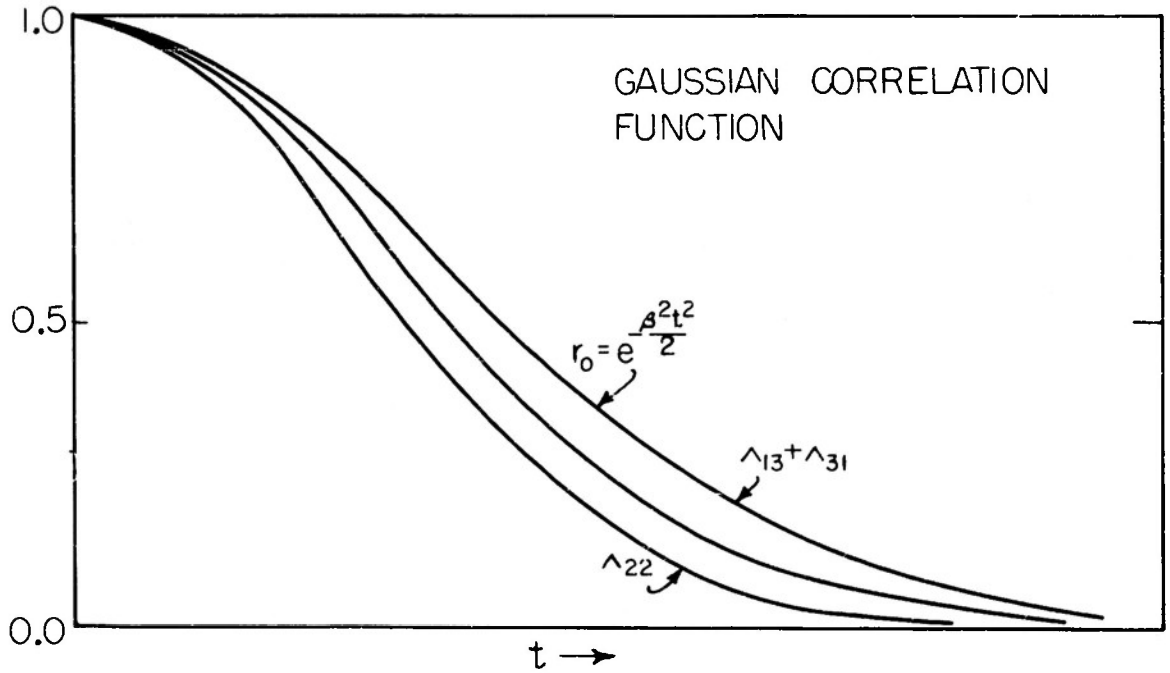

FIG. 6 NORMALIZED SEMI-INVARIANTS

also gives information about statistical dependence in time (or equivalently, the spectral distribution of power) which is most clearly exhibited by normalizing thecorrelation function so that it varies from one to zero. Accordingly, we define

$$r_{out}(t) \equiv \frac{R(t) - R(\infty)}{R(0) - R(\infty)} \quad . \tag{4.14}$$

The more rapidly $r_{out}(t)$ drops to zero, the less correlation there is between successive samples of the output wave.

Some statements about the general effects of signal-to-noise ratio and noise density can be made immediately. Passing through a nonlinear device cannot increase the correlation present in the input wave , whence $r_{out}(t) \leq r_o(t)$, regardless of the values of p or γ. Furthermore, the noise suppression effect when p is large means that the most rapid decrease of $r_{out}(t)$ will occur when no signal is present and that, with increasing signal $r_{out}(t)$ will tend to $r_o(t)$. The nongaussian suppression effect means that the difference between $r_{out}(t)$ for gaussian and nongaussian noise of fixed density and equal input power will decrease as the signal is increased. The effect of nongaussian noise on the amount of correlation in the output depends in an involved fashion on the detector law, signal-to-noise ratio, and noise model, so that the discussion of this point is best deferred till after the presentation of some specific results.

Figures 7,8 and 9 show $r_{out}(t)$ for a quadratic detector and the three different noise models. Note that the three general features of $r_{out}(t)$ mentioned above are borne out by the figures. For the quadratic detector, the exponential and gaussian models give less correlation with nongaussian noise than with gaussian, while for the linear model, the opposite is true. Because of the simplicity of the expression for the correlation function, we can see quite easily why this is so. Gaussian noise after the quadratic detector has one undistorted noise term ($2p r_o$, arising from s x n intermodulation) and one scrambled noise term (r_o^2, from n x n modulation). If the noise is nongaussian an additional n x n term enters, containing the semi-invariant $\Lambda_{22}(t)$. For the exponential and gaussian models, this term adds to the scrambled noise to make the nongaussian result less correlated than the corresponding gaussian one, while for the linear model, the semi-invariant term adds to the undistorted noise term, acting to increase the correlation over the gaussian

amount.

Table 4.3 shows the correlation functions for the linear detector. Because the expressions do not terminate, it is not possible to cover the entire range of values of p and γ. Strongly nongaussian noise ($\gamma = 1$) can be included, however, because of the numerical factors involved in the Edgeworth series. The first correction term is about the size of $2^2\Lambda_{40}/4!\psi^2$ or $1/4\gamma$. The second is in two parts, one half the square of the first term or $1/32\gamma^2$ and one involving sixth-order semi-invariants, $2^3\Lambda_{60}/6!\psi^3$ or $1/36\gamma^2$, both of which are sufficiently small to be neglected inasmuch as the first correction is itself not large compared to the gaussian part of the results. The correlation function is much more sensitive to the dependence on signal-to-noise ratio. The strong signal series is sufficiently accurate when p is greater than two; the weak signal series, however, can only be used for p = 0.5 at the most.

The normalized output correlation functions are shown for the linear detector in Figs. 10-12. Previously, with the quadratic detector the nongaussian correlation function was either always greater or always less than the corresponding gaussian one. For the linear detector, however, the correlation is greater for nongaussian noise when the signal is weak and greater for gaussian noise when the signal is strong. An additional complication is that the curves for gaussian and nongaussian noise cross each other near the origin of time when p is large, although for by far the most of the time the nongaussian curve lies below. The curves again illustrate that the difference between the two types of noise is greatest when the signal is small, and that the difference is suppressed when a strong signal is present. For the linear model the suppression is of higher order, so that the difference is particularly small.

4.6 The effect of nongaussian statistics in general

The effect of the nongaussian statistics on $r_{out}(t)$ has varied in these two cases, depending in a rather obscure manner on the law of the detector, noise model and signal-to-noise ratio, so that an investigation of general values of ν is worth while; however, since the linear and quadratic detectors are by far the most important, a qualitative look at the results for arbitrary values of ν suffices to complete the discussion of the output correlation function.

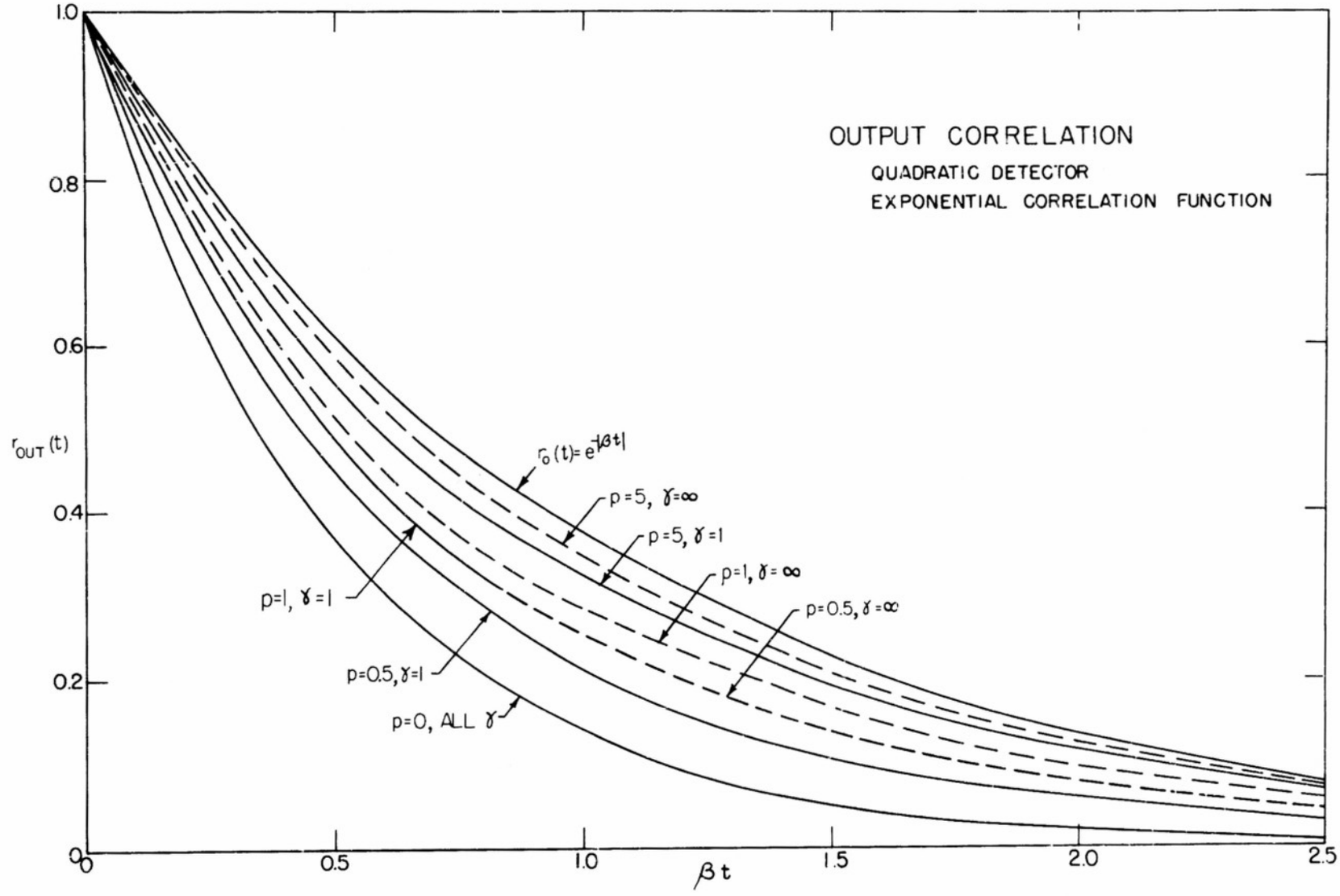
OUTPUT CORRELATION
QUADRATIC DETECTOR
EXPONENTIAL CORRELATION FUNCTION
$r_{OUT}(t)$
$r_o(t) = e^{-|\beta t|}$
p=5, γ=∞
p=5, γ=1
p=1, γ=∞
p=0.5, γ=∞
p=1, γ=1
p=0.5, γ=1
p=0, ALL γ
βt
1.0
0.8
0.6
0.4
0.2
0
0.5
1.0
1.5
2.0
2.5

FIGURE 7

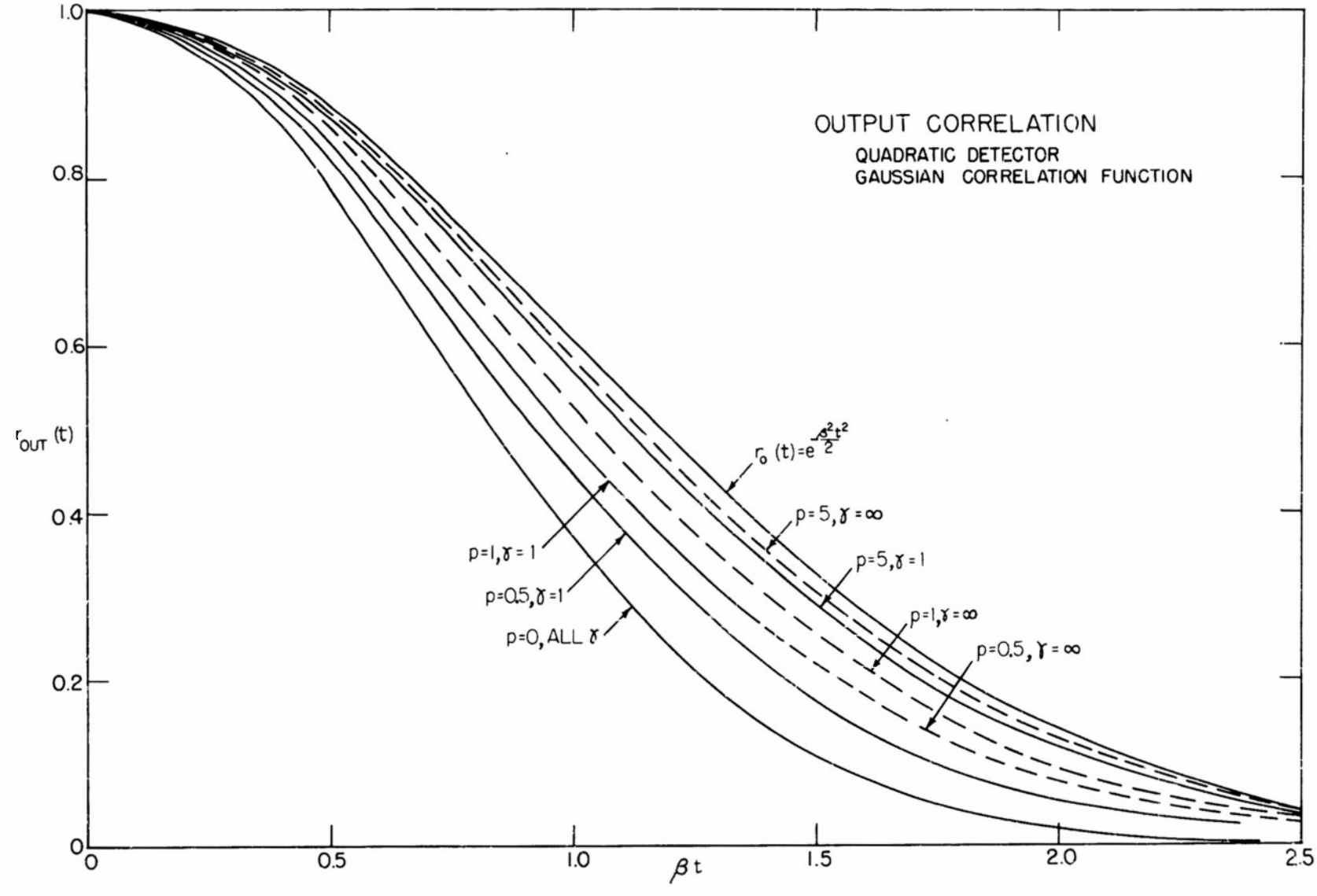
OUTPUT CORRELATION
QUADRATIC DETECTOR
GAUSSIAN CORRELATION FUNCTION
$r_{OUT}(t)$
βt
$r_o(t)=e^{-\frac{\beta^2 t^2}{2}}$
p=5, γ=∞
p=5, γ=1
p=1, γ=∞
p=0.5, γ=∞
p=1, γ=1
p=0.5, γ=1
p=0, ALL γ
1.0
0.8
0.6
0.4
0.2
0
0.5
1.0
1.5
2.0
2.5

FIGURE 8

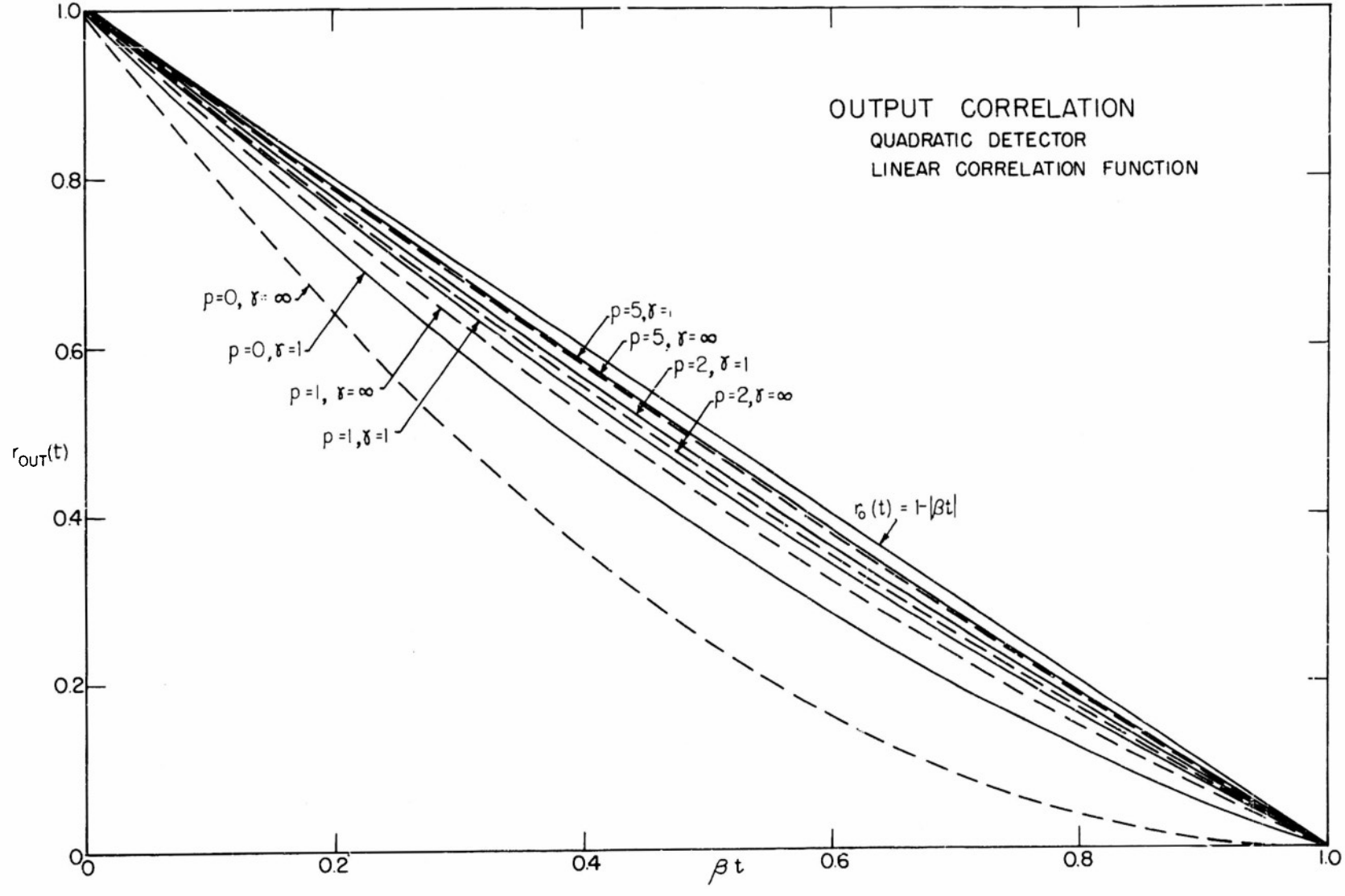
OUTPUT CORRELATION
QUADRATIC DETECTOR
LINEAR CORRELATION FUNCTION
p=0, γ=∞
p=0, γ=1
p=1, γ=∞
p=1, γ=1
p=5, γ=1
p=5, γ=∞
p=2, γ=1
p=2, γ=∞
r₀(t) = 1-|βt|
r_OUT(t)
βt
1.0
0.8
0.6
0.4
0.2
0
0.2
0.4
0.6
0.8
1.0

FIGURE 9

TABLE 4.3

CORRELATION FUNCTIONS

FOR THE LINEAR DETECTOR

a. Weak signal $p \ll 1$

1. Exponential Model: $r_o = e^{-\beta|t|}$

$$R(t) = \frac{\beta^2 \psi}{\pi^2}\left\{E(r_o) + r_o^2 B(r_o) - (1-r_o^2) / 8\gamma[2E(r_o) - K(r_o)]\right.$$

$$\left. + p[E(r_o) + r_o B(r_o) + \frac{1}{8\gamma}\left\{(1-2r_o^2)E(r_o) + r_o B(r_o)\right\}] + O(p^2, \gamma^{-2})\right\}$$

2. Gaussian Model: $r_o = e^{-\frac{\beta^2 t^2}{2}}$

$$R(t) = \frac{\beta^2 \psi}{\pi^2}\left\{E(r_o) + r_o^2 B(r_o) + \frac{1}{8\gamma\sqrt{\pi}}[4r_o^2 D(r_o) - (1-r_o^2)K(r_o) - 4r_o^{5/2} D(r_o)]\right.$$

$$\left. + p[E(r_o) + r_o B(r_o) + \frac{1}{8\gamma(1-r_o^2)\sqrt{\pi}}\left\{(1-5r_o^2 + 4r_o^{5/2})E(r_o) + r_o(3-4r_o^{\frac{1}{2}} + r_o^2)B(r_o)\right\}] + O(p^2, \gamma^{-2})\right\}$$

3. Linear Model: $r_o = \begin{cases} 1 - \beta|t| , & \beta|t| \ll 1 \\ 0 , & \beta|t| \gg 1 \end{cases}$

$$R(t) = \frac{\beta^2 \psi}{\pi^2}\left\{E(r_o) + r_o^2 B(r_o) - \frac{1-r_o}{8\gamma}[K(r_o) - 2r_o D(r_o)]\right.$$

$$\left. + p[E(r_o) + r_o B(r_o) + \frac{1-r_o}{8\gamma}\left\{\frac{3}{1+r_o} B(r_o) - D(r_o)\right\}] + O(p^2, \gamma^{-2})\right\}$$

TABLE 4.3 (cont.)

b. Strong signal $p \gg 1$

1. Exponential Model: $r_o = e^{-\beta|t|}$

$$R(t) = \frac{2\beta^2\psi p}{\pi^2}\left\{1 + \frac{1+r_o}{2p} + \frac{1-r_o}{8p^2}\left[1 - r_o + \frac{1}{4\gamma}(1 - r_o + 2r_o^2)\right]\right.$$

$$\left. + \frac{1-r_o^2}{16p^3}\left[1 - r_o + \frac{1}{4\gamma}(5 - 5r_o + 2r_o^2)\right] + O(p^{-4}, \gamma^{-2})\right\}$$

2. Gaussian Model: $r_o = e^{-\frac{\beta^2 t^2}{2}}$

$$R(t) = \frac{2\beta^2\psi p}{\pi^2}\left\{1 + \frac{1+r_o}{2p} + \frac{1}{8p^2}\left[(1-r_o)^2 + \frac{1}{4\gamma\sqrt{\pi}}(1 - 4r_o^{3/2} + 3r_o^2)\right]\right.$$

$$\left. + \frac{1}{16p^3}\left[(1-r_o^2)(1-r_o) + \frac{1+r_o}{4\gamma\sqrt{\pi}}(5 - 8r_o - 4r_o^{3/2} + 7r_o^2)\right] + O(p^{-4}, \gamma^{-2})\right\}$$

3. Linear Model: $r_o = \begin{cases} 1 - \beta|t|, & \beta|t| < 1 \\ 0, & \beta|t| > 1 \end{cases}$

$$R(t) = \frac{2\beta^2\psi p}{\pi^2}\left\{1 + \frac{1+r_o}{2p} + \frac{1-r_o}{8p^2}\left[1 - r_o + \frac{1}{4\gamma}\right] + \frac{1-r_o}{16p^3}\left[1 - r_o^2 + \frac{1}{4\gamma}(5 - 3r_o)\right] + O(p^{-4}, \gamma^{-2})\right\}$$

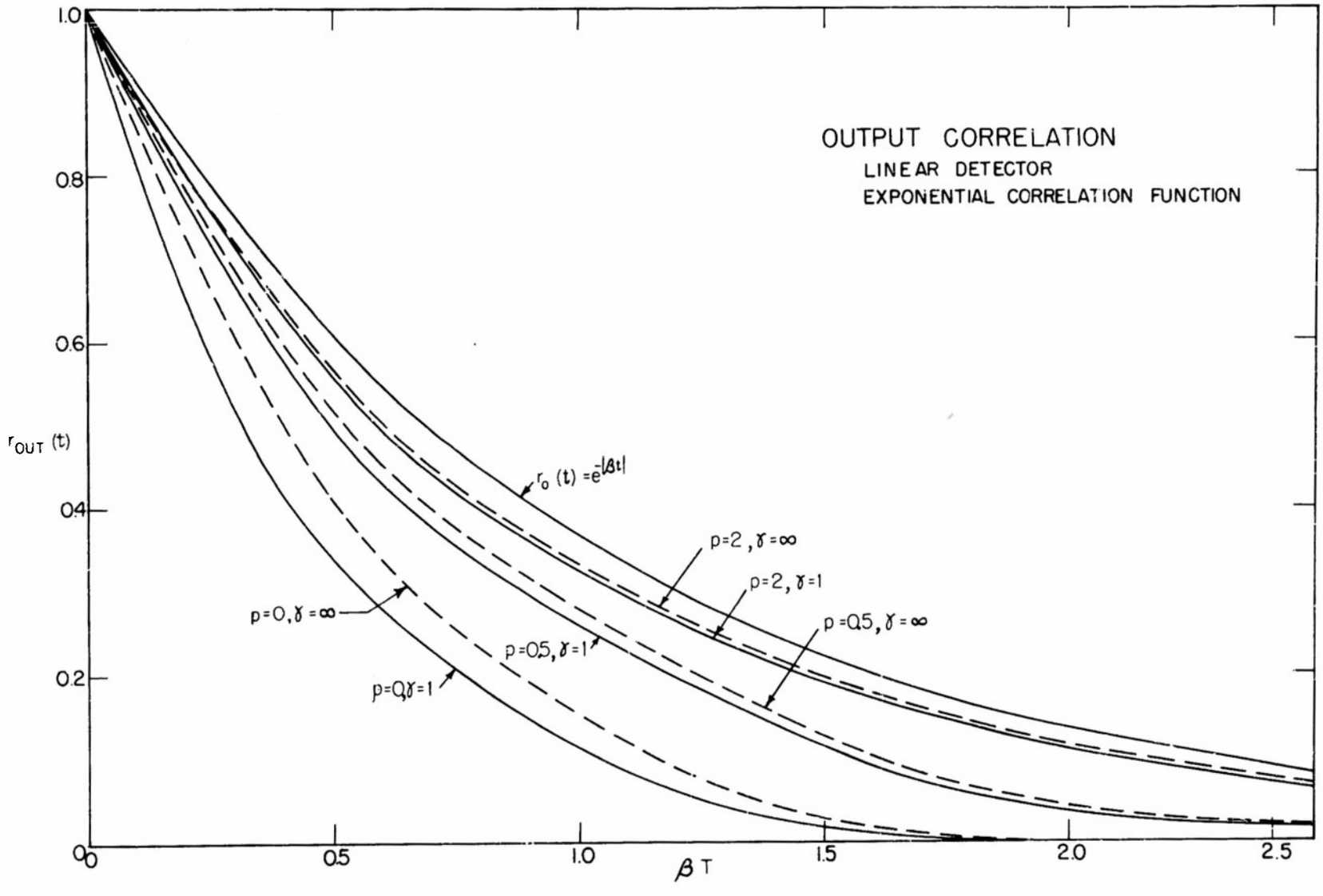
OUTPUT CORRELATION
LINEAR DETECTOR
EXPONENTIAL CORRELATION FUNCTION
$r_{OUT}(t)$
$r_o(t) = e^{-|\beta t|}$
p=2, γ=∞
p=2, γ=1
p=0.5, γ=∞
p=0.5, γ=1
p=0, γ=∞
p=0, γ=1
βT
1.0
0.8
0.6
0.4
0.2
0
0.5
1.0
1.5
2.0
2.5

FIGURE 10

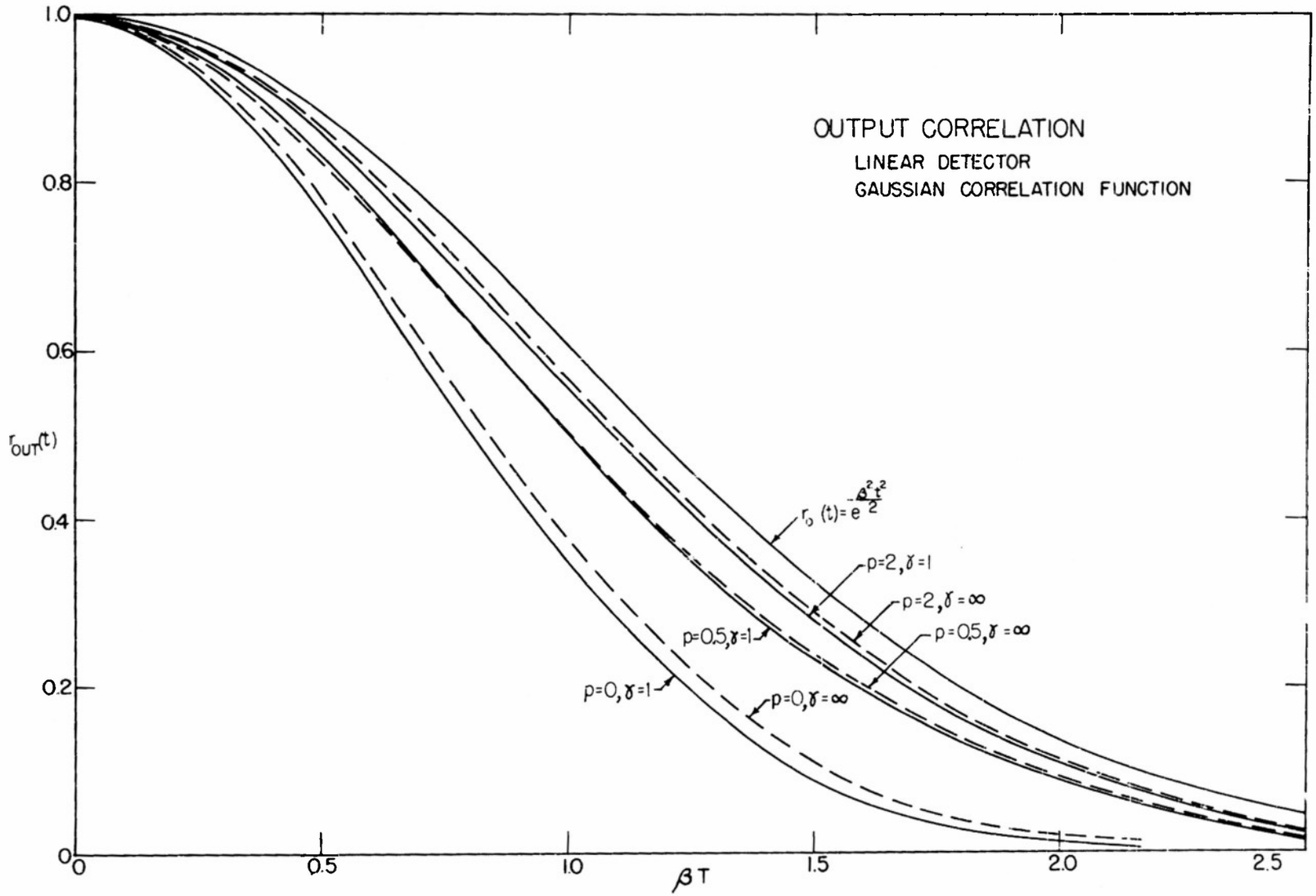
OUTPUT CORRELATION
LINEAR DETECTOR
GAUSSIAN CORRELATION FUNCTION
$r_{OUT}(t)$
$r_0(t) = e^{-\frac{\beta^2 t^2}{2}}$
p=2, γ=1
p=2, γ=∞
p=0.5, γ=1
p=0.5, γ=∞
p=0, γ=1
p=0, γ=∞
βT
0
0.2
0.4
0.6
0.8
1.0
0.5
1.0
1.5
2.0
2.5

FIGURE 11

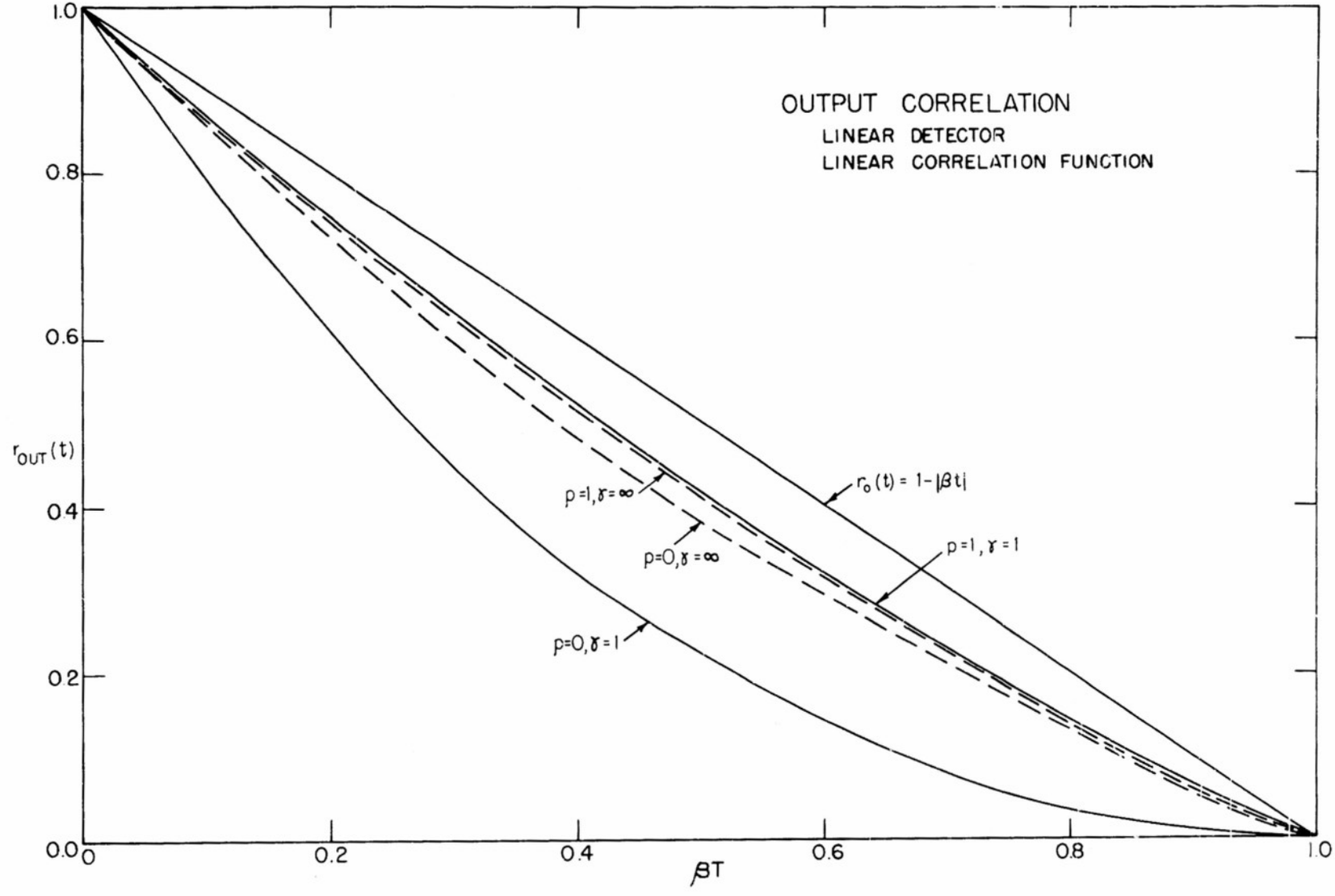
OUTPUT CORRELATION
LINEAR DETECTOR
LINEAR CORRELATION FUNCTION
$r_{OUT}(t)$
$r_o(t) = 1-|\beta t|$
p=1, γ=∞
p=0, γ=∞
p=1, γ=1
p=0, γ=1
βT
1.0
0.8
0.6
0.4
0.2
0.0
0
0.2
0.4
0.6
0.8
1.0

FIGURE 12

The primary point in question is whether nongaussian noise increases or decreases the correlation of the output compared to gaussian noise of the same input power. We have obtained the sign of the change in correlation as a function of ν and p for the special cases above and for various limiting values of ν and p, but have not been able to get a really satisfactory assurance that no additional changes of sign occur for intermediate values of ν or p. The best way to present the result is to show the first quadrant of a (ν,p)-plane in which the boundaries and regions of increased or decreased correlation are explicitly labelled.

The behavior along the lines $\nu = 1$ and $\nu = 2$ is known from the results of Figs. 7-12; and, in addition, we have found the sign of the change in correlation for large p and ν, and for $p = 0$ and all ν. Appendix VII gives the explicit forms of $r_{out}(t)$ from which Fig. 13 was constructed.

The dependence of the change in the total output power and in the d-c power on the law of the detector leads one to expect that the normalized output correlation function should also exhibit some such settled type of behavior when ν is larger than some number, perhaps not exactly two. In fact, Fig. 11 bears this out. Nonetheless, while all the information that appears in the figure is correct, and any additional changes in the behavior of $r_{out}(t)$ seem unlikely, it cannot be categorically stated that all the changes in correlation are included.

The figure shows that, with the exponential and gaussian models, when the law of the detector is greater than two, the correlation of the output noise is greater when the noise is nongaussian. Only when the detector law is less than two does the relative strength of the signal affect the result. Near $\nu = 1$, in the shaded area, the output correlation functions for gaussian and nongaussian noise cross each other so no definite assignment of this region can be made. Figures 10-12 for the linear detector show, however, that for most of the time, the correlation of nongaussian noise is less than that of gaussian. When ν is less than two, the nongaussian noise terms have signs which differ, giving a noise cancellation effect with strong and weak signals (for the specific equations, see Appendix VII).

The effect is not exactly the same in the two cases because the noise is different, coming mostly from signal-by-noise modulation products when the signal is strong and from noise-by-noise modulation products when the noise is weak.

The linear model differs from the other two in the decrease of the semi-invariants with time compared to the input correlation function. Just as in the previous discussion of the linear and quadratic detectors, one expects the correlation of this model to be greater than that of the other two. Figure 13 shows that here the nongaussian noise is more strongly correlated for all values of ν when no signal is present, and that the band of increased correlation at high signal levels has moved to larger values of ν.

The magnitude of the change in correlation will be greater when the signal is weak or absent. At large signal levels, the change is suppressed by a factor of $1/p$ for the exponential and gaussian models and by a factor of $1/p^2$ for the linear model.

4.7 The smoothing effect of finite time averages

Up to now, the discussion of the output of the detector has been concerned with average values, which implies averaging over all time. When the output is averaged over a finite time, the result is not a parameter of the output distribution as for the infinite average, but rather again a random variable, although one with a more concentrated distribution than before. In actual practice, of course, only a finite time is available in which to operate on the output of the detector. The finite averaging time makes an analysis more difficult, but the variance of the averaged output can be found [103].

The effect of a finite averaging time depends partly on the video filter. This is a low-pass filter transmitting the low-frequency spectral zone and cutting off the spectral zones at the carrier frequency and its multiples, and is followed in turn by an ideal finite time integrator. From the reference quoted above, we have the result that the variable $z = (1/T) \int_0^T I_o(t)dt$, where T is the averaging time and I_o is the low-frequency output of the detector, has as its variance,

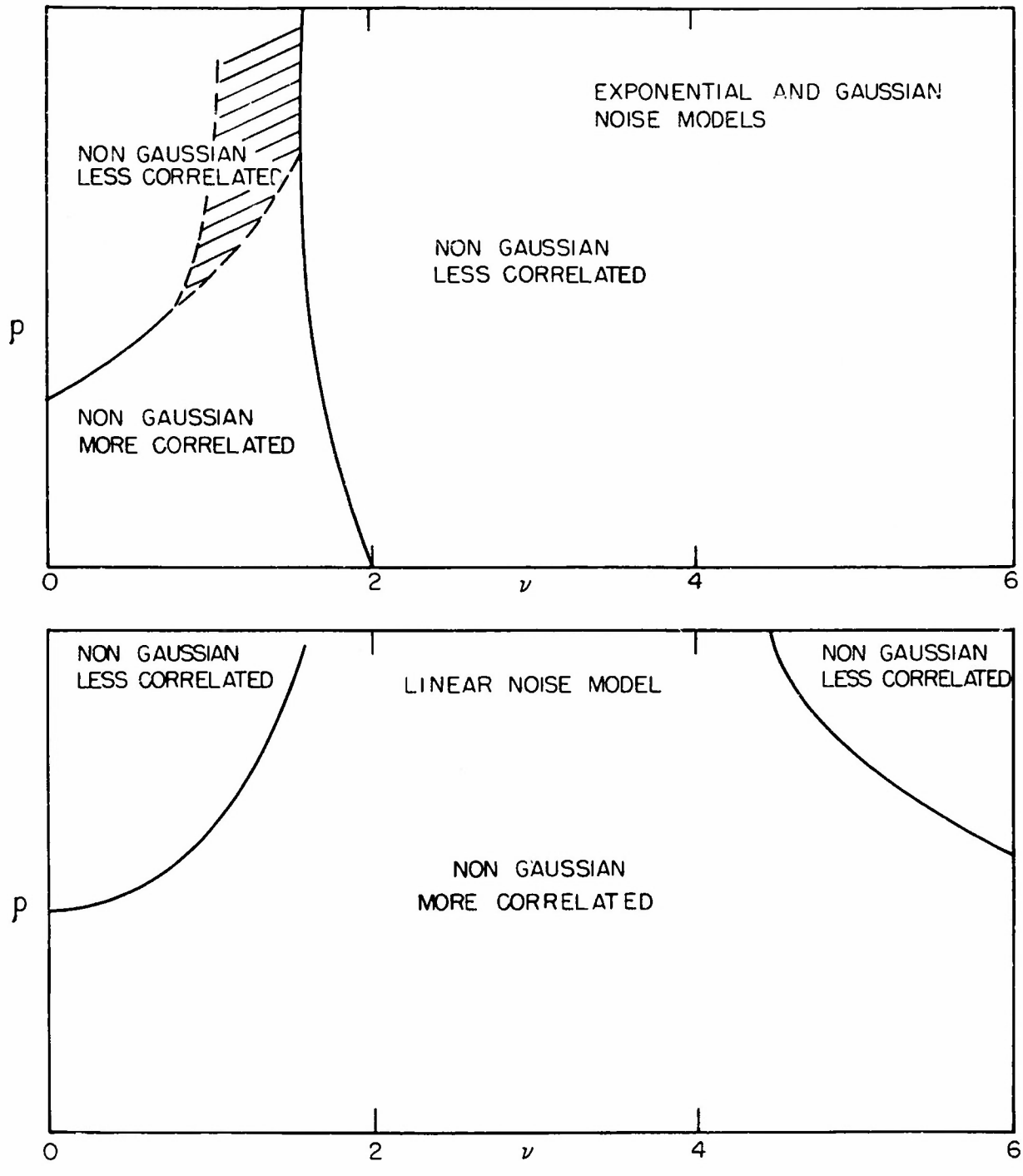

FIG. 13 EFFECT OF NON GAUSSIAN STATISTICS ON THE OUTPUT CORRELATION

$$\sigma^2 = \frac{2}{T}\int_0^T [R(t) - \overline{I}^2][1 - t/T]\,dt \quad , \tag{4.15}$$

where the averages under the integral sign are ensemble averages. Notice that to find the variance of Z requires knowing a more complicated statistic of the infinite averaging problem.

The general effect of the averaging can be readily seen. When T is shorter than the time in which the output correlation function goes to its final value, the averaging is almost entirely ineffective so that the variance of Z is as great as that of I_o. On the other hand when T is much greater than the time in which the correlation function varies, the mean and variance of Z are effectively composed of the sum of independent random variables, whose number is proportional to the averaging time. Thus for long averaging times, the relative variance $\sigma^2/\overline{I}^2$, will vanish as 1/T. Explicit results are in general difficult to obtain because t appears implicitly in the correlation function; however, for the quadratic detector, the elementary form of the output correlation function again leads to particularly simple results.

The relative variance, $\sigma^2/\overline{I}^2$, is the best measure of the elimination of noise effected by averaging. Table 4.4 gives the quadratic detector equations, and Figs. 14, 15, and 16 present graphs of the variation of the variance with time. Just as before, with increasing signal, the relative noise output becomes less and the difference between gaussian and nongaussian noise also is less pronounced. However, this orderly sequence is disturbed for weak signals and long smoothing times. The smoothing is more effective against the n x n component of the relative variance than the s x n component because the n x n part is less correlated than the other; thus, with long averaging times, the remaining fluctuation is mostly from the s x n component. At low signal levels, where the variance, even with no smoothing, is only slightly less than that with no signal, the variance with long smoothing times will be greater because the "no-signal" noise, arising entirely from n x n interaction, is more strongly suppressed.

Another interesting point is that the nearly gaussian noise always has a larger variance than gaussian for all three models, when noise alone is

present. This behavior is in contrast to that of the correlation function where the linear model differs from the other two. In fact, for finite averaging, the three models behave the same nearly everywhere in the (ν,p)-plane. Appendix VIII takes up the question in more detail; the results are that nearly gaussian noise has a greater variance than gaussian noise of the same input mean square, except when the signal is large and ν lies in the approximate range 0.5 to 1.5, in which case the nearly gaussian variance is less. The boundary of the two regions is not quite the same for the three different models, but this is the only difference between them.

TABLE 4.4

OUTPUT VARIANCE WITH QUADRATIC

DETECTOR AND FINITE AVERAGING

a. Exponential Model: $r_o(\beta t) = e^{-\beta|t|}$

$$\sigma^2/\bar{I}^2 = \frac{1}{2(\beta T)^2(1+p)^2}\left[\left(1+\frac{1}{\gamma}\right)\left(r_o^2(\beta T) + 2\beta T - 1\right) + 8p\left(r_o(\beta T) + \beta T - 1\right)\right]$$

b. Gaussian Model: $r_o(\beta t) = e^{-\frac{\beta^2 t^2}{2}}$; $\Phi(x) = \frac{2}{\sqrt{\pi}}\int_o^x e^{-y^2}\,dy$

$$\sigma^2/\bar{I}^2 = \frac{\sqrt{\pi}}{\beta T(1+\rho)^2}\left[\left(1+\frac{1}{\gamma\sqrt{\pi}}\right)\Phi(\beta T) + 2\sqrt{2}\,p\,\Phi(\beta T/\sqrt{2})\right] + \frac{1}{(\beta T)^2(1+p)^2}\left[\left(1+\frac{1}{\gamma\sqrt{\pi}}\right)\left(r_o^2(\beta T)-1\right)\right.$$

$$\left. + 4p\left(r_o(\beta T) - 1\right)\right]$$

c. Linear Model: $r_o(\beta t) = 1 - \beta|t|, |\beta t| \le 1;\ 0, |\beta t| \ge 1$

$$\sigma^2/\bar{I}^2 = \frac{1}{3(1+p)^2}\left[\left(2p+\frac{1}{\gamma}\right)(3-\beta T) + 3 - 2\beta T + \frac{1}{2}(\beta T)^2\right] \quad , \beta T \le 1;$$

$$= \frac{1}{3(\beta T)^2(1+p)^2}\left[\left(2p+\frac{1}{\gamma}\right)(3\beta T - 1) + \frac{1}{2}(4\beta T - 1)\right], \beta T \ge 1.$$

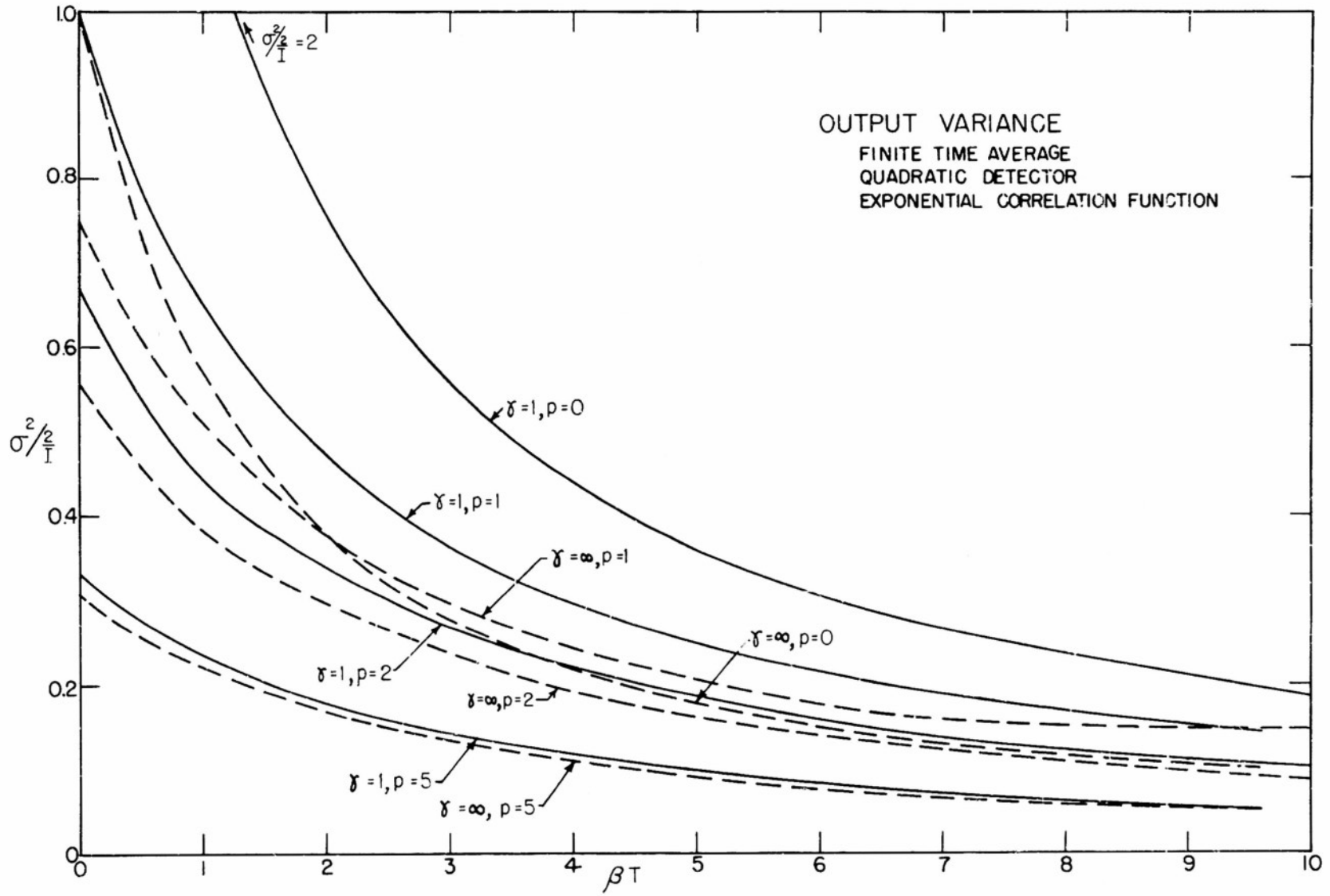
OUTPUT VARIANCE
FINITE TIME AVERAGE
QUADRATIC DETECTOR
EXPONENTIAL CORRELATION FUNCTION
$\sigma^2/\frac{2}{I}$
$\sigma^2/\frac{2}{I}$ = 2
γ = 1, p = 0
γ = 1, p = 1
γ = ∞, p = 1
γ = ∞, p = 0
γ = 1, p = 2
γ = ∞, p = 2
γ = 1, p = 5
γ = ∞, p = 5
βT
0
0.2
0.4
0.6
0.8
1.0
1
2
3
4
5
6
7
8
9
10

FIGURE 14

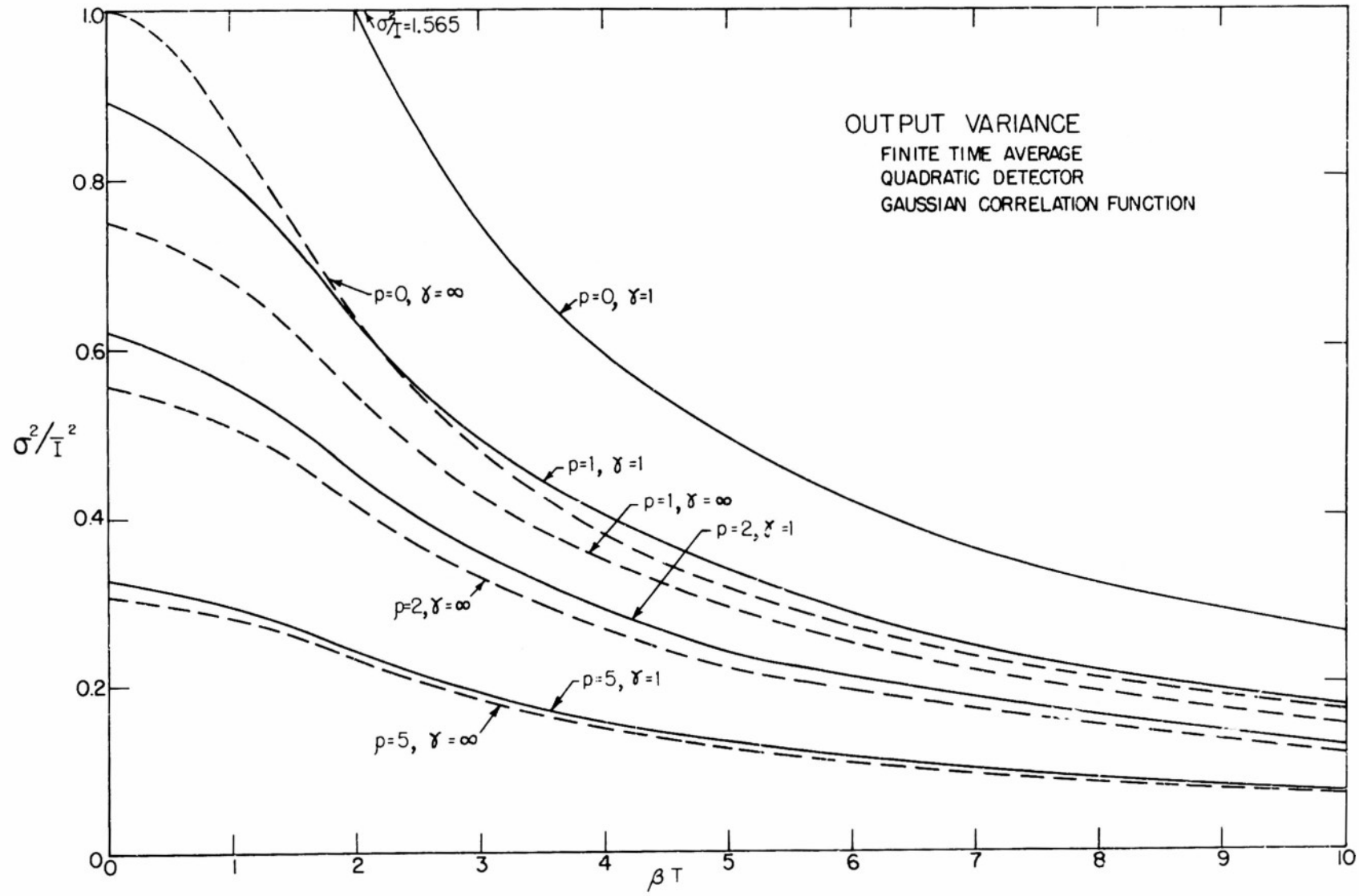
OUTPUT VARIANCE
FINITE TIME AVERAGE
QUADRATIC DETECTOR
GAUSSIAN CORRELATION FUNCTION
σ_I^2=1.565
p=0, γ=∞
p=0, γ=1
p=1, γ=1
p=1, γ=∞
p=2, γ=1
p=2, γ=∞
p=5, γ=1
p=5, γ=∞
$\sigma^2/\bar{I}^2$
βT
0
0.2
0.4
0.6
0.8
1.0
1
2
3
4
5
6
7
8
9
10

FIGURE 15

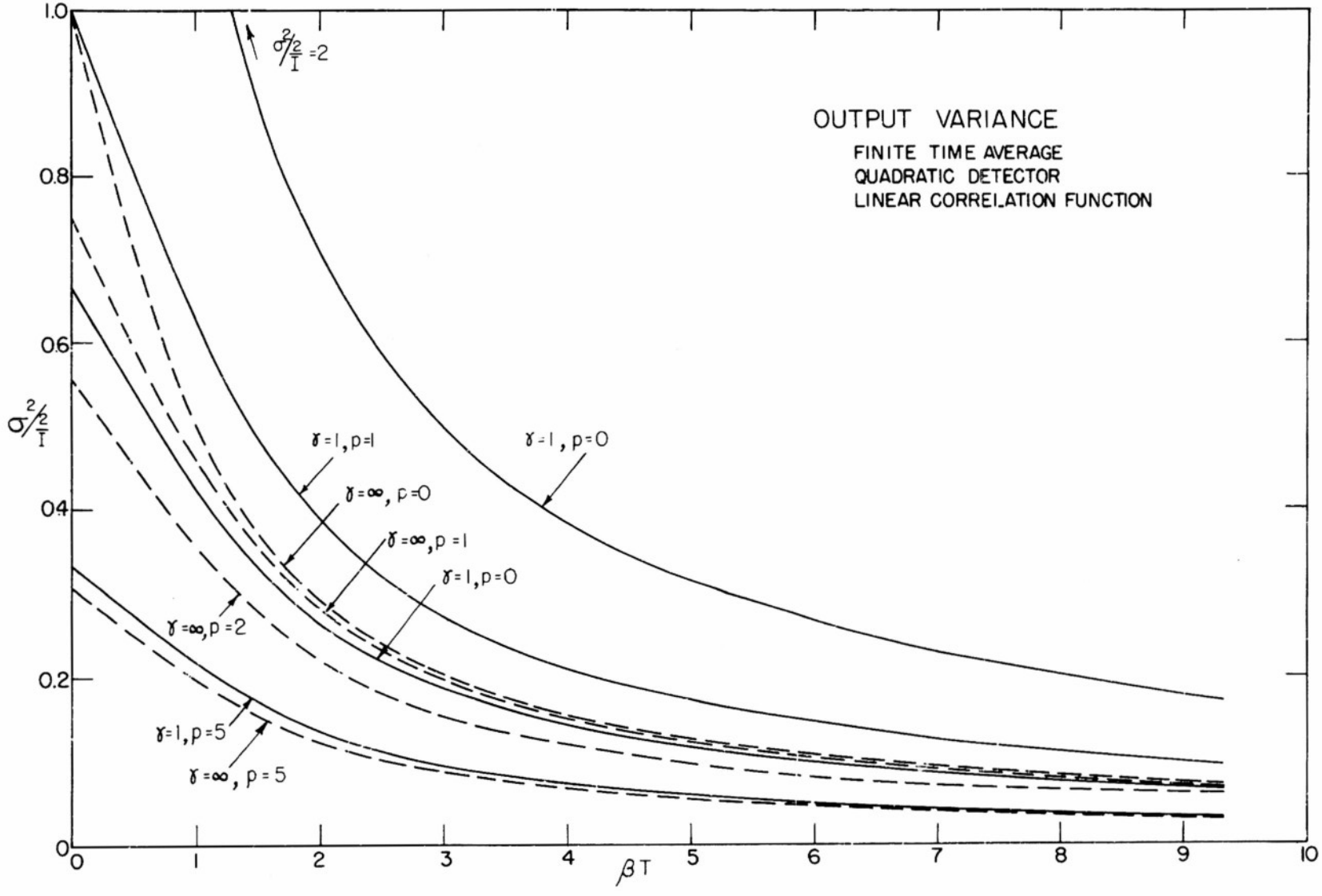
OUTPUT VARIANCE
FINITE TIME AVERAGE
QUADRATIC DETECTOR
LINEAR CORRELATION FUNCTION
$\sigma^2/\bar{I}^2 = 2$
$\gamma = 1, p = 1$
$\gamma = 1, p = 0$
$\gamma = \infty, p = 0$
$\gamma = \infty, p = 1$
$\gamma = 1, p = 0$
$\gamma = \infty, p = 2$
$\gamma = 1, p = 5$
$\gamma = \infty, p = 5$
$\sigma^2/\bar{I}^2$
βT
0
0.2
0.4
0.6
0.8
1.0
1
2
3
4
5
6
7
8
9
10

FIGURE 16

V

Conclusion

In the preceding sections, we have discussed the form of the nearly gaussian distributions and the physical noise sources that may be expected to produce nearly normal random noise. In the previous section, the problem of the rectification of nongaussian noise has been considered and most of the important statistical parameters of the output determined in general, although in perhaps intractable form. The qualitative effect of nongaussian statistics on the output power, output correlation function, and finitely averaged output have been determined in reasonable generality, with explicit formulae and graphs for the most important special cases.

Acknowledgments

We wish to express our thanks to Miss Anne F. Downey, Miss Janet Connolly and to Leon S. Levy, who performed the calculations for this report.

Appendix I

Stationarity

Even though the instantaneous value of the noise wave is stationary, in general the slowly varying components are not; however, since the noise is narrow-band, to a satisfactory degree of approximation, they may be assumed so. The difficulty is the same as with a modulated carrier, viz., a phase shift is involved which spoils stationarity unless the phase distribution is uniform.

The importance of establishing stationarity lies in the fact that analytic results are obtained from statistical averages, while experimental results are obtained from time averages. If the random process involved is stationary or, more precisely, is composed of stationary subsets that possess no non-trivial stationary subsets, then the two kinds of averages are equal (to within a subset of measure zero).

To discuss stationarity, it is most convenient to use the ensemble representation.* For the Poisson ensemble, we may use

$$V(t;t',\psi) = R(t-t') \cos\left(\omega_o[t-t'] - \psi\right) , \qquad (I.1)$$

where t' is uniformly distributed.

Equation (I.1) is not a random function; it is a particular member of the ensemble fixed by the ensemble parameters t' and ψ and as such is a determinate function. At a later time τ, the time of Eq. (I.1), is replaced by $t + \tau$. This generates a new ensemble which can be compared to the old one only when the time difference τ is absorbed into the ensemble parameters by some appropriate transformation. After the two ensembles have the same time value, they may be compared to see if they are the same, which is the stationarity requirement. In this case, τ can be added to t',

$$V(t+\tau;\, t',\, \psi) = V(t;\, t' - \tau,\, \psi) . \qquad (I.2)$$

Since t' is uniformly distributed the translation by τ will leave the overall ensemble invariant.

*An ensemble is a set of functions together with a probability distribution defined over the set.

For the in-phase and quadrature components, a further restriction is needed. We have specifically

$$\left.\begin{aligned} X(t;t',\psi) &= R(t-t')\cos(\omega_o t' + \psi) \\ Y(t;t',\psi) &= R(t-t')\sin(\omega_o t' + \psi) \end{aligned}\right\} \qquad (I.3)$$

and

$$X(t+\tau;t',\psi) = X(t;t'-\tau, \psi + \omega_o \tau) \quad . \qquad (I.4)$$

This last equation indicates that, for the slowly varying components to be stationary, the phase must be purely random as well as the time t'; however, the narrow-band character permits a relaxation of this result for nearly gaussian distributions.

Since we have a Poisson ensemble, the semi-invariants of X and Y are simply related to the moments of the individual pulses.

$$\mu_{mn} = \langle X^m Y^n \rangle = \gamma \left\langle h^{m+n}(\beta[t-t']) \cos^m[\omega_o t' + \psi] \times \sin^n[\omega_o t' + \psi] \right\rangle_{av} \qquad (I.5)$$

The trigonometric part can be written as a Fourier series and each term interpreted as the sine or cosine transform of $h^{m+n}(\beta[t-t'])$, evaluated as a multiple of the central frequency, (the phase may be absorbed in t' since t' is uniformly distributed). The pulse envelope varies much more slowly than the central frequency part, so that its transform will have hardly any spectral components at the central frequency. This will also be true of the transforms of the smaller powers of the pulse envelope, so that all terms in the Fourier series may be neglected except the leading one, corresponding to the zeroth harmonic, which gives the isotropic result. Thus, for nearly gaussian noise where the higher-order moments are negligible, the distribution is effectively isotropic. The conclusion can not be extended to a narrow-band distribution in general, because of the different behavior of the high-order moments. Since the energy in an individual pulse is finite, the pulse envelope must either last for a finite amount of time or vanish sufficiently strongly at infinity. Taking powers of envelopes of the decreasing class will increase the rate of fall and broaden the spectrum, until, for large values of m+n, the spectral components at harmonics of the

central frequency are no longer negligible and the distribution thus not isotropic.

Table I.1 illustrates the above remarks, for three different types of pulse envelopes: (i) exponential pulses, characteristic of a single tuned circuit, (ii) gaussian pulses, characteristic of a multi-stage amplifier, and (iii) square pulses of finite duration. The duration of the major part of the pulse is $1/\beta$, so that β is roughly half the bandwidth of the i-f circuits involved; accordingly, the ratio of harmonic term to isotropic term is expressed in terms of Q, the reciprocal of the fractional bandwidth. Fractional bandwidths in radar are about 0.1, so that the moment for which a harmonic term first reaches 5% of the isotropic one is the fifth moment for exponential pulses and the thirty-fifth for gaussian pulses. Square pulses do not present the same problem, since all the moments behave the same as far as the relative contributions of harmonics are concerned; for the assumed Q, the first harmonic is 5% of the isotropic term and higher harmonics all contribute less.

The above remarks show that, for nearly gaussian Poisson ensembles, isotropy follows from the narrow-band structure, so that the in-phase and quadrature components are stationary under the same restrictions as placed on the instantaneous value; this is sufficient for our purposes.

Table I.1

Envelope Moments and Spectra

$h(\beta t)$ Pulse envelope	$\int_0^\infty h^m(\beta t)\cos p\omega_o t\,dt \quad p<m$	$\int_0^\infty h^m \cos p\omega_o t\,dt \Big/ \int_0^\infty h^m dt$
$e^{-\beta t}$	$\frac{m\beta}{(m\beta)^2+(p\omega_o)^2}$	$\frac{1}{1+(\frac{p2Q}{m})^2}$
$e^{-\beta^2 t^2}$	$\sqrt{\frac{\pi}{4m\beta^2}}\, e^{-\frac{p^2\omega_o^2}{4m\beta^2}}$	$e^{-\frac{p^2Q^2}{m}}$
$1 \quad 0<t<\beta^{-1}$ $0 \quad \beta^{-1}<t$	$\frac{\sin p\omega/\beta}{p\omega}$ $Q = \omega_o/2\beta$	$\frac{\sin 2pQ}{2pQ}$

Appendix II

Nearly Gaussian Distributions in Terms of Parametric Derivatives

This series is useful when the noise ensemble has a phase uniformly distributed, independent of the envelope. As has been shown, nearly gaussian narrow-band noise waves have a structure equivalent to this. Thus the random variable to be considered is

$$Z(t) = R(t) \cos [\omega_o t - \theta(t)] \quad , \tag{II.1}$$

where

$$W(R,\theta) = \begin{cases} W(R)/2\pi & 0 < \theta < 2\pi \, , \\ 0 & \text{elsewhere.} \end{cases}$$

The first-order moments are easily calculated.

$$\mu_u = \langle R^u \rangle_{av} \int_0^{2\pi} \cos^u(\omega_o t - \theta) d\theta / 2\pi \, ,$$

$$= \frac{[1 + (-1)^n]}{2} \frac{\Gamma(\frac{n+1}{2})}{\sqrt{\pi}\,\Gamma(\frac{n}{2} + 1)} \langle R^u \rangle \, . \tag{II.2}$$

$$\therefore \quad \mu_{2u+1} = 0 \, ,$$

and

$$F_Z(\xi) = \sum_{k=0}^{\infty} \frac{\mu_{2k}}{(2k)!} (i\xi)^{2k} \, . \tag{II.3}$$

The odd semi-invariants are also zero, as may be seen by comparing their power series, Eq. (2.5), with the one for the moments. We have accordingly

$$\ln F_Z(\xi) - \sum_{k=1}^{\infty} \frac{(i\xi)^k}{k!} \lambda_k = \ln \left[1 + \sum_{m=1}^{\infty} \frac{\mu_{2m}}{(2m)!} (i\xi)^{2m} \right]$$

$$= \sum_{k-1}^{\infty} \frac{(-1)^{k-1}}{k} \left\{ \sum_{m=1}^{\infty} \frac{\mu_{2m}}{(2m)!} (i\xi)^{2m} \right\}^k \quad . \tag{II.4}$$

Since only even powers appear in the series for the moments, the same must be true for the semi-invariant series, which implies that $\lambda_{2k+1} = 0$. Consequently,

$$F_Z(\xi) = \exp \left\{ \sum_{k=1}^{\infty} \frac{\lambda_{2k}}{(2k)!} (i\xi)^{2k} \right\} \quad . \tag{II.5}$$

The exponential can be expanded in a power series except for its first term; the leading terms will be

$$F_Z(\xi) = \left\{ 1 + \frac{\lambda_4}{4!}(i\xi)^4 + \frac{\lambda_6}{6!}(i\xi)^6 + \frac{\lambda_4^2}{2!(4!)^2}(i\xi)^8 + O(\gamma^{-3}) \right\} e^{-\frac{\psi\xi^2}{2}} \tag{II.6}$$

Clearly this equation can be written in terms of derivatives with respect to ψ, viz.:

$$F_Z(\xi) = \left\{ 1 + \frac{\lambda_4}{3!} \frac{\partial^2}{\partial\psi^2} - \frac{\lambda_6}{6!} 8 \frac{\partial^3}{\partial\psi^3} + \frac{\lambda_4^2}{2!(3!)^2} \frac{\partial^4}{\partial\psi^4} + O(\gamma^{-3}) \right\} e^{-\frac{\psi\xi^2}{2}} \quad . \tag{II.7}$$

The corresponding series for the second-order distribution is more involved, since the narrow-band structure appears explicitly in the moments. The second-order moments are

$$\mu_{mn}(t) = \langle R_1^m R_2^n \rangle_{av} \langle \cos^m(\omega_o t_o - \theta_1) \cos^n(\omega_o [t_o + t] - \theta_2) \rangle_{av} \quad , \tag{II.8}$$

which gives, after expanding the second cosine,

$$\mu_{mn}(t) = \langle R_1^m R_2^n \rangle_{av} \sum_{k=0}^{n} C_k^n (-1)^k \langle \cos^{n-k}(\omega_o t - \theta) \sin^k(\omega_o t - \theta) \rangle_{\theta\, av}$$

$$\times \langle \cos^{m+n-k}(\omega_o t_o - \theta_1) \sin^k(\omega_o t_o - \theta_1) \rangle_{\theta_1\, av} \tag{II.9}$$

where

$$\theta = \theta_2 - \theta_1 \quad . \tag{II.9}$$

The average over θ_1 will be different from zero only when both k and m +n- k are even; thus all odd-order moments again vanish. As before, the same is true of the semi-invariants. The average over the phase change, θ, must be postponed until the end in order to use the series of derivatives. The first set of terms in the semi-invariant series, Eq. (2.5), is

$$-\frac{1}{2}[\psi_1 \xi_1^2 + 2\psi r_o \xi_1 \xi_2 \cos(\omega_o t-\theta) + \psi_2 \xi_2^2] \quad , \tag{II.10}$$

where the subscripts to the ψ's have been inserted to permit differentiation of each of the terms separately. In order to obtain a series in parametric derivatives, it must be shown that the appropriate powers of ξ_1, ξ_2, and $\cos(\omega_o t - \theta)$ in a given term of the expansion of the exponent can be found by taking appropriate derivatives of the expression in Eq. (II.10). Since k in Eq. (II.9) is even, the sine factor can be expressed in terms of cosines and expanded, so that the m, nth moment term contains $\xi_1^m \xi_2^n \cos^{n-j}(\omega_o t-\theta)$, where m+n and j are even, and $j \leq n$. Then by taking n-j derivatives with respect to ψr_o, j/2 derivatives with respect to ξ_2, and (m-n+j)/2 derivatives with respect to ξ_1, the explicit dependence on both the variables and the narrow-band structure is suppressed. This is a total of (m+n)/2 derivatives, just half the number an Edgeworth series would require. Once assured that the series can be written down, it is easier to find the terms directly, rather than to search for a general formula.

For Poisson noise, the leading terms are

$$F_2(\xi_1, \xi_2; t) = \left\langle \left\{ 1 + \frac{\lambda_{40} \xi_1^4}{4!} + \frac{\Lambda_{31}(t) \cos(\omega_o t-\theta)}{3!} \xi_1^3 \xi_2 \right.\right.$$
$$\left. + \frac{\Lambda_{22}(t)}{12} \xi_1^2 \xi_2^2 [2\cos^2(\omega_o t-\theta) + 1] + \frac{\Lambda_{13}(t)}{3!} \cos(\omega_o t-\theta) \xi_1 \xi_2^3 + \frac{\Lambda_{40}}{4!} \xi_2^4 \right\}$$
$$\left. \times \exp\left\{ -\frac{1}{2}[\psi_1 \xi_1^2 + 2\psi r_o \xi_1 \xi_2 \cos(\omega_o t-\theta) + \psi_2 \xi_2^2] \right\} \right\rangle_{\theta \text{ av}} , \tag{II.11}$$

giving at once

$$F_2(\xi_1,\xi_2;t)=\left\langle\left\{1+\frac{\lambda_{40}}{3!}\left[\frac{\partial^2}{\partial\psi_1^2}+\frac{\partial^2}{\partial\psi_2^2}\right]+\frac{1}{3\partial\psi r_o}\left[\Lambda_{31}(t)\frac{\partial}{\partial\psi_1}+\Lambda_{13}(t)\frac{\partial}{\partial\psi_2}\right]\right.\right.$$

$$\left.\left.+\frac{\Lambda_{22}(t)}{3!}\left[\frac{\partial^2}{\partial(\psi r_o)^2}+2\frac{\partial^2}{\partial\psi_1\partial\psi_2}\right]\right\}\right.$$

$$\left.\times\exp\left\{-\frac{1}{2}\left[\psi_1\xi_1^2+2\psi r_o\xi_1\xi_2\cos(\omega_o t-\theta)+\psi_2\xi_2^2\right]\right\}\right|_{\psi_1=\psi_2=\psi}\Bigg\rangle_{\theta\ av}. \quad \text{(II.12)}$$

After the derivatives have been found, the subscripts are no longer desirable since the noise is stationary. Eq. (II.12) is the natural generalization of Eq. (II.7) as can be seen by expressing the differential operator in matrix form

$$F_2(\xi_1,\xi_2;t)=\left\langle\left\{1+\frac{1}{3!}\left\|\frac{\partial}{\partial\psi_1}\ \frac{\partial}{\partial\psi r_o}\ \frac{\partial}{\partial\psi_2}\right\|\left\|\begin{matrix}\Lambda_{40}&\Lambda_{31}&\Lambda_{22}\\ \Lambda_{31}&\Lambda_{22}&\Lambda_{13}\\ \Lambda_{22}&\Lambda_{13}&\Lambda_{40}\end{matrix}\right\|\left\|\begin{matrix}\frac{\partial}{\partial\psi_o}\\ \frac{\partial}{\partial\psi\Lambda_o}\\ \frac{\partial}{\partial\psi_2}\end{matrix}\right\|\right\}\right.$$

$$\left.\times F_2(\xi_1,\xi_2;t)_{gauss}\right|_{\psi_1=\psi_2=\psi}\Bigg\rangle_{\theta\ av}. \quad \text{(II.13)}$$

Appendix III

Envelope and Phase Distributions

Often the distributions of the slowly varying components are needed. It is obviously desirable to relate these to the distributions of the instantaneous value which are usually previously known. Again it is most convenient to work with the characteristic function and the series for the moments. The in-phase and quadrature components are defined from Eq. (2.19), $V(t) = X(t) \cos \omega_o t + Y(t) \sin \omega_o t$. The first-order moments are then

$$\mu_{mn} = \langle X^m Y^n \rangle_{av} = \langle R^{m+n} \cos^m \theta' \sin^n \theta' \rangle_{av} \qquad \text{(III.1)}$$

The characteristic function when written in polar coordinates is

$$F_{X,Y}(\rho\cos\phi, \rho\sin\phi) = \sum_{\substack{M=0 \\ m+n=M}}^{\infty} \frac{\mu_{mn}}{m!n!} (i\rho)^{m+n} \cos^m\phi \sin^n\phi \qquad \text{(III.2)}$$

Substituting Eq. (III.1) in Eq. (III.2), and using the binomial theorem on the terms of fixed value of M, we find that

$$F_{X,Y}(\rho\cos\phi, \rho\sin\phi) = \sum_{M=o}^{\infty} \frac{(i\rho)^M}{M!} \langle R^M \cos^M(\theta' - \phi) \rangle_{av} \qquad \text{(III.3)}$$

If θ is independent of R and uniformly distributed, the average may be carried out to give the Mth moment of V; otherwise, the shift in the angle by an amount ϕ may change the value of the average so that it is not the Mth moment. In the former case, we have the desired result

$$F_{X,Y}(\rho \cos \phi, \rho \sin \phi) = F_V(\rho) \quad . \qquad \text{(III.4)}$$

To obtain the distribution of the envelope alone, the restriction may be relaxed. In general, we have that

$$W(R,\theta) = \frac{R}{(2\pi)^2} \int_o^{\infty} \int_o^{2\pi} \rho\, d\rho\, d\phi\, e^{i\rho R\cos(\theta-\phi)} F_{X,Y}(\rho\cos\phi, \rho\sin\phi) \quad . \qquad \text{(III.5)}$$

The integration over θ can be performed, after which ϕ will appear only in the characteristic function. Then the cosine factor in Eq. (III.3) can be averaged over ϕ, which is now isotropic, making the distribution of θ' in Eq. III.3 immaterial. The final result is

$$W(R) = R\int_0^\infty \rho\, J_o(\rho R)\; F_V(\rho)\, d\rho \quad . \tag{III.6}$$

This equation is stronger than the usual relation between the Hankel transform and two-dimensional Fourier transform of an isotropic function [104]. For one thing, the condition of isotropy has been shown to be unnecessary here; furthermore, when the characteristic function is isotropic, it is not only a function of R alone, which is true in general, but also is a function with physical meaning as a one-dimensional Fourier transform (Eq. III.4).

The extension of these results to second-order distributions is easily accomplished. The moments are

$$\mu_{mnpq}(t) = \langle X_1^m Y_1^n X_2^p Y_2^q \rangle_{av} = \langle R_1^{m+n} R_2^{p+q} \cos^m\theta_1 \sin^n\theta_1 \times \cos^p\theta_2 \sin^q\theta_2 \rangle_{av} \tag{III.7}$$

The characteristic function can be put in the form corresponding to Eq. (III.3), namely,

$$F_{2X,Y}(\rho_1\cos\phi_1,\ \rho_1\sin\phi_1;\ \rho_2\cos\phi_2,\ \rho_2\sin\phi_2;\ t)$$

$$= \sum_{M+P=0}^{\infty} \frac{(i\rho_1)^M (i\rho_2)^P}{M!P!} \langle R_1^M R_2^P \cos^M(\theta_1'-\phi_1)\cos^P(\theta_2'-\phi_2)\rangle_{av} \tag{III.8}$$

If θ_1 is uniformly distributed, the average can be carried out, giving

$$F_{2X,Y}(\rho_1\cos\phi_1, \rho_1\sin\phi_1;\ \rho_2\cos\phi_2,\ \rho_2\sin\phi_2;t) = F_{2V}(\rho_1, \rho_2; t, \cos(\phi_2-\phi_1)) \ , \tag{III.9}$$

that is, wherever $\cos\omega_o t$ appeared in the characteristic function for V, $\cos(\phi_2-\phi_1)$ will now appear.

If the distribution of θ_1 is not required, then, as before, integrations

over first θ_1, then ϕ_1 gives the analogue to Eq. (III.6)

$$W_2(R_1,R_2,\theta,t) = R_1R_2\int_0^\infty \int_0^\infty \int_0^{2\pi} \frac{d\phi}{(2\pi)^2} d\,\rho_1\, d\rho_2\, \rho_1\rho_2$$

$$\times J_o\left(\left[\rho_1^2R_1^2 + \rho_2^2R_2^2 + 2\rho_1\rho_2R_1R_2\cos(\theta-\phi)\right]^{1/2}\right)$$

$$\times F_{2v}(\rho_1,\rho_2;t,\cos\phi) \quad , \qquad \text{(III.10)}$$

where

$$\theta = \theta_2 - \theta_1 \quad , \quad \text{and} \quad \phi = \phi_2 - \phi_1 \quad .$$

Appendix IV.

Clutter Fluctuations due to Movement of the Scatterers

If the scatterers in one resolving volume move between pulses, e.g., are blown by the wind, then the position of the kth scatterer will change in the time t by an amount $d_k = v_k t$, where v_k is the component of the scatterer's velocity along the radius vector to the radar; t is assumed short enough so that v_k is constant. The change in distance will alter the time of arrival of the pulse reflected from the scatterer by an amount $\Delta t'_k = t'_{2k} - t'_{1k} = 2v_k t/c$. The clutter return at time t_z is then

$$V(t_2) = \sum_{k=1}^{K} a_{2k} h\left(\frac{t_1 - t'_{1k}}{\tau} - \frac{2v_k t}{c\tau}\right) \cos\left\{\omega_o (t_1 + t) - \omega_T \frac{2v_k t}{c} - \psi_{2k}\right\} . \quad \text{(IV.1)}$$

Because the start of each transmitter pulse serves as a new origin of time, the time difference $t = t_2 - t_1$, appears in the envelope factor only in t'_2, the time of arrival of the new transmitter pulse; furthermore, the phase change in the rapidly varying part depends on the transmitter frequency, ω_T, not on the i-f frequency, ω_o. From this equation and Eq. (3.1) the semi-invariants are found to be

$$\lambda_{mn}(t) = \gamma \left\langle a_1^m a_2^n \int_{-\infty}^{\infty} h^m(x) h^n\left(x + \frac{2vt}{c\tau}\right) \cos^m(\omega_o \tau x - \psi_1) \right.$$

$$\left. x \cos^m\left(\omega_o \tau x + \omega_T \frac{2vt}{c} + \omega_o t - \psi_2\right) dx \right\rangle_{av} , \quad \text{(IV.2)}$$

where $x = t/\tau$.

The effect of moving scatterers may be illustrated by studying the correlation function. We have

$$r(t) = \frac{\lambda_{11}(t)}{\lambda_{20}} = r_o(t) \cos(\omega_o t + \alpha) ,$$

$$r_o(t) = r_a(t)\left| \left\langle r_h\left(2\frac{vt}{c\tau}\right) e^{\frac{2i\omega_T vt}{c} - i\psi} \right\rangle_{v,\,\psi\,av} \right|$$

$$\tan\alpha = \frac{\left\langle r_h\left(2\frac{vt}{c\tau}\right) \sin\left(\omega_T \frac{2vt}{ch} - \psi\right)\right\rangle_{av}}{\left\langle r_h\left(2\frac{vt}{c\tau}\right) \cos\left(\omega_T \frac{2vt}{c} - \psi\right)\right\rangle_{av}} \quad . \tag{IV.3}$$

Here $\psi = \psi_2 - \psi_1$, $r_a(t) = \langle a_1 a_2 \rangle / \langle a^2 \rangle$,

and

$$r_{h\frac{(t)}{\tau}} = \int_{-\infty}^{\infty} h(x)\, h\left(x+\frac{t}{\tau}\right) dx \Big/ \int_{-\infty}^{\infty} h^2(x)\, dx \quad .$$

This equation corresponds to the one first found by Siegert,[105] except that here the pulsed nature of the clutter is included in the analysis, appearing through the correlation function of the pulse envelope $r_h(2vt/c\tau)$.

In particular situations, the correlation function is usually simpler than Eq. (IV.3) seems to indicate. Almost always the motion of the scatterers varies the envelope dependence so much more slowly than the phase factor that the envelope correlation function, $r_h(t)$, may be taken as unity during the time of significant variations in $r_o(t)$. The pulse envelope correlation function will drop to near zero when the argument, $2vt/c\tau$, is near unity, i.e., a time difference comparable to the pulse duration. One can argue that up to $2vt/c\tau \sim 0.1$, this correlation function may be taken as one. Then the velocity average becomes

$$\int_{-\infty}^{\infty} r_h\left(\frac{2vt}{c\tau}\right) e^{\frac{2i\omega_T vt}{c}} W(v)\, dv = \int_{\frac{-c\tau}{20t}}^{\frac{c\tau}{20\tau}} e^{\frac{2i\omega_T vt}{c}} W(v)\, dv \tag{IV.4}$$

With a 1-μsec pulse, these limits are $\frac{5.00}{t}$, (velocities in m/sec), so that if the probability of velocities exceeding this limit is sufficiently small, the limits on the right-hand side can be made infinite, giving

$$\left\langle r_h\left(\frac{2vt}{c\tau}\right) e^{\frac{2i\omega_T vt}{c}} \right\rangle_v \doteq F_v\left(\frac{2\omega_T t}{c}\right) \quad , \tag{IV.5}$$

where F_v is the characteristic function of the velocity distribution. A reasonable upper limit on significant velocity values is $\bar{v} + 3\sigma_v$, which for "window" is about 2-5 m/sec. Thus up to times of the order of one second, the correlation function assumes the simple form of Eq. (IV.5). The argument of the characteristic function is then sufficiently large, so that the correlation function $r_o(t)$ is negligibly small.

As a specific illustration, consider the case of square pulses reflected from clutter with a gaussian velocity distribution. Then

$$\left| \left\langle r_h \left(\frac{2vt}{c\tau}\right) e^{\frac{2i\omega_T vt}{c}} \right\rangle_v \right| = \left| \left\langle \left(1 - \frac{2vt}{c\tau}\right) e^{\frac{2i\omega_T vt}{c}} \right\rangle_v \right|$$

$$= \left| \left(1 + \frac{i}{\tau}\frac{d}{d\omega_T}\right) F_v\left(\frac{2\omega_T t}{c}\right) \right|$$

$$= \left| 1 - \frac{2\bar{v}t}{c\tau} - i\,\frac{4\sigma_v^2 \omega_T t^2}{c^2 \tau} \right| e^{-\frac{2\sigma_v^2 \omega_T^2 t^2}{c^2}}$$

$$= \left| 1 - \bar{v}t\,(6.7\times10^{-3}) - i\,\sigma_v^2 t^2\,(2.5\times10^{-2}) \right| e^{-\sigma_v^2 t^2\, 800.0} \qquad \text{(IV.6)}$$

Clearly, the exponential will ensure the effective vanishing of the whole expression before the effect of the envelope correlation function can be felt at all, even for the case of an airborne radar measuring ground clutter ($\bar{v} \sim 500$ mph $\doteq$ 250 m/sec, $\sigma_v \sim 1$ m/sec).

The normalized correlation function of Eq. (IV.3) is thus

$$r_o(t) = r_a(t) \left| F_v\left(\frac{2\omega_T t}{c}\right) F_\psi(-1, 1; t) \right| , \qquad \text{(IV.7)}$$

where $F_\psi(\xi_1, \xi_2; t)$ is the second-order characteristic function of the phase.

Furthermore, the change in amplitude of the return due to the change in range is so small as to be negligible, so that the amplitude correlation function $r_a(t)$ depends only on changes in aspect of the scatterers with time.

Where the aspect of the scatterer either changes very slowly or does not affect the amplitude of the return (e.g., "window" sea return), then $r_a(t)$ is also unity. The phase of the scatterers, ψ_h, is usually the same from pulse to pulse so that the correlation function reduces to the magnitude of the velocity characteristic function alone.

Not very much is known about the velocity distribution of scatterers. T.S. George [106] has considered the problem of a moving radar and fixed clutter, obtaining fluctuation values through numerical integration without explicitly calculating the correlation function. Both Hilst [107] and Fleisher [108] have studied the inference of velocity distributions from experimentally observed correlation functions; however, as yet the time dependence of the correlation function is not a settled question. In particular, all of the three types of time dependence considered in section IV of this report are valid possibilities on the present experimental evidence.

Appendix V

Output Power

To calculate the output power requires finding a general moment of the input envelope, as Eq. (4.4) shows. Using the nearly gaussian envelope distribution, Eq. (2.26), we have

$$\langle R^{2\nu}\rangle_{av} = \left[1 + \frac{\lambda_{40}}{3!}\frac{\partial^2}{\partial\psi^2} + O(\gamma^{-2})\right]\int_0^\infty \frac{R^{2\nu+1}}{\psi} I_o\left(\frac{A_o R}{\psi}\right) e^{-\frac{R^2+A_o^2}{2\psi}} dR \qquad (V.1)$$

The integral is a generalization of Weber's exponential integral [109] well known to give

$$\langle R^{2\nu}\rangle_{av} = \left[1 + \frac{\lambda_{40}}{3!}\frac{\partial^2}{\partial\psi^2} + O(\gamma^{-2})\right]\Gamma(\nu+1)(2\psi)^\nu {}_1F_1(-\nu;1;-p) \qquad (V.2)$$

where ${}_1F_1(-\nu;1;-p)$ is the confluent hypergeometric function and $p = A_o^2/2\psi$ is the input signal-to-noise power ratio. The indicated differentiation can be carried out most easily by using the series for the hypergeometric function, (Eq. VI.8), to give the final result

$$\langle R^{2\nu}\rangle_{av} = \Gamma\left(\frac{\nu}{2}+1\right)(2\psi)^\nu \left[{}_1F_1(-\nu;1;-p) + \frac{\lambda_{40}}{3!\psi^2}\nu(\nu-1){}_1F_1(-\nu+2;1;-p) + O(\gamma^{-2})\right] \qquad (V.3)$$

For the d-c power, the square of the νth-moment is required, which is found by replacing 2ν by ν in Eq. (V.3). The 2νth-moment is slightly more convenient to use in discussing the nearly gaussian correction term so the next paragraph treats only the total power.

The nearly gaussian deviation in total power, as a function of ν and p, depends on $\nu(\nu-1)\,{}_1F_1(-\nu+2;1;-p)$. The general behavior of the hypergeometric function can be found by examining the cases of integral ν, and interpolating, which is possible because the hypergeometric function is a continuous function of its parameters. A graph of these functions is shown in Fig. 17. When ν is greater than one, both $\nu(\nu-1)$ and the hypergeometric function are positive, so the correction term is positive. When ν is less than one, $\nu(\nu-1)$ is negative; and the hypergeometric function

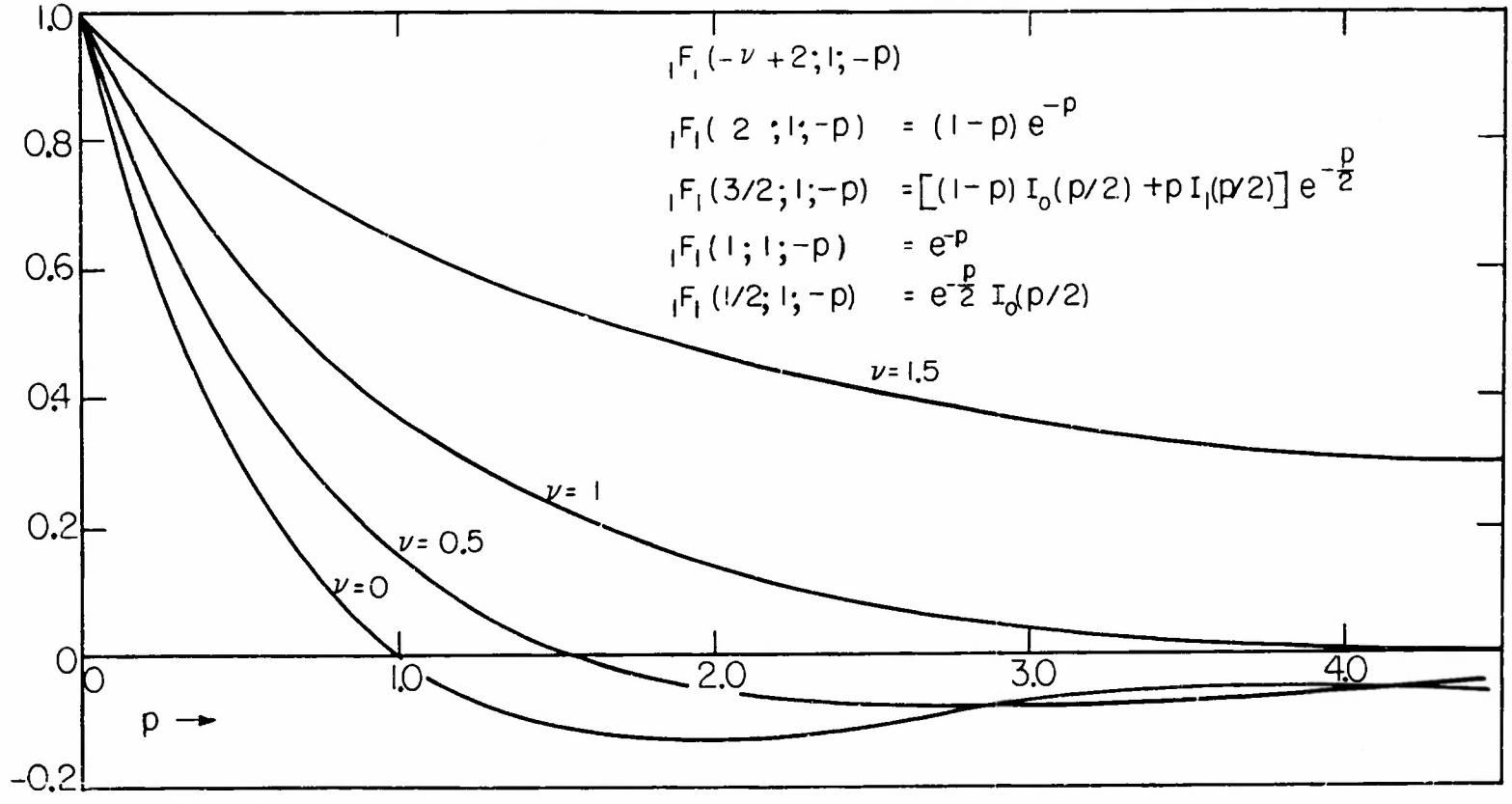

FIG. 17 CONFLUENT HYPERGEOMETRIC FUNCTIONS

changes sign at a value of p greater than one. Thus the correction term is negative if p is less than one, and is first positive and then negative if p is greater than one, the zero of the correction term moving toward $\nu = 1$ as p increases.

Appendix VI

Evaluation of the Output Correlation Function

The total output correlation function is given by Eq. (4.8),

$$R_T(t) = \int_C \frac{dz_1}{2\pi} \int_C \frac{dz_2}{2\pi} f(iz_1)\, f(iz_2)\, F_2(z_1, z_2)\, F_2(z_1, z_2)_{sig} \qquad (VI.1)$$

All the functions appearing here are known except for the characteristic function of the sine wave signal, which can be evaluated from its definition as an average, as done below. To form an ensemble from the determinate sine wave, we take a random phase as the ensemble parameter.

$$X(t;\phi) = A_o \cos(\omega_o t + \phi) \quad , \qquad (VI.2)$$

where

$$W(\phi) = \begin{cases} \frac{1}{2\pi} & \phi < 2\pi \\ 0 & \phi > 2\pi \end{cases}$$

Then

$$F_2(z_1, z_2)_{sig} = \frac{1}{2\pi} \int_o^{2\pi} e^{iz_1 A_o \cos(\omega_o t_o + \phi) + iz_2 A_o \cos(\omega_o [t_o + t] + \phi)} d\phi$$

$$= J_o\left(A_o \sqrt{z_1^2 + z_2^2 + 2z_1 z_2 \cos \omega_o t}\right)$$

$$= \sum_{n=0}^{\infty} \epsilon_n (-1)^n J_n(A_o z_1) J_n(A_o z_2) \cos n\omega_o t \, , \qquad (VI.3)$$

where we have used well known formulas of the theory of Bessel functions.

The characteristic function of the noise is

$$F_2(z_1, z_2) = [1 + L] \exp\left\{ -\frac{1}{2}[\psi_1 z_1^2 + \psi_2 z_2^2 + 2\psi r_o z_1 z_2 \cos \omega_o t] \right\} \Big|_{\psi_1 = \psi_2 = \psi} \qquad (VI.4)$$

where L is the differential operator in ψ_1, ψ_2 and ψr_o that appears in Eq. (2.18).

The correlation function can be separated into its zonal parts by expanding the trigonometric term in the exponent of Eq. (VI.4) as a Fourier series and combining with the Fourier series of Eq. (VI.3). The result is

$$R_T(t) = [1+L]\sum_{n=0}^{\infty}\sum_{m=0}^{\infty}\frac{(-1)^n}{2}\epsilon_m \cos m\omega_o t$$

$$\times \beta^2 \int_C \frac{dz_1}{2\pi}\frac{\Gamma(\nu+1)}{(iz_1)^{\nu+1}} e^{-\frac{\psi_1}{2}z_1^2} J_n(A_o z_1)\int_C \frac{dz_2}{2\pi}\frac{\Gamma(\nu+1)}{(iz_2)^{\nu+1}} e^{-\frac{\psi_2}{2}z_2^2} J_n(A_o z_2)$$

$$\times [(-1)^{m+n}\epsilon_{m+n} I_{m+n}(\psi r_o z_1 z_2) + (-1)^{|m-n|}\epsilon_{|m-n|} I_{|m-n|}(\psi r_o z_1 z_2)] . \qquad (VI.5)$$

This equation may be further simplified by noting that, for the receiver problem, only the low frequency zone, m=0, is required. Then the two contour integrals may be separated by expanding the modified Bessel function in a power series, giving

$$R(t) = [1+L]\sum_{n=0}^{\infty}\sum_{k=0}^{\infty}\frac{\epsilon_n(\frac{\psi r_o}{2})^{n+2k}}{k!(k+n)!} H_{n,k}(A_o,z_1) H_{n,k}(A_o,z_2)\Big|_{\psi_1=\psi_2=\psi} \qquad (VI.6)$$

where

$$H_{n,k}(A_o,z_j) = \frac{\beta\Gamma(\nu+1)}{2\pi i^{\nu+1}}\int_C dz_j\, e^{-\frac{\psi_j z_j^2}{2}} J_n(A_o z_j) z_j^{n+2k-\nu-1} ,$$

and the low-frequency correlation function R(t) appears. The $H_{n,k}$ functions may be evaluated by taking as the contour the real axis indented downward at the origin (see sec. 4 and App. III of ref. 100).

$$H_{n,k}(A_o,z_j) = \frac{\beta\Gamma(\nu+1)}{2\pi i^{\nu+1}}[1-(-1)^{\nu}]\int_o^{\infty} x^{n+2k-\nu-1} e^{-\frac{\psi_j x^2}{2}} J_n(A_o x)dx ,$$

provided $n+k > \nu/2$, so that the integral around the indentation vanishes.

The real integral is Weber's first exponential integral [110], so that the final result is

$$H_{n,k}(A_o,z_j) = \frac{\beta\Gamma(\nu+1)\left(-\frac{\nu}{2}\right)_{n+k}}{2\Gamma\left(\frac{\nu}{2}+1\right)}(-1)^{n+k}\,\frac{p_j^{\frac{n}{2}}\,\psi_j^{\frac{\nu}{2}-\frac{n+2k}{2}}}{n!}\,{}_1F_1\left(-\frac{\nu}{2}+n+k;n+1;-p_j\right) . \tag{VI.7}$$

In this equation, $p_j = A_o^2/2\psi_j$, and ${}_1F_1$ is the confluent hypergeometric function. The generalized hypergeometric function is defined formally as

$${}_pF_q(a_1,\ldots a_p;\, b_1,\ldots b_q;x) \equiv \sum_{n=o}^{\infty} \frac{\prod_{i=1}^{p}(a_i)_n}{\prod_{i=1}^{q}(b_i)_n}\,\frac{x^n}{n!} , \tag{VI.8}$$

where

$$(a)_n \equiv \frac{\Gamma(a+n)}{\Gamma(a)} = \prod_{i=o}^{n-1}(a+i) .$$

In this report, only the three functions ${}_1F_1$, ${}_2F_1$, and ${}_2F_0$ are needed.

Equation (VI.7) is an integral function of $n + k - \nu/2$ and, therefore, by analytic continuation $H_{n,k}(A_o,z_j)$ equals the right side of Eq. (VI.7) without any restriction on ν. The correlation function is thus

$$R(t) = [1+L]\frac{\beta^2\Gamma^2(\nu+1)}{4\Gamma^2\left(\frac{\nu}{2}+1\right)}\left(\frac{\psi_1\psi_2}{4}\right)^{\frac{\nu}{2}}$$

$$\times\sum_{n=o}^{\infty}\sum_{k=o}^{\infty}\frac{\epsilon_n(p_1p_2)^{\frac{n}{2}}}{k!\,n!^2(k+n)!}\left(\frac{\psi^2 r_o^2}{\psi_1\psi_2}\right)^{\frac{n+2k}{2}}\left(-\frac{\nu}{2}\right)_{n+k}^2$$

$$\times\,{}_1F_1\left(-\frac{\nu}{2}+n+k;n+1;-p_1\right){}_1F_1\left(-\frac{\nu}{2}+n+k;n+1;-p_2\right)\Bigg|_{\psi_1=\psi_2=\psi} \tag{VI.9}$$

By expanding the hypergeometric functions and summing over k, an alternate form may be found, viz.,

$$R(t) = [1 + L]\,\frac{\beta^2\Gamma^2(\nu+1)}{4\Gamma^2(\frac{\nu}{2}+1)}\left(\frac{\psi_1\psi_2}{4}\right)^{\frac{\nu}{2}}$$

$$\times\sum_{n=o}^{\infty}\sum_{i=o}^{\infty}\sum_{j=o}^{\infty}\frac{\epsilon_n(-1)^{i+j}\,p_1^{\,i+\frac{n}{2}}\,p_2^{\,j+\frac{n}{2}}}{i!\,j!(i+n)!\,(j+n)!\,n!}\left(\frac{\psi^2 r_o^{\,2}}{\psi_1\psi_2}\right)^{\frac{n}{2}}(-\tfrac{\nu}{2})_{i+n}(-\tfrac{\nu}{2})_{j+n}$$

$$\times\,{}_2F_1\left(-\frac{\nu}{2}+i+n,\,-\frac{\nu}{2}+j+n;\,n+1;\,\frac{\psi^2 r_o^{\,2}}{\psi_1\psi_2}\right)\Bigg|_{\psi_1=\psi_2=\psi}\quad . \qquad \text{(VI.10)}$$

When p is small, this last is the better form, since it is a power series in p. For large p, the ordinary asymptotic expansion of the confluent hypergeometric function may be substituted into Eq. (VI.9) to give a formal asymptotic expansion of the correlation function

$${}_1F_1(a;c;-x)\simeq\frac{\Gamma(c)}{\Gamma(c-a)}\,x^{-a}\;{}_2F_0\left(a,1+a-c;\frac{1}{x}\right)+O\left(e^{-x}\right)\quad , \qquad \text{(VI.11)}$$

$$|x|>> a \quad , \quad |x|>> c \quad .$$

$$R(t)\simeq[1+L]\,\frac{\beta^2\Gamma^2(\nu+1)}{4\Gamma^4(\frac{\nu}{2}+1)}\left(\frac{A_o^{\,2}}{4}\right)^{\nu}$$

$$\times\sum_{n=o}^{\infty}\sum_{k=o}^{\infty}\frac{\epsilon_n}{k!\,(k+n)!}\,(-\tfrac{\nu}{2})_k^2\,(-\tfrac{\nu}{2})_{n+k}^2\,\left(\frac{r_o}{p}\right)^{n+2k}$$

$$\times\;{}_2F_0\left(-\frac{\nu}{2}+n+k,\,-\frac{\nu}{2}+k;\,\frac{1}{p_1}\right)\;{}_2F_0\left(-\frac{\nu}{2}+n+k,\,-\frac{\nu}{2}+k;\,\frac{1}{p_2}\right)\quad . \qquad \text{(VI.12)}$$

Notice that as p tends to infinity, the correlation function reduces to that for the signal alone, as it should; however, the asymptotic nature of the equation is not assured at present, since Eq. (VI.11) is not valid for values of n and/or k comparable to or greater than p. In these cases, by using the asymptotic expansions appropriate to $n>> p, k$; $k>> p, n$; $n,k>> p$;

$n \doteq p$; $k \doteq p$; $n \doteq k \doteq p$; [111] it can be shown that the leading term in the asymptotic expansion is of exponential order. Thus the terms which are neglected in using a finite part of Eq. (VI.12) are actually of even smaller order than the equation indicates so that the asymptotic expansion is valid, with the restriction that p must be larger than the largest value of n or k appearing in the finite approximation. In the event that ν is an even integer, all the series involved terminate, and the left-and right-hand sides of Eq. (VI.12) are equal.

The remaining step is to evaluate the derivatives contained in the operator L. The strong signal case, Eq. (VI.12), contains only positive powers of the quantities to be differentiated, so that the result is simply obtained using the formula

$$\frac{d}{dx}\,{}_2F_0(a,b;cx) = abc\;{}_2F_0(a+1,b+1;cx) \quad . \tag{VI.13}$$

The result is, in abbreviated form,

$$R(t) \simeq \frac{\beta^2 \Gamma^2(\nu+1)}{4\Gamma^4(\frac{\nu}{2}+1)} \left(\frac{p\psi}{2}\right)^{\nu} \sum_{n=o}^{\infty}\sum_{k=o}^{\infty} \frac{\epsilon_n}{k!\,(n+k)!} \left(\frac{r_o}{p}\right)^{n+2k}$$

$$\times \left\{ \mathcal{J}^2(0) + \frac{\lambda_{40}}{3p^2\psi^2}\,\mathcal{J}(2)\mathcal{J}(0) + \frac{\Lambda_{31}(t)+\Lambda_{13}(t)}{3p^2\psi^2}\,(n+2k)\left(\frac{r_o}{p}\right)^{-1} \times \mathcal{J}(1)\mathcal{J}(0) \right.$$

$$\left. + \frac{\Lambda_{22}(t)}{3p^2\psi^2}\left[\frac{1}{2}(n+2k)(n+2k-1)\left(\frac{r_o}{p}\right)^{-2}\mathcal{J}^2(0) + \mathcal{J}^2(1)\right] \right\} \quad , \tag{VI.14}$$

where

$$\mathcal{J}(a) = \left(-\frac{\nu}{2}\right)_{n+k+a}\left(-\frac{\nu}{2}\right)_{k+a}\,{}_2F_0\left(-\frac{\nu}{2}+n+k+a, -\frac{\nu}{2}+k+a; \frac{1}{p}\right)$$

The weak signal case is more complicated, but with the analogue of Eq. (VI.13) for the ${}_2F_1$ function, and the additional formula

$$\frac{d}{dx}\left[x^a\,{}_2F_1(a,b;c;x)\right] = ax^{a-1}\,{}_2F_1(a+1,b;c;x) \quad ,$$

the result corresponding to Eq. (VI.14) is, also in abbreviated form,

$$R(t) = \frac{\beta^2 \Gamma^2(\nu+1)}{4\Gamma^2(\frac{\nu}{2}+1)} \left(\frac{\psi}{2}\right)^{\nu} \sum_{k=o}^{\infty} \sum_{m=o}^{\infty} \sum_{n=o}^{\infty} \frac{\epsilon_k (-1)^{m+n} r_o^{\,k} p^{k+m+n}}{k!(k+m)!m!(k+n)!n!}$$

$$\times \left\{ \mathcal{F}(0,0,0) + \frac{\lambda_{40}}{3\psi^2} \mathcal{F}(200) + \frac{\Lambda_{31}(t)+\Lambda_{13}(t)}{3\psi^2} \left[\frac{k}{r_o} \mathcal{F}(1,0,0) + \frac{2r_o}{k+1} \mathcal{F}(2,1,1) \right] \right.$$

$$\left. + \frac{\Lambda_{22}(t)}{3\psi^2} \left[\frac{k(k-1)}{2r_o^{\,2}} \mathcal{F}(0,0,0) + \frac{3k+2}{k+1} \mathcal{F}(1,1,0) + \frac{r_o^{\,2}}{(k+1)^2(k+2)} \mathcal{F}(2,2,2) \right] \right\}$$

where

$$\mathcal{F}(a,b,c) = (-\tfrac{\nu}{2})_{k+m+a} (-\tfrac{\nu}{2})_{k+m+b} \; {}_2F_1(-\tfrac{\nu}{2}+k+n+a, -\tfrac{\nu}{2}+k+m+b; k+1+c; r_o^{\,2}) \; .$$

When ν is an integer, the hypergeometric functions reduce to polynomials if ν is even, or to complete elliptic integrals if ν is odd.

Appendix VII

Effect of Nearly Gaussian Statistics on the Output Correlation Function

To determine whether the correlation in the output is increased or decreased by nongaussian noise as compared to gaussian noise, we study various special cases of $r_{out}(t)$.

When p is large, we may use the strong signal expression for the correlation function, Eq. (4.13), to obtain finally

$$r_{out}(t) = r_{out}(t)_{gauss}\left\{1+\frac{1}{6p\psi^2}\left[\nu\left(\frac{\nu}{2}-1\right)\left\{\frac{\Lambda_{31}(t)+\Lambda_{13}(t)}{r_o}-2\Lambda_{40}\right\}\right.\right.$$
$$\left.\left.+\left\{2\left(\frac{\nu}{2}\right)^2+\left(\frac{\nu}{2}-1\right)^2\right\}\left\{\frac{\Lambda_{22}(t)}{r_o}-\Lambda_{40}\right\}\right]+O(p^{-2},\gamma^{-2})\right\} \qquad \text{(VII.1)}$$

For the exponential and gaussian models, we see from Table 4.1 that the semi-invariant expressions in the inner braces are negative so that when ν is greater than two, the output correlation is reduced. When ν is quite small, the second term alone is important and again the output correlation is reduced. Near $\nu = 1$, the sign of the change in correlation varies because the output correlation functions cross each other. The boundaries between this region and those in which the nongaussian output correlation is less lie in the ranges $\nu = 0.4\text{-}.6$, $1.2\text{-}1.4$ for both models.

The boundary is not sharply defined since inside the region the gaussian and nearly gaussian curves cross each other.

For the linear model the nongaussian part of Eq. (VII.1) vanishes. We must then start again from the general strong signal result, Eq. (VI.14), including p^{-3} terms specialized for the linear model. Carrying this procedure through gives

$$r_{out}(t) = r_{out}(t)_{gauss}\left\{1-\frac{1-r_o}{64p^2\gamma}\left[7\nu^4-54\nu^3+126\nu^2-128\nu+56\right]+O(p^{-3},\gamma^{-2})\right\} \qquad \text{(VII.2)}$$

The difference between gaussian and nongaussian noise is of smaller order here than for the other two noise models. The polynomial has two real roots, when ν equals 1.55 and 4.54, between which points the nongaussian result has more correlation.

When no signal is present, Eq. (VI.15), which contains hypergeometric functions, must be used. The behavior of the correlation function as a function of ν is then still too difficult to predict for all times t; however, by expanding the hypergeometric functions in powers of $r_o^2(t)$ and $1 - r_o^2(t)$, the change in correlation can be found separately for large times and small times. Since the two results agree, we have confidence in the indicated answers.

For large times, the input correlation function is small and the expansion of the hypergeometric function around the origin is appropriate (Eq. (VI.8)). The normalized output correlation functions for the noise models are then

$$r_{out}(t) = r_o^2\left\{1 - \frac{(\frac{\nu}{2} - 1)}{\gamma} + O\left[\gamma^{-2}, \nu^2 r_o^2/4\right]\right\}, \text{ exponential model (VII.3)}$$

$$r_{out}(t) = r_o^2\left\{1 - \frac{\frac{\nu}{2} - 1}{\gamma\sqrt{\pi}}(3 - 2\sqrt{r_o}) + O\left[\gamma^{-2}, \nu^2 r_o^2/4\right]\right\} \text{ gaussian model (VII.4)}$$

$$r_{out}(t) = r_o^2\left\{1 + \frac{(\frac{\nu}{2} - 1)^2}{r_o\gamma} + O\left[\gamma^{-2}, \nu^2/4\right]\right\} \qquad \text{linear model (VII.5)}$$

These equations indicate that nongaussian noise of the linear type is always more correlated than the corresponding gaussian noise, with identical results for the exponential and gaussian models when ν is less than two, and opposite results for ν greater than two.

For small times, the expansion of the hypergeometric function in powers of $1 - r_o^2$ is needed. [112].

$$F(a,b;c;z) = \frac{\Gamma(c)\Gamma(c-a-b)}{\Gamma(c-a)\Gamma(c-b)} F(a,b;a+b-c+1;1-z)$$

$$+ \frac{\Gamma(c)\Gamma(a+b-c)}{\Gamma(a)\Gamma(b)} (1-z)^{c-a-b} F(c-a,c-b;c-a-b+1;1-z) \quad . \qquad \text{(VII.6)}$$

Integral values of c-a-b, which correspond to integral values of ν, are exceptional; however, the modifications of Eq. (VII.6) that are then needed when ν is greater than one are of higher order than the terms appearing in Eqs. (VII.7-9)[113]. For the linear detector the results are already known (Table 4.3) so that a special treatment of this case here is unnecessary.

The normalized output correlation functions are

exponential model:

$$r_{cut}(t) = r_{out}(t)_{gauss}\left\{1 - \frac{\Lambda_{40}(1-r_o^2)}{48\psi^2\left[1-\frac{\Gamma^2(\frac{\nu}{2}+1)}{\Gamma(\nu+1)}\right]^2}\frac{\nu^2}{\nu-1}\left[30-4-\frac{\Gamma^2(\frac{\nu}{2}+1)}{\Gamma(\nu+1)}(\nu^2+2\nu-4)\right]\right.$$

$$\left. + \frac{\Lambda_{40}(1-r_o^2)^\nu}{3\psi^2\left[1-\frac{\Gamma^2(\frac{\nu}{2}+1)}{\Gamma(\nu+1)}\right]}\nu\frac{\Gamma^4(\frac{\nu}{2}+1)}{\Gamma^2(\nu+1)} + O(\gamma^{-2}(1-r_o^2)^2)\right\} \qquad \text{(VII.7)}$$

gaussian model:

$$r_{out}(t) = r_{out}(t)_{gauss}\left\{1 - \frac{\Lambda_{40}(1-r_o^2)2\nu^2}{48\psi^2\left[1-\frac{\Gamma^2(\frac{\nu}{2}+1)}{\Gamma(\nu+1)}\right]^2}\left[1-\frac{\Gamma(\frac{\nu}{2}+1)\Gamma(\frac{\nu}{2}+2)}{\Gamma(\nu+1)}\right] + O(\gamma^{-2},(1-r_o^2)^2)\right\} \qquad \text{(VII.8)}$$

linear model:

$$r_{cut}(t) = r_{out}(t)_{gauss}\left\{1 + \frac{\Lambda_{40}(1-r_o^2)}{48\psi^2\left[1-\frac{\Gamma^2(\frac{\nu}{2}+1)}{\Gamma(\nu+1)}\right]^2}\frac{\nu}{\nu-1}\left[2(\frac{\nu}{2}-1)^2+\frac{\Gamma^2(\frac{\nu}{2}+1)}{\Gamma(\nu+1)}(\nu^3-\frac{3}{2}\nu^2+2\nu-2)\right]\right.$$

$$\left. + \frac{\Lambda_{40}(1-r_o^2)^\nu}{6\psi^2\left[1-\frac{\Gamma^2(\frac{\nu}{2}+1)}{\Gamma(\nu+1)}\right]}\nu\frac{\Gamma^4(\frac{\nu}{2}+1)}{\Gamma^2(\nu+1)} + O(\gamma^{-2},(1-r_o^2)^2)\right\} \qquad \text{(VII.9)}$$

Appendix VIII

The Effect of Nearly Gaussian Statistics with Finite Averaging

When the signal-to-noise ratio is large, the output correlation function is comparatively simple, Eq. (4.13), so that the variance for general ν can be found, following Eq. (4.15),

exponential model:

$$\sigma_E^2 = \frac{2K}{x^2}\left\{\left[2+\frac{\nu(\nu-2)}{p}\left(1+\frac{1}{4\gamma}\right)\right]\left[e^{-x}+x-1\right]\right.$$
$$+\frac{1}{4p}\left[\left(\frac{\nu}{2}\right)^2+\left(\frac{\nu}{2}-1\right)^2+\frac{1}{2\gamma}\left\{2\left(\frac{\nu}{2}\right)^2+\left(\frac{\nu}{2}-1\right)^2\right\}\right]\left[e^{-2x}+2x-1\right]$$
$$\left.+\frac{1}{4p\gamma}\frac{\nu}{2}\left(\frac{\nu}{2}-1\right)\left[e^{-3x}+3x-1\right]+O(p^{-2},\gamma^{-2})\right\} \qquad \text{(VIII.1)}$$

gaussian model:

$$\sigma_G^2 = \frac{\sqrt{2\pi}\,K}{x}\left\{\left[2+\frac{\nu(\nu-2)}{p}\right]\Phi\left(\frac{x}{\sqrt{2}}\right)\right.$$
$$+\frac{1}{p\sqrt{2}}\left[\left(\frac{\nu}{2}\right)^2+\left(\frac{\nu}{2}-1\right)^2+\frac{1}{2\gamma\sqrt{\pi}}\left\{2\left(\frac{\nu}{2}\right)^2+\left(\frac{\nu}{2}-1\right)^2\right\}\right]\Phi(x)$$
$$\left.+\frac{\nu(\nu-2)}{p\gamma\sqrt{6\pi}}\Phi\left(\frac{x\sqrt{3}}{2}\right)+O(p^{-2},\gamma^{-2})\right\}$$
$$+\frac{K}{x^2}\left\{\left[2+\frac{\nu(\nu-2)}{p}\right]\left[e^{-\frac{x^2}{2}}-1\right]+\frac{1}{2p\sqrt{2}}\left[\left(\frac{\nu}{2}\right)^2+\left(\frac{\nu}{2}-1\right)^2\right.\right.$$
$$\left.+\frac{1}{2\gamma\sqrt{\pi}}\left\{2\left(\frac{\nu}{2}\right)^2+\left(\frac{\nu}{2}-1\right)^2\right\}\right]\left[e^{-x^2}-1\right]$$
$$\left.+\frac{\nu(\nu-2)}{3p\gamma\sqrt{\pi}}\left[e^{-\frac{3x^2}{4}}-1\right]+O(p^{-2},\gamma^{-2})\right\} \qquad \text{(VIII.2)}$$

linear model:

$$\sigma_L^2 = \frac{K}{3}\left\{\left[2 + \frac{\nu(\nu-2)}{p} + \frac{1}{2p\gamma}\left\{2\left(\frac{\nu}{2}\right)^2 + \nu(\nu-2) + \left(\frac{\nu}{2}-1\right)^2\right\}\right][3-x]\right.$$

$$\left. + \frac{1}{p}\left[\left(\frac{\nu}{2}\right)^2 + \left(\frac{\nu}{2}-1\right)^2\right][3 - 2x + \frac{x^2}{2}] + O(p^{-2}, \gamma^{-2})\right\}, \quad x \leq 1;$$

$$= \frac{K}{3x^2}\left\{\left[2 + \frac{\nu(\nu-2)}{p} + \frac{1}{2p\gamma}\left\{2\left(\frac{\nu}{2}\right)^2 + \nu(\nu-2) + \left(\frac{\nu}{2}-1\right)^2\right\}\right][3x-1]\right.$$

$$\left. + \frac{1}{2p}\left[\left(\frac{\nu}{2}\right)^2 + \left(\frac{\nu}{2}-1\right)^2\right][4x-1] + O(p^{-2}, \gamma^{-2})\right\} \quad x \geq 1; \qquad \text{(VIII. 3)}$$

where

$$x = \beta T$$

$$\Phi(x) = \frac{2}{\sqrt{\pi}}\int_0^x e^{-t^2}\, dt$$

and

$$K = \frac{\beta^2 \Gamma^2(\nu+1)}{4\Gamma^4(\frac{\nu}{2}+1)}\left(\frac{p\psi}{2}\right)^{\nu} .$$

When the signal is large, the nongaussian terms are all of higher order than p^{-1} and so will not appear in $\bar{I}^2$, to the order used above. Thus the effect of the nearly gaussian statistics on $\sigma^2/\bar{I}^2$ is entirely fixed by the terms appearing in Eqs. (VIII. 1-3). For large x, the variances reduce to

exponential model:

$$\sigma_E^2 = \frac{2K}{x}\left\{2 + \frac{1}{2p}\left[8\frac{\nu}{2}\left(\frac{\nu}{2}-1\right) + \left(\frac{\nu}{2}\right)^2 + \left(\frac{\nu}{2}-1\right)^2\right]\right.$$

$$+ \frac{1}{p\gamma}\left[\frac{4}{3}\frac{\nu}{2}\left(\frac{\nu}{2}-1\right) + \frac{1}{2}\left(\frac{\nu}{2}\right)^2 + \frac{1}{4}\left(\frac{\nu}{2}-1\right)^2\right]$$

$$\left. + O(x^{-1}, p^{-2}, \gamma^{-2})\right\} \qquad \text{(VIII. 4)}$$

gaussian model:

$$\sigma_G^2 = \frac{K\sqrt{2\pi}}{x}\left\{2 + \frac{1}{p\sqrt{2}}\left[\left(\frac{\nu}{2}\right)^2 + 4\sqrt{2}\,\frac{\nu}{2}\left(\frac{\nu}{2}-1\right) + \left(\frac{\nu}{2}-1\right)^2\right]\right.$$

$$\left. + \frac{1}{p\gamma\sqrt{2\pi}}\left[\left(\frac{\nu}{2}\right)^2 + \frac{4}{\sqrt{3}}\,\frac{\nu}{2}\left(\frac{\nu}{2}-1\right) + \frac{1}{2}\left(\frac{\nu}{2}-1\right)^2\right] + O(x^{-1}, p^{-2}, \gamma^{-2})\right\}, \qquad \text{(VIII.5)}$$

linear model:

$$\sigma_L^2 = \frac{K}{x}\left\{2 + \frac{2}{3p}\left[\left(\frac{\nu}{2}\right)^2 + 6\,\frac{\nu}{2}\left(\frac{\nu}{2}-1\right) + \left(\frac{\nu}{2}-1\right)^2\right]\right.$$

$$\left. + \frac{1}{2p\gamma}\left[2\left(\frac{\nu}{2}\right)^2 + 4\,\frac{\nu}{2}\left(\frac{\nu}{2}-1\right) + \left(\frac{\nu}{2}-1\right)^2\right] + O(x^{-1}, p^{-2}, \gamma^{-2})\right\} \qquad \text{(VIII.6)}$$

The nongaussian part of all three of these is positive for large and small ν and negative for ν near one. The two values of ν at which the nongaussian part of the variance changes sign are for the exponential model 0.33 and 1.42, for the gaussian model 0.38 and 1.33, and for the linear model, 0.46 and 1.26.

For the no-signal results, it is most convenient to start from an alternate expression for the relative variance.

$$\frac{R(t) - \bar{I}^2}{\bar{I}^2} = \frac{R(t) - R(\infty)}{R(0) - R(\infty)} \cdot \frac{R(0) - R(\infty)}{R(\infty)}$$

$$= r_{out}(t)\left(\frac{P_o - P_{d\text{-}c}}{P_{d\text{-}c}}\right). \qquad \text{(VIII.7)}$$

This form enables us to use the results already found for the behavior of $r_{out}(t)$. For noise alone, from Eqs. (4.5, 4.6), we have

$$\frac{P_o - P_{d\text{-}c}}{P_{d\text{-}c}} = \frac{\Gamma(\nu+1)}{\Gamma^2\left(\frac{\nu}{2}+1\right)}\left\{1 - \frac{\Gamma^2\left(\frac{\nu}{2}+1\right)}{\Gamma(\nu+1)} + \frac{\Lambda_{40}\nu^2}{12\psi^2} + O(\gamma^{-2})\right\} \qquad \text{(VIII.8)}$$

so that the nongaussian part of the power ratio is always positive. The relative variance is then

$$\frac{\sigma^2}{\bar{I}^2} = \left(\frac{P_o - P_{d\text{-}c}}{P_{d\text{-}c}}\right)\frac{2}{T}\int_o^T r_{out}(t)\left[1 - \frac{t}{T}\right]dt, \qquad \text{(VIII.9)}$$

in which 1 - t/T is always positive.

Since $r_{out}(t)$ is always greater for nearly gaussian noise for the linear model, it follows immediately that the nongaussian variance is always greater. When ν is less than two, the same is true of the exponential and gaussian models; however, for these, when ν is greater than two, $r_{out}(t)$ is less for nongaussian noise, so the answer is not immediately obvious. For the two models with r_o^2 small, from Eqs.(VII.3,4)

exponential model:

$$\frac{R(t)-\bar{I}^2}{\bar{I}^2} = r_o^2 \frac{\Gamma(\nu+1)}{\Gamma^2(\frac{\nu}{2}+1)}\left\{1 - \frac{\Gamma^2(\frac{\nu}{2}+1)}{\Gamma(\nu+1)} + \frac{1}{8\gamma}\left[\nu^2 + 4(2-\nu)\left\{1 - \frac{\Gamma^2(\frac{\nu}{2}+1)}{\Gamma(\nu+1)}\right\}\right] + O(\gamma^{-2}, r_o^2)\right\}, \qquad \text{(VIII.10)}$$

gaussian model:

$$\frac{R(t)-\bar{I}^2}{\bar{I}^2} = r_o^2 \frac{\Gamma(\nu+1)}{\Gamma^2(\frac{\nu}{2}+1)}\left\{1 - \frac{\Gamma^2(\frac{\nu}{2}+1)}{\Gamma(\nu+1)} + \frac{1}{8\gamma\sqrt{\pi}}\left[\nu^2 + 4(2-\nu)(3-2\sqrt{r_o})\left\{1 - \frac{\Gamma^2(\frac{\nu}{2}+1)}{\Gamma(\nu+1)}\right\}\right] + O(\gamma^{-2}, r_o^2)\right\}, \qquad \text{(VIII.11)}$$

The nongaussian part of both of these are now positive for all values of ν. When $1 - r_o^2$ is small, from Eqs. (VII.7,8), we have

exponential model:

$$\frac{R(t)-\bar{I}^2}{\bar{I}^2} = r_{out}(t)_{gauss} \frac{\Gamma(\nu+1)}{\Gamma^2(\frac{\nu}{2}+1)}\left\{1 - \frac{1}{32\gamma\left\{1 - [\Gamma^2(\frac{\nu}{2}+1)/\Gamma(\nu+1)]\right\}} \frac{\nu^2}{\nu-1}\right.$$

$$\left. \times \left[\nu(4 - 3\{1-r_o^2\}) + 4r_o^2 + \frac{\Gamma^2(\frac{\nu}{2}+1)}{\Gamma(\nu+1)}\left\{4r_o^2 - 2\nu(1+r_o^2) + \nu^2(1-r_o^2)\right\}\right] + O(\gamma^{-2}, (1-r_o^2)^2)\right\}, \qquad \text{(VIII.12)}$$

gaussian model:

$$\frac{R(t)-\bar{I}^2}{\bar{I}^2} = r_{out}(t)_{gauss} \frac{\Gamma(\nu+1)}{\Gamma^2(\frac{\nu}{2}+1)} \left\{ 1 + \frac{\nu^2}{32\gamma\sqrt{\pi}\left[1-\Gamma^2(\frac{\nu}{2}+1)/\Gamma(\nu+1)\right]} \right.$$

$$\times \left[(4 - 2\{1-r_o^2\}) \left(1 - \frac{\Gamma^2(\frac{\nu}{2}+1)}{\Gamma(\nu+1)} \right) + \frac{\Gamma^2(\frac{\nu}{2}+1)}{\Gamma(\nu+1)} \nu(1-r_o^2) \right]$$

$$\left. + O(\gamma^{-2}, (1-r_o^2)^2) \right\} \qquad \text{(VIII.13)}$$

These are also larger when the noise is nongaussian, so that finally we have the result that the variance is always larger with nongaussian noise than with gaussian noise when no signal is present.

This same approach can be used to find the change in the variance when nongaussian noise is present and the signal is strong. The power ratio is now

$$\frac{P_o - P_{d-c}}{P_{d-c}} = \frac{\nu^2}{2p} \left\{ 1 + \frac{2\nu^2+3\nu+8}{8p} + \frac{\Lambda_{40}}{6p\psi^2} \frac{7\nu^2-12\nu+14}{4} + O(p^{-2}, \gamma^{-2}) \right\} . \qquad \text{(VIII.14)}$$

The nongaussian part is negative between $\nu = 0.45$ and $\nu = 1.26$. Since the nongaussian part of $r_{out}(t)$ for the linear noise model is of order p^{-2}, the power ratio alone will determine the sign of the change in the variance. So with these two noise models, the zeros of Eq. (VIII.14) correspond rather closely to those of $r_{out}(t)$ so that when ν is small, the nongaussian variance is more; when ν is near one, it is less; and when ν is two or more, it is greater again. Finding more exact boundaries by this method is not worth while since they are already known from the first part of this appendix.

References

1. F. Y. Edgeworth, Trans. Camb. Phil. Soc. 20 (1905), p. 36.

2. K. Pearson, Drapers Co. Res. Mem. Biometric Series III, 1906, "Mathematical Theory of Migration."

3. M. Crofton, ref. 1 and 9th ed. Encyclopedia Brittanica, "Probability."

4. J. L. Lawson and G. E. Uhlenbeck, Threshold Signals. McGraw Hill 1950, Sec. 3.1, p. 33.

5. J. L. Doob, Stochastic Processes, Wiley, 1953, Sec. 2.1, p. 46.

6. S. O. Rice, Bell Syst. Tech. J. 23, 282 (1944); 24, 46 (1945).

7. M. C. Wang and G. E. Uhlenbeck, Rev. Mod. Phys. 17, 322 (1945).

8. J. L. Doob, op. cit., Sec. 2.6, p. 80.

9. H. Cramér, Mathematical Methods of Statistics, Princeton, 1946, Chap. 10.

10. J. L. Doob, op. cit., Sec. 1.11, p. 37.

11. J. L. Doob, op. cit., Sec. 2.8, p. 94.

12. N. Wiener, Acta Math. 55, 117 (1930).

13. A. Khintchine, Math. Ann. 109, 604 (1934).

13a. H. Hurwitz and M. Kac, Ann. Math. Stat. 15, 173 (1944).

14. W. Feller, Probability Theory, Vol. 1, Wiley, 1950, Sec. 6.5.

15. J. C. Kluyver, Proc. Sec. of Sci., K. Akad. van Wet. (Amsterdam) 8, 341 (1906).

16. D. Middleton, J. Appl. Phys. 22, 1143, 1153, 1326 (1951).

17. For a rigorous proof of the asymptotic nature of this expansion see H. Cramér, Random Variables and Probability Distributions, Cambridge Tracts in Math. 36 (1937).

18. Ref. 4, Chap. 6.

19. D. E. Kerr, ed., Propagation of Short Radio Waves, McGraw-Hill, 1951, Chaps. 6,7.

20. F. Block, M. Hamermesh, and M. Philips, RRL Report, 411-TM-127, 19 Jun 44, "Return Cross Sections from Randomly Oriented Resonant Half-wave Length Chaff."

21. Kerr, op. cit., Sec. 6.21.

22. Lawson and Uhlenbeck, op. cit., Sec. 6.5.

23. Kerr, op. cit., Chap. 7.

24. W. Trinks, Ann. Phys. 22, 561, 1935.

25. Kerr, op. cit. Sec. 8.6-8.7.

26. J. O. Laws and D. A. Parsons, Trans. Am. Geophys. Union, 1943, pt 2, p. 452.

27. L. J. Andrews et al, Naval Electronics Laboratory, Proc. I.R.E. 35, 351 (1947).

28. G. T. Rado, RL Rep. 603, 7 Mar 45, "Measurements of the Attenuation of K-band Waves by Rain."

29. W. J. Humphreys, Physics of the Air, McGraw-Hill, second ed, 1940.

30. D. B. Kerr, op. cit., Secs. 6.6-6.12.

31. G. G. Macfarlane and H. Davies, Proc. Phys. Soc. 58, 717(1946).

32. Kerr, op. cit. Sec. 6.10.

33. Kerr, op. cit. Sec. 6.9.

34. Kerr, op. cit. Fig. 6.20, p. 516.

35. Electronics, August 1946, p. 88.

36. Physics of Sound in the Sea, Summary Technical Report of Div. 6 NDRC, Vol. 8, Washington, D. C. 1946.

37. Principles of Underwater Sound. Extracted from Sum. Tech. Rep., Div. 6, NDRC, Vol. 7.

38. C. F. Eyring, R. J. Christenson, R. W. Raitt, J. Acoust. Soc. Am. 20, 462 (1948).

39. Principles of Underwater Sound, supra, Sec. 5, 4.2.

40. D. P. Loye and D. A. Proudfoot, J. Acoust. Soc. Am. 18, 446 (1947).

41. M. B. Dobrin, Science 105, 19 (1947).

42. F. A. Everest, R. W. Young, and M. W. Johnson, J. Acoust. Soc. Am. 20, 137 (1948).

43. Johnson, Everest, and Young, Bio. Bull. 93, 122 (1947).

44. W. W. Lewis, Protection of Transmission Systems against Lightning, Wiley, 1950.

45. B. F. J. Schonland, The Flight of Thunderbolts, Oxford, 1950.

46. H. Norinder, Tellus 1, no. 2, p. 1 (1949).

47. Ross Gunn et al., Proc. I.R.E. 34, 156P, 161P, 167P, 234, 241, 276 (1946).

48. W. H. Huggins, Final Report of Precipitation Static Reduction Research at Oregon State College, June 1941-March 1943, Commo. Sec. NDRC, OSRD No. 1907 (Edwards Bros. 1943).

49. C. G. Miller and L. B. Loeb, J. Appl. Phys. 22, 494, 614 (1951).

50. G. W. Trichel, Phys. Rev. 55, 384 (1938).

51. Gunn et al., op. cit., p. 241.

52. K. E. Fitzsimmons, Phys. Rev. 61, 175 (1942).

53. H. M. Hucke, Proc. I.R.E. 27, 301 (1939).

54. H. C. Vander Hulst, A Course in Radio Astronomy, Leiden, 1951.

55. J. L. Pawsey and D. E. Yabsley, Aust. J. Sci. Res. 2 A, 198 (1949).

56. M. Ryle, Proc. Roy. Soc. 195A, 82 (1949).

57. J. P. Wild, Aust. J. Sci.Res. 3A, 541 (1950).

58. J. P. Wild, Aust. J. Sci. Res. 3A, 599 (1950).

59. R. Payne-Scott and A. S. Little, Aust. J. Sci. Res. 5A, 32 (1952).

60. J. P. Wild, Aust. J. Sci. Res. 4A, 36 (1951).

61. R. Payne-Scott and A. S. Little, Aust. J. Sci. Res. 4A, 489,508 (1951).

62. J. H. Piddington and H. C. Minnett, Aust. J. Sci. Res. 2A 539 (1949).

63. V. A. Bailey, Phys. Rev. 78, 428 (1950).

64. D. Bohm and E. P. Gross, Phys. Rev. 75, 1851, 1864 (1949).

65. O. Bunemann, Nature 165, 474 (1950).

66. E. J. Blum, J. F. Denisse, and J. L. Steinberg, Compt. Rend. 232, 483 (1951).

67. A. V. Haeff, Phys. Rev. 75, 1546 (1949).

68. J. C. Jaeger and K. C. Westfold, Aust. J. Sci. Res. 2A, 322 (1949).

69. Yves Rocard, Compt. Rend. 232, 598 (1951).

70. E. J. Blum, J. F. Denisse, and J. L. Steinberg, Compt. Rend. 232, 387 (1951).

71. W. Schottky, Ann. Physik 57, 541-567 (1918).

72. D. O. North, RCA Rev. 4, 441, 5, 244 (1940).

73. W. S. Shockley and J. A. Pierce, Proc. I.R.E. 26, 321 (1938).

74. R. D. Sard, J. Appl. Phys. 17, 768 (1946).

75. R. W. Engstrom, J. Opt. Soc. Am. 37, 420 (1947).

76. J. W. Coltman, Proc. I.R.E. 37, 671 (1949).

77. J. S. Allen, Proc. I.R.E. 38, 346 (1950).

78. J. B. Johnson, Phys. Rev. 32, 97 (1932); H. Nyquist, Phys. Rev. 32, 110 (1932).

79. F. C. Williams, J. I.E.E 81, 751 (1937).

80. P. Drude, Ann. Physik 1, 566 (1900).

81. R. Becker, Theorie der Elektrizität, Teubner, 1933.

82. W. Shottky, Phys. Rev. 28, 74-103 (1926).

83. G. G. Macfarlane, P.P.S. 59, pt. 3, 366-374 (1947); B63, 807-814 (1950).

84. A. van der Ziel, Physica 16, 359-372 (1950).

85. R. H. Campbell, Jr. and R. A. Chipman, Proc. I.R.E. 37, 938-942 (1949).

86. H. C. Montgomery, Bell Syst. Tech J. 31, 950-975 (1952).

87. W. Shockley, Electrons and Holes in Semiconductors. Van Nostrand, 1950, Sec. 3.16

88. W. Shockley, op. cit., p. 290.

89. W. Shockley, op. cit., pp. 20, 285.

90. G. B. Herzog and A. van der Ziel, Phys. Rev. 84, 1249 (1951).

91. R.H. Mattson and A. van der Ziel, J. Appl. Phys. 24, 222 (1953).

92. Charles Kittel, Rev. Mod. Phys. 21, 541-583 (1949).

93. H.J. Williams and W. Shockley, Phys. Rev. 75, 178-183 (1949).

94. T. Hofbauer and K.M. Koch, Z. Phys. 130, 409-414 (1951).

95. T. Kamei, J. Phys. Soc. Jap. 6, 260-265 (1951).

96. M. Kac and A.J. Siegert, J. Appl. Phys. 18, 383 (1947).

97. Maurice Meyer, On Some Distributions of Functions in the Theory of Random Noise, Harvard Thesis, 1952; also M. Meyer and D. Middleton, J. Appl. Phys. 25(July, 1954).

98. N.M. Blachman, J. Appl. Phys. 24, 783 (1953).

99. S.O. Rice, Bell Syst. Tech. J. 23, 282 (1944).

100. D. Middleton, Q. Appl. Math. 5, 445 (1948).

101. Jahnke and Emde, Funktionentafeln, Dover, 1943, p. 78.

102. J. L. Doob, op. cit., Chap. V, Sec. 8.

103. W.B. Davenport, D. Middleton, R.A. Johnson, J. Appl. Phys. 23, 377(1952).

104. Ian Sneddon, Fourier Transforms, Wiley, Sec. 11, p. 62.

105. Lawson and Uhlenbeck, op. cit., Sec. 6.2, p. 128, eq. (7).

106. T.S. George, Proc. Inst. E.E. 99, Pt. IV, p. 92 (1952).

107. G. R. Hilst, M.I.T., Dept. of Met., Tech. Rep. 9A, 1 Nov. 1949, "Audio-Frequency Fluctuations in Radar Storm Echoes."

108. Aaron Fleisher, M.I.T., Dept. of Met., Tech. Rep. 22, 15 Jan. 1953 "The Information Contained in Weather Noise."

109. G. N. Watson, Bessel Functions, p. 393, eq. (2).

110. A. Erdélyi, et al, Higher Transcendental Functions, Vol. I., McGraw-Hill, 1953, Vol. 2, Sec. 7.7, eq. 22.

111. Erdélyi et al, Secs. 6.13, 26.13.3.

112. Erdélyi et al, op. cit., Vol. 1, Sec. 2.10, eq. 1.

113. Erdélyi et al, op. cit., Vol. 1, Sec. 2.3.1.

DISTRIBUTION LIST

Technical Reports

2	Chief of Naval Research (427) Department of the Navy Washington 25, D. C.
1	Chief of Naval Research(460) Department of the Navy Washington 25, D. C.
1	Chief of Naval Research (421) Department of the Navy Washington 25, D. C.
6	Director (Code 2000) Naval Research Laboratory Washington 25, D. C.
2	Commanding Officer Office of Naval Research Branch Office 150 Causeway Street Boston, Massachusetts
1	Commanding Officer Office of Naval Research Branch Office 1000 Geary Street San Francisco 9, California
1	Commanding Officer Office of Naval Research Branch Office 1030 E. Green Street Pasadena, California
1	Commanding Officer Office of Naval Research Branch Office The John Crerar Library Building 86 East Randolph Street Chicago 1, Illinois
1	Commanding Officer Office of Naval Research Branch Office 346 Broadway New York 13, New York
3	Officer-in-Charge Office of Naval Research Navy No. 100 Fleet Post Office New York, N. Y.

1	Chief, Bureau of Ordnance (Re4) Navy Department Washington 25, D. C.
1	Chief, Bureau of Ordnance (AD-3) Navy Department Washington 25, D. C.
1	Chief, Bureau of Aeronautics (EL-1) Navy Department Washington 25, D. C.
2	Chief, Bureau of Ships (810) Navy Department Washington 25, D. C.
1	Chief of Naval Operations (Op-413) Navy Department Washington 25, D. C.
1	Chief of Naval Operations (Op-20) Navy Department Washington 25, D. C.
1	Chief of Naval Operations (Op-32) Navy Department Washington 25, D. C.
1	Director Naval Ordnance Laboratory White Oak, Maryland
2	Commander U. S. Naval Electronics Laboratory San Diego, California
1	Commander (AAEL) Naval Air Development Center Johnsville, Pennsylvania
1	Librarian U. S. Naval Post Graduate School Monterey, California
50	Director Signal Corps Engineering Laboratories Evans Signal Laboratory Supply Receiving Section Building No. 42 Belmar, New Jersey

3	Commanding General (RDRRP) Air Research and Development Command Post Office Box 1395 Baltimore 3, Maryland
2	Commanding General (RDDDE) Air Research and Development Command Post Office Box 1395 Baltimore 3, Maryland
1	Commanding General (WCRR) Wright Air Development Center Wright-Patterson Air Force Base, Ohio
1	Commanding General (WCRRH) Wright Air Development Center Wright-Patterson Air Force Base, Ohio
1	Commanding General (WCRE) Wright Air Development Center Wright-Patterson Air Force Base, Ohio
2	Commanding General(WCRET) Wright Air Development Center Wright-Patterson Air Force Base, Ohio
1	Commanding General (WCREO) Wright Air Development Center Wright-Patterson Air Force Base, Ohio
2	Commanding General (WCLR) Wright Air Development Center Wright-Patterson Air Force Base, Ohio
1	Commanding General (WCLRR) Wright Air Development Center Wright-Patterson Air Force Base, Ohio
2	Technical Library Commanding General Wright Air Development Center Wright-Patterson Air Force Base, Ohio
1	Commanding General (RCREC-4C) Rome Air Development Center Griffiss Air Force Base Rome, New York
1	Commanding General (RCR) Rome Air Development Center Griffiss Air Force Base Rome, New York

2	Commanding General (RCRW) Rome Air Development Center Griffiss Air Force Base Rome, New York
6	Commanding General (CRR) Air Force Cambridge Research Center 230 Albany Street Cambridge 39, Massachusetts
1	Commanding General Technical Library Air Force Cambridge Research Center 230 Albany Street Cambridge 39, Massachusetts
2	Director Air University Library Maxwell Air Force Base, Alabama
1	Commander Patrick Air Force Base Cocoa, Florida
2	Chief, Western Division Air Research and Development Command P. O. Box 2035 Pasadena, California
1	Chief, European Office Air Research and Development Command Shell Building 60 Rue Ravenstein Brussels, Belgium
1	U. S. Coast Guard (EEE) 1300 E Street, N. W. Washington, D. C.
1	Assistant Secretary of Defense (Research and Development) Research and Development Board Department of Defense Washington 25, D. C.
5	Armed Services Technical Information Agency Document Service Center Knott Building Dayton 2, Ohio

1	Director Division 14, Librarian National Bureau of Standards Connecticut Avenue and Van Ness St., N. W.
1	Director Division 14, Librarian National Bureau of Standards Connecticut Avenue and Van Ness St., N. W.
1	Office of Technical Services Department of Commerce Washington 25, D. C.
1	Commanding Officer and Director U. S. Underwater Sound Laboratory New London, Connecticut
1	Federal Telecommunications Laboratories, Inc. Technical Library 500 Washington Avenue Nutley, New Jersey
1	Librarian Radio Corporation of America RCA Laboratories Princeton, New Jersey
1	Sperry Gyroscope Company Engineering Librarian Great Neck, L. I., New York
1	Watson Laboratories Library Red Bank, New Jersey
1	Professor E. Weber Polytechnic Institute of Brooklyn 99 Livingston Street Brooklyn 2, New York
1	University of California Department of Electrical Engineering Berkeley, California
1	Dr. E. T. Booth Hudson Laboratories 145 Palisade Street Dobbs Ferry, New York
1	Cornell University Department of Electrical Engineering Ithaca, New York

1	University of Illinois Department of Electrical Engineering Urbana, Illinois
1	Johns Hopkins University Applied Physics Laboratory Silver Spring, Maryland
1	Professor A. von Hippel Massachusetts Institute of Technology Research Laboratory for Insulation Research Cambridge, Massachusetts
1	Director Lincoln Laboratory Massachusetts Institute of Technology Cambridge 39, Massachusetts
1	Signal Corps Liaison Office Massachusetts Institute of Technology Cambridge 39, Massachusetts
1	Mr. Hewitt Massachusetts Institute of Technology Document Room Research Laboratory of Electronics Cambridge, Massachusetts
1	Stanford University Electronics Research Laboratory Stanford, California
1	Professor A. W. Straiton University of Texas Department of Electrical Engineering Austin 12, Texas
1	Yale University Department of Electrical Engineering New Haven, Connecticut
1	Mr. James F. Trosch, Administrative Aide Columbia Radiation Laboratory Columbia University 538 West 120th Street New York 27, N. Y.
1	Dr. J.V.N. Granger Stanford Research Institute Stanford, California